

KENTUCKY TRANSPORTATION CENTER

College of Engineering

**BASELINE MODELING OF THE MAYSVILLE CABLE-STAYED
BRIDGE OVER THE OHIO RIVER**





UNIVERSITY OF KENTUCKY

College of Engineering
Kentucky Transportation Center

Our Mission

We provide services to the transportation community through research, technology transfer and education. We create and participate in partnerships to promote safe and effective transportation systems.

We Value...

Teamwork -- Listening and Communicating, Along with Courtesy and Respect for Others
Honesty and Ethical Behavior
Delivering the Highest Quality Products and Services
Continuous Improvement in All That We Do

For more information or a complete publication list, contact us

KENTUCKY TRANSPORTATION CENTER

176 Raymond Building
University of Kentucky
Lexington, Kentucky 40506-0281

(859) 257-4513
(859) 257-1815 (FAX)
1-800-432-0719
www.ktc.uky.edu
ktc@engr.uky.edu

The University of Kentucky is an Equal Opportunity Organization

Research Report
KTC-05-10/FRT104-00-1F

BASELINE MODELING OF THE MAYSVILLE CABLE-STAYED BRIDGE OVER THE OHIO RIVER

by

I. E. Harik

Professor of Civil Engineering and Program Manager, Structures and Coatings Section,
Kentucky Transportation Center

Jindong Hu

Visiting Professor, Kentucky Transportation Center

Suzanne Weaver Smith

Associate Professor, Department of Mechanical Engineering

Wei-Xin Ren

Visiting Professor, Kentucky Transportation Center

Tong Zhao

Visiting Professor, Kentucky Transportation Center

Jennie E. Campbell

Graduate Student, Department of Mechanical Engineering

and

R. Clark Graves

Associate Program Manager, Pavements Section, Kentucky Transportation Center

Kentucky Transportation Center
College of Engineering, University of Kentucky

In cooperation with

Transportation Cabinet
Commonwealth of Kentucky

and

Federal Highway Administration
U.S. Department of Transportation

The contents of this report reflect the views of the authors who are responsible for the facts and accuracy of the data presented herein. The contents do not necessarily reflect the official views or policies of the University of Kentucky, the Kentucky Transportation Cabinet, nor the Federal Highway Administration. This report does not constitute a standard, specification or regulation. The inclusions of manufacturer or trade names are for identification purposes and are not to be considered as endorsement.

July 2005

Technical Report Documentation Page

1. Report No. KTC-05-10/FRT104-00-1F		2. Government Accession No.		3. Recipient's Catalog No.	
4. Title and Subtitle BASELINE MODELING OF THE MAYSVILLE CABLE-STAYED BRIDGE OVER THE OHIO RIVER				5. Report Date July 2005	
				6. Performing Organization Code	
				8. Performing Organization Report No. KTC-05-10/FRT104-00-1F	
7. Author(s): I.E. Harik, J.D. Hu, S.W. Smith, W.X. Ren, T. Zhao, J.E. Campbell and R. C. Graves				10. Work Unit No. (TRAIS)	
9. Performing Organization Name and Address Kentucky Transportation Center College of Engineering University of Kentucky Lexington, Kentucky 40506-0281				11. Contract or Grant No.	
				13. Type of Report and Period Covered Final	
				14. Sponsoring Agency Code	
12. Sponsoring Agency Name and Address Kentucky Transportation Cabinet State Office Building Frankfort, Kentucky 40622					
15. Supplementary Notes Prepared in cooperation with the Kentucky Transportation Cabinet and the U.S. Department of Transportation, Federal Highway Administration.					
16. Abstract This report presents the baseline modeling of the Maysville cable-stayed bridge which connects Maysville, Kentucky and Aberdeen, Ohio over the Ohio River. The objective of this study is to establish the bridge baseline model via the dynamics-based technique and finite element method. The scope of research includes finite element modeling and modal analysis, field free vibration testing, finite element model calibration using field test results, and cable dynamic testing and modeling. It is demonstrated that a cable-stayed bridge is a highly pre-stressed structure. The stress stiffening of cable elements plays an important role in both static and dynamic analysis. The large deflection analysis has shown that large deflection has the limited effect on the member deflections. Dominate dynamic response modes in the low frequency range contain vertical and transverse directions. The free vibration modes of the bridge are complicated and coupled. A good agreement of frequencies has been found between finite element modeling and in field free vibration testing after calibrating the finite element model. But, the better matching for higher modes is not expected and not realistic, as the experimental model properties of the bridge come from the output-only measurement. The calibrated finite element model may be used as a baseline in the future structural analysis and monitoring of the Maysville cable-stayed bridge.					
17. Key Words Cable-stayed bridge; Finite element model; Modal analysis; Free vibration testing; Natural frequency; Baseline model; Cable model; Kentucky.			18. Distribution Statement Unlimited with approval of Kentucky Transportation Cabinet		
19. Security Classif. (of this report) Unclassified		20. Security Classif. (of this page) Unclassified		21. No. of Pages 148	22. Price

EXECUTIVE SUMMARY

Research Objectives

Maysville cable-stayed bridge, dedicated as the William H. Harsha Bridge, connects Maysville (Mason County), Kentucky and Aberdeen (Brown County), Ohio over the Ohio River as seen in the photographs in Figures 1.1 and 1.2. The bridge was officially opened to traffic on January 12, 2001. The objective of this investigation is to analyze the dynamic characteristics of the bridge and establish a finite element model as a baseline in the structural analysis and monitoring of the Maysville cable-stayed bridge.

To achieve the objective, this study contains the following four tasks:

- 1) On-site ambient vibration testing;
- 2) Finite element modeling and modal analysis;
- 3) Finite element model updating (calibration) using field test results;
- 4) Cable testing and modeling.

Background

Cable-stayed bridges have become one of the most frequently used bridge systems throughout the world because of their aesthetic appeal, structural efficiency, enhanced stiffness compared with suspension bridges, ease of construction and small size of substructures. Over the past 40 years, rapid developments have been made on modern cable-stayed bridges. With the main span length increasing, more shallow and slender stiffness girders used in modern cable-stayed bridges, the safety of the whole bridge under service loadings and environmental dynamic loadings, such as impact, wind and earthquake loadings, presents increasingly important concerns in design, construction and service. It has become essential to synthetically understand and realistically predict their response to these loadings. The unique structural styles of cable-stayed bridges make the span length longer and beautify the environment, but also add to the difficulties in

accurate structural analysis. It is known that these long span and cable-stayed bridges constitute complex structural components with high geometric nonlinearity. In addition, the initial equilibrium configuration under dead loads has a significant effect on the structural behavior of cable-stayed bridges.

The discretized finite element method provides a convenient and reliable idealization of the structural continua and is particularly effective when using digital-computer analyses. The finite deformation theory with a discrete finite element model is the most powerful tool used in the nonlinear analysis of modern cable-stayed bridges. However, it is not an easy task to establish a real and reliable finite element model of such complex structures. The process requires the combination of the bridge field testing and analysis. The initial finite element model has to be updated or calibrated by the field test results.

Field Free Vibration Testing

On-site dynamic testing of a bridge provides an accurate and reliable description of its dynamic characteristics. Matching the actual dynamic characteristics of bridges has become an integral part of dynamics-based structure evaluation in order to eliminate the uncertainties and assumptions involved in analytical modeling. The current dynamic characteristics (frequencies and mode shapes) of the Maysville cable-stayed bridge were obtained from the field free vibration test results under the excitation due to running the loaded trucks. These dynamic characteristics were subsequently used as the basis for calibrating the finite element model to establish a baseline for the bridge.

Finite Element Modeling and Calibration

A three-dimensional finite element model was constructed in the ANSYS, one of the most powerful engineering design and analysis commercial software packages. The established finite element model is then used to conduct both static and dynamic analysis of the Maysville cable-stayed bridge. Starting from the deformed equilibrium

configuration, the modal analysis is performed. The modal analysis of the cable-stayed bridge is therefore a “pre-stressed” modal analysis. All possible frequencies and mode shapes can be calculated.

One of the advantages of finite element modeling and analysis is that parametric studies can be performed. The structural and material parameters that affect the modal properties of the bridge can be identified from such parametric studies. From the parametric studies, it is found that the key parameters affecting the vertical modal properties are the mass, cable sectional area, cable elastic modulus and deck vertical bending stiffness. The key parameters affecting the transverse and torsion modal properties are the mass, cable sectional area, cable elastic modulus and deck lateral bending stiffness. The parametric studies reported here not only prove the efficiency of the finite element methodology, but also demonstrate the variation in modal response caused by a variation in the input parameters.

Finite element model calibration was then carried out by adjusting its structural or material parameters, which affect the modal properties of the bridge, such that the FEM predicted frequencies and mode shape match the experimentally observed frequencies and mode shapes. The first eight frequencies determined through free vibration measurements in the system identified modes and FEM predictions are summarized in Tables E-1. This table shows that good agreement exist between the experimental and calibrated analytical results.

Table E-1 Comparison of Frequencies

Mode	Test (Hz)	FE Model (Hz)	Mode classification
1	0.3945	0.43	Vertical
2	0.5	0.507	Transverse; Transverse + Torsion for FEM
3	0.5222	0.556	Vertical
4	0.6556	0.646	Transverse + torsion
5	0.7778	0.709	Torsion
6	0.8444	0.824	Vertical
7	0.9333	-	Longitudinal
8	1	0.964	Vertical

Cable Testing and Modeling

Cable testing and modeling for the Maysville Bridge included the following accomplishments:

- Three field tests of the cables were conducted (on 1/10/01, 5/22/01 and 8/13/01), including tests with loaded trucks and with ambient (typical traffic and wind) excitation. Tests were conducted over a range of temperatures.
- Finite element models for the cables were developed using the as-built cable properties. Models included a set of ten cables. Both unrestrained and restrained models were developed.
- Comparison of finite-element model results to field test results showed good correlation.

Notable results include the following:

- Field measurement of all cables can be performed in approximately 1.5 days using short time records and Cepstrum signal processing techniques.
- Field tests of the cables in May 2001 and August 2001 resulted in consistent fundamental frequencies that differed for the longest cables from results of the first test just before bridge opening in January 2001. Possible explanations for the differences include a “breaking-in” period for castings and temperature effects.
- A rain event occurred during testing in May 2001. Response of two restrained cables was recorded during the rain showing persistent amplitude-modulated response unrelated to the anchor motion. This response stopped when the rain stopped. Rivulets were noted and photographed on the underside of the cables. The helical strikes included on the surface of the cables do not significantly disrupt the rivulet path down the cable. The motion of the cables was limited (by the restrainers), however, to acceleration amplitudes less than those seen with typical heavy traffic.
- No model refinement for the cable models was required for good correlation between model and field test results.

Conclusions and Recommendations

On site free vibration testing provides a fast way to obtain the real dynamic properties of a structure. The peak picking identification is very fast and efficient since no model has to be fitted to the data. For real applications, the peak picking method could be used on site to verify the quality of the measurements. But the mode shapes for the transverse are not too good since the transverse excitation is not enough. The bump-and-brake test does not improve the identified results.

A good agreement of frequencies has been found between the results of the calibrated finite element model and in *situ* free vibration testing results. The identified frequencies from the High-speed and Bump-brake measurements are quite stable. The better matching for higher modes is not expected and not realistic too, as the experimental modal properties of the bridge come from the output-only measurement. The calibrated finite element model may be used as a baseline in the future structural analysis and monitoring of the Maysville cable-stayed bridge.

Related to cable modeling and testing, we conclude the following: 1) as-built information on the cable construction was used to develop verified finite-element models of the 80 cables which can be used as a baseline for future evaluation of cable stiffness and structural integrity, 2) field-survey testing of all cables can be accomplished with ambient (traffic) excitation in 1.5 days, so periodic monitoring of the cables is possible without permanent installation of a measurement system, 3) the helical strikes on the surface of the cables do not appreciably affect the formation or flow of water rivulets; restrainers (cable-ties) seemed effective in limiting motion of the cables during one rain event that was measured and 4) periodic measurement of the cable response is recommended to monitor the continuing effectiveness of the restrainers and structural integrity of the cables.

ACKNOWLEDGEMENTS

The financial support for this project was provided the Kentucky Transportation Cabinet and Federal Highway Administration. The assistance of the staff in the Pavement Section in the Kentucky Transportation Center in coordinating and conducting the bridge testing is especially noteworthy. The authors are also grateful to the assistance provided by the engineers and the staff in Kentucky Highway District 9.

TABLE OF CONTENTS

EXECUTIVE SUMMARY	i
ACKNOWLEDGEMENTS	vi
TABLE OF CONTENTS	vii
LIST OF TABLES	ix
LIST OF FIGURES	x
1. INTRODUCTION	
1.1. General.....	1
1.2. Bridge Description.....	3
1.3. On-Site Dynamic Testing.....	5
1.4. Finite Element Modeling and Calibration.....	6
1.5. Cable Testing and Modeling.....	8
1.6. Scope of Work.....	8
2. FIELD DYNAMIC TESTING	
2.1. General.....	10
2.2. Output-Only Dynamic Testing.....	12
2.3. Peak Picking (PP) System Identification.....	16
2.4. Remarks.....	24
3. FINITE ELEMENT MODELING AND CALIBRATION	
3.1. General.....	26
3.2. Initial Finite Element Model.....	29
3.3. Static Analysis under Dead Load.....	50
3.4. Modal Analysis.....	56
3.5. Parametric Studies.....	72
3.6. Finite Element Model Calibration.....	83
3.7. Remarks.....	89
4. CABLE TESTING AND MODELING	
4.1. General.....	93

4.2. Field Testing of the Maysville Bridge Stay Cables.....97
4.3. Finite Element Analysis.....115
4.4. Remarks.....122

5. CONCLUSIONS AND RECOMMENDATIONS

5.1. General.....124
5.2. Finite Element Modeling and Dynamic Properties.....124
5.3. Free Vibration Testing and Model Calibration.....126
5.4. Cable Testing and Modeling.....126

REFERENCES.....128

LIST OF TABLES

Table No.	Description	Page No.
E-1	Comparison of Frequencies	iii
2.1	Instrumentation Per Setup	15
2.2	Possible Frequencies of High-speed Test (Hz)	22
2.3	Possible Frequencies of Bump-and-Brake Test (Hz)	22
2.4	Summary of Identified Frequencies (Hz)	23
3.1	Member Details Extracted from the Plan	30
3.2	Preliminary Material Properties	36
3.3	Preliminary Real Constants	38
3.4	Material Properties	41
3.5	Real Constants	42
3.6	Details of the Model	44
3.7	Initial Tension Forces in the Cables	52
3.8	Comparison of Maximum Deflections (absolute value, foot)	56
3.9	Comparison of Frequencies (Hz)	58
3.10	Natural Frequencies (Hz) and Mass Fraction	60
3.11	Natural Frequencies (Hz) and Participation Factors	61
3.12	Frequencies (Hz) for Different Deck Mass Densities	73
3.13	Frequencies (Hz) for Different Cable Areas	75
3.14	Frequencies (Hz) for Different Cable Moduli	77
3.15	Frequencies (Hz) for Different Deck Vertical Stiffnesses	79
3.16	Frequencies (Hz) for Different Lateral Deck Stiffnesses	81
3.17	Calibrated Real Constants	83
3.18	Calibrated Material Properties	85
3.19	Comparison of Frequencies	86
4.1	Nominal Cable Designs (Cables 21-40 are Symmetric to Cables 1–20)	96
4.2	Numerical Results from Cepstrum Analysis of All Tested Cables	114
4.3	Cable Geometry and Material Properties for Downstream Cables 21-30	116
4.4	Finite Element Model Fundamental Frequency Results with Tests and String Model	117
4.5	Cable Geometry and Material Properties for Downstream Cables 1-40	120
4.6	Cable Geometry and Material Properties for Upstream Cables 1-40	121

LIST OF FIGURES

Fig. No.	Description	Page No.
1.1	Aerial View of the Maysville Cable-Stayed Bridge	3
1.2	Side View of the Maysville Cable-Stayed Bridge	4
1.3	Plan and Elevation of the Maysville Cable-Stayed Bridge	5
2.1	Measurement Instrumentation Plan	14
2.2	Typical Acceleration Time Histories at Location U20	15
2.3	Full Data Averaged Vertical Response Spectra (High-speed Test)	19
2.4	Full Data Averaged Transverse Response Spectra (High-speed Test)	19
2.5	Full Data Averaged Longitudinal Response Spectra (High-speed Test)	20
2.6	Full Data Averaged Vertical Response Spectra (Bump-and-brake Test)	20
2.7	Full Data Averaged Transverse Response Spectra (Bump-and-brake Test)	21
2.8	Full Data Averaged Longitudinal Response Spectra (Bump-and-brake Test)	21
2.9	Identified First Vertical Mode Shape of Maysville Bridge ($f = 0.3889 \text{ Hz}$)	23
2.10	Identified First Transverse Mode Shape of Maysville Bridge ($f = 0.5 \text{ Hz}$)	24
3.1	BEAM4 3-D Elastic Beam Element	33
3.2	3-D Tension-only Truss Element	34
3.3	3-D structural solid element	36
3.4	Elevation of Finite Element Model	46
3.5	Plan of Finite Element Model	46
3.6	Isotropic Elevation of Finite Element Model	49
3.7	1st Mode Shape ($f = 0.432 \text{ Hz}$, Vertical)	62
3.8	2nd Mode Shape ($f = 0.517 \text{ Hz}$, Transverse + Torsion)	63
3.9	3rd Mode Shape ($f = 0.558 \text{ Hz}$, Vertical)	64
3.10	4th Mode Shape ($f = 0.679 \text{ Hz}$, Transverse + Torsion)	65
3.11	5th Mode Shape ($f = 0.711 \text{ Hz}$, Torsion)	66
3.12	6th Mode Shape ($f = 0.827 \text{ Hz}$, Vertical)	67
3.13	7th Mode Shape ($f = 0.972 \text{ Hz}$, Vertical)	68
3.14	8th Mode Shape ($f = 0.987 \text{ Hz}$, Torsion)	69
3.15	9th Mode Shape ($f = 1.010 \text{ Hz}$, Tower Sway)	70
3.16	10th Mode Shape ($f = 1.017 \text{ Hz}$, Tower Sway)	71
3.17	Frequencies vs Deck Mass Density	74
3.18	Frequencies vs Cable Section Area	76
3.19	Frequencies vs Cable Elastic Modulus	78
3.20	Frequencies vs Deck Vertical Bending Stiffness	80
3.21	Frequencies vs Deck Lateral Bending Stiffness	82

3.22	Comparison of First Vertical Mode Shape	87
3.23	Comparison of Second Vertical Mode Shape	87
3.24	Comparison of Third Vertical Mode Shape	88
3.25	Comparison of First Transverse Mode Shape	88
3.26	Comparison of Second Transverse Mode Shape	89
4.1	Aerial View of the Maysville Bridge, January 2001	94
4.2	Elevation Drawing of the Maysville Bridge	94
4.3	Recorded Changes to Design Tensions for Deck Alignment and Profile Adjustment	94
4.4	Steel Strands in Template (left) and Helical Strikes and Cross-ties (right)	95
4.5	Restrainer (Cross-tie) Design Detail	95
4.6	High-speed (left) and Bump-and-brake (right) tests on January 10, 2001	97
4.7	Typical Traffic Including Heavy Trucks During Test on August 13, 2001	98
4.8	Typical Accelerometer Mounting (top left) and Orientation on Cable (top right) and Anchor (bottom)	99
4.9	Anchor 29W Acceleration Time Histories: Fast (left) and Bump-and-brake (right)	100
4.10	Cable 29W Acceleration Time Histories: Fast (left) and Bump-and-brake (right)	100
4.11	29W Fast Test Acceleration Spectra: Anchor (left) and Cable (right)	101
4.12	29W Bump and Brake Acceleration Spectra: Anchor (left) and Cable (right)	102
4.13	A Typical Cepstrum Analysis to Determine Fundamental Frequency: Time History (left), Spectrum (middle) and Cepstrum (right)	102
4.14	Frequencies of Cables 21-40W: String Models and First Field Test Results	104
4.15	Temperatures Recorded for All Field Tests: Surface Temperatures (1/10/01) and Air Temperatures (5/22/01 and 8/13/01)	104
4.16	Second field test: in the rain (top left), measuring wind speed (top right) and data acquisition system (bottom)	106
4.17	Typical Accelerations for Heavier Traffic, Cable 32 W (left) and Lighter Traffic, Cable 33 W (right) on May 22, 2001	106
4.18	Typical Spectra for Heavier Traffic, Cable 32 W (left) and Lighter Traffic, Cable 33 W (right) on May 22, 2001	107
4.19	Frequencies of Cables 1-40W: String Models, First and Second Test Results	108
4.20	Underside rivulet on Cable 40W (top left and right, with contrast enhanced), Rivulet Stream Leaving Cable (bottom left), and Restrainer Collar Ribbons Showing Wind Speed and Direction and Underside Rivulet (bottom right)	109
4.21	Transverse (z) acceleration of Cable 40W overlaid with tri-axial anchor accelerations in rain with light traffic (left) and heavy traffic (right)	110

4.22	Transverse (z) acceleration of Cable 39W with tri-axial anchor accelerations in rain with light traffic (left) and after rain has stopped with heavy traffic (right)	110
4.23	Third field test in progress (top left), data acquisition (top right), measuring wind speed and direction (bottom left), and cable / anchor sensor placement (bottom middle / right)	112
4.24	Frequencies of Cables 21-40W: String Model and All Field Test Results	112
4.25	Frequencies of Cables 1-40E: String Model and All Field Test Results	113
4.26	Finite Element Model of Ten Unrestrained Cables of the Maysville Bridge	117
4.27	Comparison of Finite Element Model Fundamental Frequency Results for Cables 21-30 W to Experimental and String Model Frequencies	118
4.28	Finite Element Model of Ten Restrained Cables of the Maysville Bridge	119
4.29	Final Comparison of Finite Element Model Results to Field Test Results	122

1. INTRODUCTION

1.1. General

Cable-stayed bridges have become one of the most frequently used bridge systems throughout the world because of their aesthetic appeal, structural efficiency, enhanced stiffness compared with suspension bridges, ease of construction and small size of substructures. Over the past 40 years, rapid developments have been made in modern cable-stayed bridges. With the main span length increased and more shallow and slender stiffness girders used in modern cable-stayed bridges, their safety of the whole bridges under service loadings and environmental dynamic loadings, such as impact, wind and earthquake loadings, presents increasingly important concerns in design, construction and service. It has become essential to synthetically understand and realistically predict their response to these loadings. The unique structural styles of cable-stayed bridges make the span length longer and beautify the environment, but also add to the difficulties in accurate structural analysis. It is known that these long span and cable-stayed bridges constitute complex structural components with high geometric nonlinearity. In addition, the initial equilibrium configuration under dead loads has a significant effect on the structural behavior of cable-stayed bridges.

A long span cable-stayed bridge exhibits nonlinear characteristics under any load conditions. These nonlinear sources may come from

- The sag effect of inclined stay cables;
- The combined axial load and bending moment interaction effect of the girders and towers;
- The large displacement effect;
- The nonlinear stress-strain behavior of materials.

The discretized finite element method provides a convenient and reliable idealization of the structural continua and is particularly effective when using digital-computer analyses. The finite deformation theory with a discrete finite element model is the most powerful tool used in the nonlinear analysis of modern cable-stayed bridges.

However, it is not an easy task to establish a real and reliable finite element model of such complex structures. The process requires the combination of bridge field test results and analyses. The initial finite element model has to be updated or calibrated by field test results.

For a long span bridge, it is useful to establish both the analytical dynamic characteristics from the finite element predictions and the measured dynamic characteristics from the field testing. Many investigations of the dynamic characteristics of the cable-stayed bridge have been conducted over the years (Fleming and Egeseli 1980, Wilson and Gravelle 1991, Wilson and Liu 1991, Yang and Fonder 1998, Ren and Obata 1999, Zhu et al. 2000, Chang et al. 2001, Zhang et al., Cunha et al. 2001 and Au et al. 2001). In these works, the ambient structural response due to wind and/or traffic loads has been proven to be useful for determining the dynamic characteristics of bridges. The structural model updating as a form of calibration is a rapidly developing technology, and provides a “global” way to evaluate the structural state. Detailed literature reviews have been performed by Doebling et al. (1996), Salawu (1997) and Stubbs et al. (1999). While its applications have been diverse and scattered (Casas and Aparicio 1994, Chen et al. 1995, Hearn and Testa 1991, Harik et al. 1997, Harik et al. 1999, Juneja et al. 1997, Liu 1995, Mazurek and Dewolf 1990). Once a finite element model is calibrated according to the measured dynamic characteristics, the model can then be used for aerodynamic and /or seismic response predictions. Furthermore, the calibrated finite element model can be used as a baseline for health assessments of a bridge structure in the future.

The present work focuses on the comprehensive research to conceive a three-dimensional finite element model of the Maysville cable-stayed bridge. Therefore, a three-dimensional finite element model has been created in the ANSYS, one general purpose commercial finite element software. All geometrically nonlinear sources are included such as cable sags, large deflections and axial force and bending moment interactions. The initial equilibrium configuration is achieved to account for the effect of dead loads. The finite element model is further updated through the use of free vibration field test results. The analytical model calibrated with experimental results is used to study both static and dynamic responses of the bridge to various parametric changes. This

calibrated finite element model can be utilized as a baseline in the structural analysis and monitoring of the Maysville cable-stayed bridge. Cable testing and modeling for the Maysville cable-stayed bridge are performed separately. They included field tests and finite element modeling of the cables. The outcomes of this research could be applied to provide useful information and data for the development of more refined design and analysis tools with future long span cable-stayed bridges.

1.2. Bridge Description

Maysville cable-stayed bridge, dedicated as the William H. Harsha Bridge, connects Maysville (Mason County), Kentucky and Aberdeen (Brown County), Ohio over the Ohio River as seen in the photographs in Figures 1.1 and 1.2. The main bridge with a total length of 2,100 ft. includes two anchor spans with each being 125 ft. long, two flanking spans with each being 400 ft. long, and the cable-stayed span being 1,050 ft. in length. Whole bridge width of 58'-6" includes two 12 ft. traffic lanes and two 12 ft. shoulders. The main cable-stayed superstructure consists of a concrete deck supported by two main 84 to 60 inch deep steel plate girders with floor beams spaced at 16'-8". The deck consists of pre-cast deck sections with cast-in-place joints and post-tensioning in both longitudinal and transverse directions. The elevation drawing is shown in Figure 1.3. The bridge was officially opened to traffic on January 12, 2001.



Figure 1.1 Aerial View of the Maysville Cable-Stayed Bridge



Figure 1.2 Side View of the Maysville Cable-Stayed Bridge

Steel stay cables are arranged in a two plane semi harped system with stays spaced at 50 foot intervals along each edge of the deck. The eighty cables are nominally four sets of twenty cables. All cable-stayed bridges have had problems with stay wind gallop when the right combination of light rain and wind occur. However, the stay cable system of the Maysville cable-stayed bridge is state-of-the-art. A co-extruded high density polyethylene pipe has been used which has a brilliant white outer layer eliminating the necessity to use a tape wrap. The outer layer has a small spiral bead around the pipe to break up air flow when there is light rain and wind to help prevent cable gallop. In addition, stay damping cables are connected between the stay cables with soft neoprene collars to further dampen galloping.

Two main towers have a goal post configuration with an upper and lower strut. The towers are 332 ft. tall and are supported on 16 concrete filled drilled shafts. Abutments are conventional concrete units supported by steel H piles.

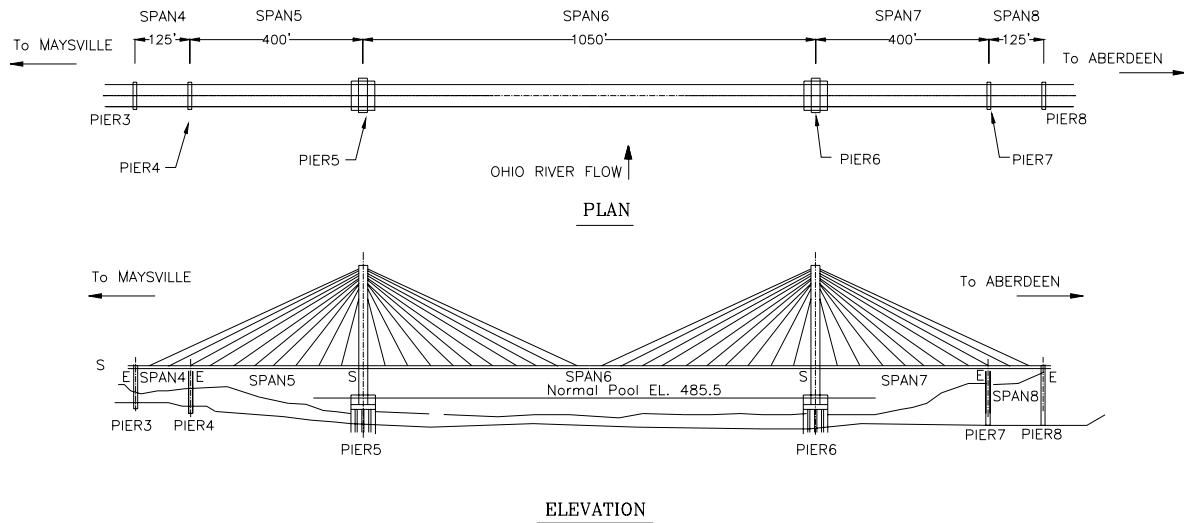


Figure 1.3 Plan and Elevation of the Maysville Cable-Stayed Bridge

1.3. On-Site Dynamic Testing

On-site dynamic testing of a bridge provides an accurate and reliable description of its dynamic characteristics. In the civil engineering, structures such as bridges or buildings are considered systems and the system identification (experimental modal analysis) means the extraction of modal parameters (frequencies, damping ratios and mode shapes) from dynamic measurements. These modal parameters will be utilized as a basis in the finite element model updating, structural damage detection, structural safety evaluation, and structural health monitoring on service.

There are three main types of bridge dynamic testing: (1) forced vibration testing; (2) free vibration testing; and (3) ambient vibration testing. In forced vibration testing and free vibration testing, the structure is excited by artificial means such as shakers, drop weights or test vehicle. By suddenly dropping a load on the structure, a condition of free vibration is induced. The disadvantage of this method is that traffic has to be shut down for an extended period of time. It is clear that this can be a serious problem for bridges that carry significant vehicular traffic.

In contrast, ambient vibration testing does not affect the traffic on the bridge because it uses existing vehicular traffic and natural wind loading to excite the bridge. This method is obviously cheaper than forced vibration testing since no extra equipment is needed to excite the structure. However, relatively long records of response measurements are required and the measured data are more stochastic. Consequently, the system identification results may be less reliable than such results obtained from a known forced vibration.

For the Maysville cable-stayed bridge, on-site dynamic testing was performed using the free vibration testing method. Dynamic characteristics (frequencies and mode shapes) of the Maysville cable-stayed bridge were extracted from the peak of the average normalized power spectral densities (ANPSDs). These vibration properties are subsequently used as a basis for updating the finite element model of the bridge.

1.4. Finite Element Modeling and Calibration

With modern commercial finite element programs it is possible to accurately predict both static and dynamic structural behavior of cable-stayed bridges. The discretized finite element model provides a convenient and reliable idealization of the structure. Thanks to rapid computer developments and the wealth of matrix analysis studies on nonlinear problems available, finite deformation theory with a discrete finite element model is one of the most powerful tools used in the analysis and design of cable-stayed bridges. An important advantage of the finite element method is that structural complexities can be considered effectively. Application of the finite deformation theory can include the effect of all nonlinear cable-stayed bridge sources such as cable sags, large deflections, and axial force and bending moment interactions. Another advantage of the finite element method lies in the capability of in-depth dynamic analysis.

A complete three-dimensional finite element model of the Maysville cable-stayed bridge has been developed for the ANSYS (ANSYS 5.7) commercial finite element

program. The ANSYS has been chosen because of the program's significant capability to account for cable stress stiffening and pre-stressed modal analysis capability. The finite element model of the Maysville cable-stayed bridge is composed of three element types: 3-D elastic beam elements, 3-D tension-only truss elements, and 3-D structural solid elements. The model consists of 994 nodes and 1321 finite elements with a total of 5168 active degrees of freedom (DOF).

In the design of cable-stayed bridges, the dead load often contributes most of bridge load. In the finite element analysis, the dead load influence is included through static analysis under dead loads before the live load or dynamic analysis is carried out. The objective of the static analysis process is to achieve the deformed equilibrium configuration of the bridge due to dead loads where the structural members are "pre-stressed". The initial tension in the cables due to the dead load is determined by on-site testing. In addition, the geometric nonlinear effect has been studied by including the stress stiffening and large deflection.

A cable-stayed bridge is a highly pre-stressed structure. Starting from the deformed equilibrium configuration, the modal analysis is performed. Therefore, the dead load effect to the stiffness is included in the modal analysis through the specification of the pre-stress forces in the cables. The modal analysis is consequently a "pre-stressed" modal analysis, from which possible frequencies and mode shapes can be calculated. A coupled mode can be included, which gives a comprehensive understanding of the dynamic behavior of cable-stayed bridges. Parametric studies can also be performed by using the following parameters: deck self-weight, cable stiffness, and edge girder and sub-stringer bending stiffness.

Due to deviations in the structure's original geometric or material properties it is difficult to establish the initial finite element model for structural evaluation. The original finite element model has to be updated or calibrated using field testing results in order to approximate the current conditions of the bridge. Finite element model updating is carried out until the finite element analytic frequencies and mode shapes match the field

testing results, maintaining physically realistic material properties. The updated finite element model is used as the baseline model for future evaluations of the bridge.

1.5. Cable Testing and Modeling

Separate consideration of the cable response is motivated by the occurrence of wind-induced vibrations of bridge stay cables worldwide. Observed and documented since the mid-1980's, a particularly troublesome vibration has been observed in light-to-moderate wind combined with light rain. "Rain-wind" vibrations led to failure of anchor details on many bridges. Researchers worldwide continue to study factors affecting wind-induced stay cable vibration toward the goal of developing design approaches for prevention and mitigation.

The eighty cables of the Maysville cable-stayed bridge are unique flexible structures whose dynamic response characteristics depend on material properties, tension, and possibly temperature. To bring the bridge deck into alignment side-to-side as the constructed sections met in the center and to smooth the vertical deck profile, cable design tensions were adjusted from those in the original plans. Cable testing and modeling for the Maysville cable-stayed bridge included three field tests of the cables. The first of these was just before the bridge opened with excitation provided by loaded trucks. The second and third tests used ambient (typical traffic and wind) excitation. Signal processing analysis of the recorded acceleration time histories identified fundamental frequencies of the cables. Finite element models were developed for all cables using the as-built cable properties and compared to field test results showing good correlation.

1.6. Scope of Work

The primary aim of this investigation is to evaluate the structural dynamic characteristics of the Maysville cable-stayed bridge and to establish the baseline model of the bridge. Dynamics-based structural evaluation will be used. To achieve the goal, the scope of work will be divided into the following five parts:

- (1). Conduct finite element modeling and modal analysis;
- (2). Extract the dynamic characteristics from on-site free vibration testing;
- (3). Calibrate the finite element model by the results of the field testing;
- (4). Conduct field tests of stay cables and finite element modeling of them;
- (5). Understand the structural behavior under service loadings and environmental dynamic loadings.

2. FIELD DYNAMIC TESTING

2.1. General

On-site dynamic testing of a bridge provides an accurate and reliable description of its real dynamic characteristics. There are three main types of dynamic bridge testing:

- *Forced Vibration Test*
- *Free Vibration Test*
- *Ambient Vibration Test*

In the first two methods, the structure is excited by artificial means such as shakers, drop weights or testing vehicle. By suddenly dropping a load on the structure, a condition of free vibration is induced. The disadvantage of these methods is that traffic has to be shut down for a rather long time, especially for large structures such as long-span bridges, and requires numerous test setups. It is clear that this can be a serious problem for bridges that have high traffic volumes. In contrast, ambient vibration testing does not affect the traffic on the bridge because it uses the traffic and wind as natural excitation. This method is obviously cheaper than forced vibration testing since no extra equipment is needed to excite the structure. However, relatively long records of response measurements are required and the measured data are more stochastic. Consequently, accurately identifying the system response modes is less accurate.

Basically, the system identification procedure is carried out according to both input and output measurement data through the frequency response functions (FRFs) in the frequency domain or impulse response functions (IRFs) in the time domain. For civil engineering structures, the dynamic responses (output) are the direct records of the sensors that are installed at several locations. However, the input or excitation of the real structure in the operational condition often can be hardly realized. It is extremely difficult to measure the input excitation forces acting on a large-scale structure. Although forced excitations (such as heavy shakers and drop weights) and correlated input-output

measurements are sometime available, testing or structural complexity and achievable data quality restrict these approaches to dedicated applications.

The output data-only dynamic testing has the advantage of being inexpensive since no equipment is needed to excite the structure. The ambient vibration is a kind of output data-only dynamic testing. The service state does not have to be interrupted by using this technique. The output data-only dynamic testing has been successfully applied to many large scale cable-supported bridges such as the Golden Gate Bridge (Abdel-Ghaffer and Scanlan 1985), the Quincy Bayview Bridge (Wilson and Gravelle 1991), the Fatih Sultan Mehmet Suspension Bridge (Brownjohn et al. 1992), the Tsing Ma Suspension Bridge (Xu et al. 1997), the Hitsuishijima Bridge, one of the Honshu-Shikoku Bridge (Okauchi et al. 1997), the Vasco da Gama Cable-Stayed Bridge (Cunha et al. 2001), the Kap Shui Mun Cable-Stayed Bridge (Chang et al. 2001), and the Roebling Suspension Bridge (Ren et al. 2001). In the case of output data-only dynamic testing, only response data are measured while actual loading conditions are unknown. A system identification procedure will therefore need to base itself on output-only data.

System Identification using output-only measurements presents a challenge requiring the use of special identification techniques, which can deal with very small magnitudes of ambient vibration contaminated by noise without the knowledge of input forces. There have been several output-only data system identification techniques available that were developed by different investigators or for different uses such as: peak-picking from the power spectral densities (Bendat and Piersol 1993), auto regressive-moving average (ARMA) model based on discrete-time data (Andersen et al. 1996), natural excitation technique (NExT) (James et al. 1995), and stochastic subspace identification (Van Overschee and De Moor 1996; Peeters and De Roeck 2000). The mathematical background for many of these methods is often very similar, differing only from implementation aspects (data reduction, type of equation solvers, sequence of matrix operations, etc.). The benchmark study was carried out to compare system identification techniques for evaluating the dynamic characteristics of a real building on operation conditions from ambient vibration data (De Roeck et al. 2000).

For the Maysville cable-stayed bridge, on-site free vibration tests have been conducted. The Maysville cable-stayed bridge consists of a 1050' main span, two 400' flanking spans and two 125' anchor spans. The bridge has the width of 58'-6" with two 12' traffic lanes and two 12' shoulders. The output data-only dynamic testing and system identification of the Maysville cable-stayed bridge are performed. The field dynamic testing was carried out just prior to opening the bridge in order to obtain the baseline dynamic characteristics of the bridge. Loaded trucks were run to excite dynamic responses from the bridge. The acceleration responses of 80 deck stations were recorded as trucks drove a high-speed pass and a slower bump-and-brake pass. The modal characteristics of the bridge are extracted from the peak picking of the average normalized power spectral densities (ANPSDs) in frequency domain. The dynamic test results will be used to calibrate the finite element model and then to establish the baseline finite element model that reflects the built-up structural conditions for the long-term structural evaluation, damage identification and health monitoring of the bridge.

2.2. Output-Only Dynamic Testing

Just prior to opening the bridge, loaded trucks were run to excite dynamic responses from the bridge and the cables. Two loaded truck cases were used. The high-speed test is the case where two loaded trucks, weighing 64,010 and 60,750 lbs drove a fast pass. The bump-and-brake test case used the 64,010 lbs truck in a slower bump-and-brake pass method. The objective of the bump-and-brake test is to give the bridge more excitation.

The equipment used to measure the acceleration-time responses of instrumentation consisted of triaxial accelerometers linked to its own data acquisition system. The system contained a Keithly MetraByte 1800HC digital recording strong motion accelerograph. Two units contained internal accelerometers, while the two remaining units were connected to Columbia Research Labs, SA-107 force balance accelerometers. The accelerometers are capable of measuring accelerations up to 2g's at frequencies up to DC-50Hz. The data was stored in a personal computer for further processing.

Sets of three accelerometers were mounted to aluminum blocks in orthogonal directions to form a triaxial accelerometer station. A block was positioned at each station with the accelerometers oriented in the vertical, transverse and longitudinal directions. To prevent any shifting of the accelerometers during testing, 25-pound bags of lead shot were laid on top of the accelerometer blocks once in position. To ensure the blocks were placed in level, adjustable feet and carpenters level were attached to each block. Accelerometers were connected to the data acquisition system by shielded cables.

Measurement stations were chosen to be between two cable planes. Instruments were placed on the pavement due to the limited access to the actual floor beams. As a result, a total of 80 locations (40 points per side) were measured. A view on the measurement instrumentations is shown in Figure 2.1. Twenty test setups are conceived to cover the planned testing area of the cable-stayed span of the bridge. A reference location, hereinafter referred as the base station, is selected based on the mode shapes from the preliminary finite element model. Each setup is composed of three base triaxial accelerometer stations and four moveable triaxial accelerometer stations. Each setup yields a total of twelve sets of data from moveable stations and nine sets of base station data. Table 2.1 shows the distribution of the different stations (locations) per setup.

Testing began at the Maysville side and progressed to the Aberdeen side. In each test set up, response data were measured for both the high-speed test and bump-and-brake test. Once the data were collected in one set up, the four moveable stations were then relocated to the next positions while the base stations remained stationary. This sequence was repeated twenty times to get output-only measurements on all stations. The sampling frequency on site is chosen to be as high as 1,000 Hz to capture the short-time transient signals of the ambient vibration in full detail. The output-only measurement is simultaneously recorded for 90 seconds at all accelerometers, which results in a total of 90,000 data points per channel. The typical acceleration records at the location U20 (span center) are as shown in Figure 2.2 for both the high-speed and bump-and-brake tests.

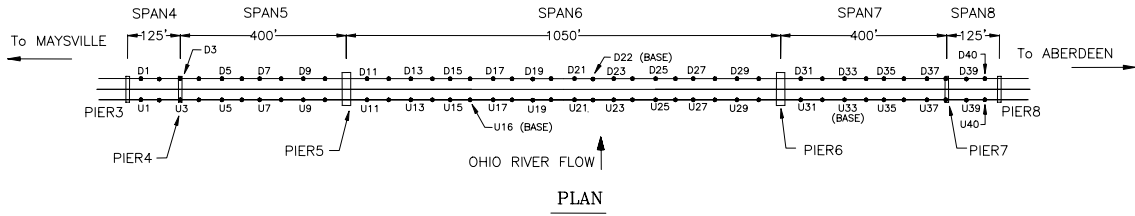
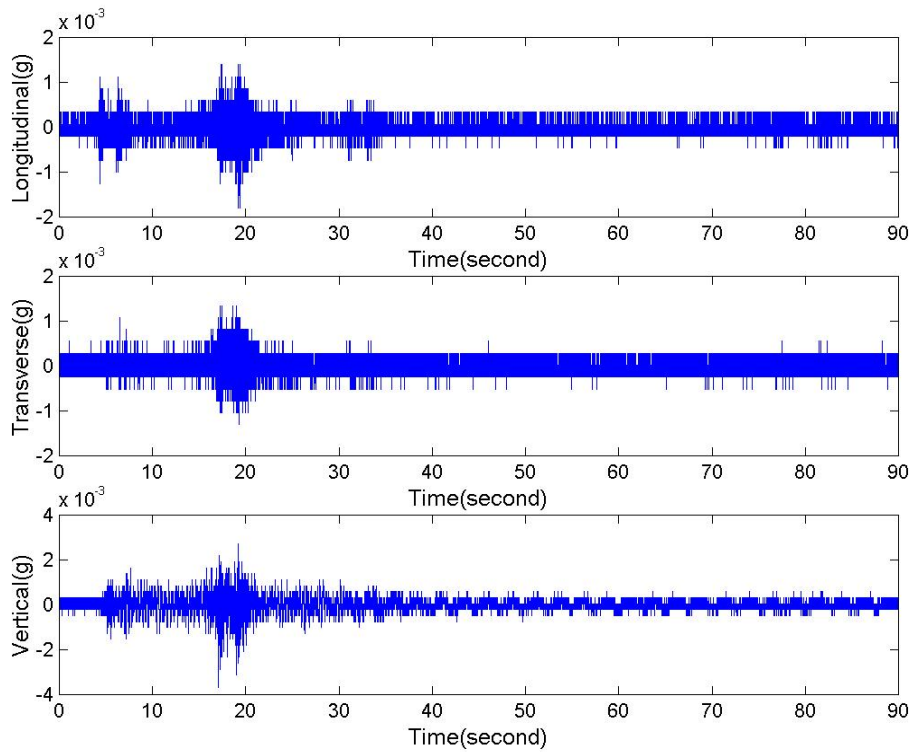
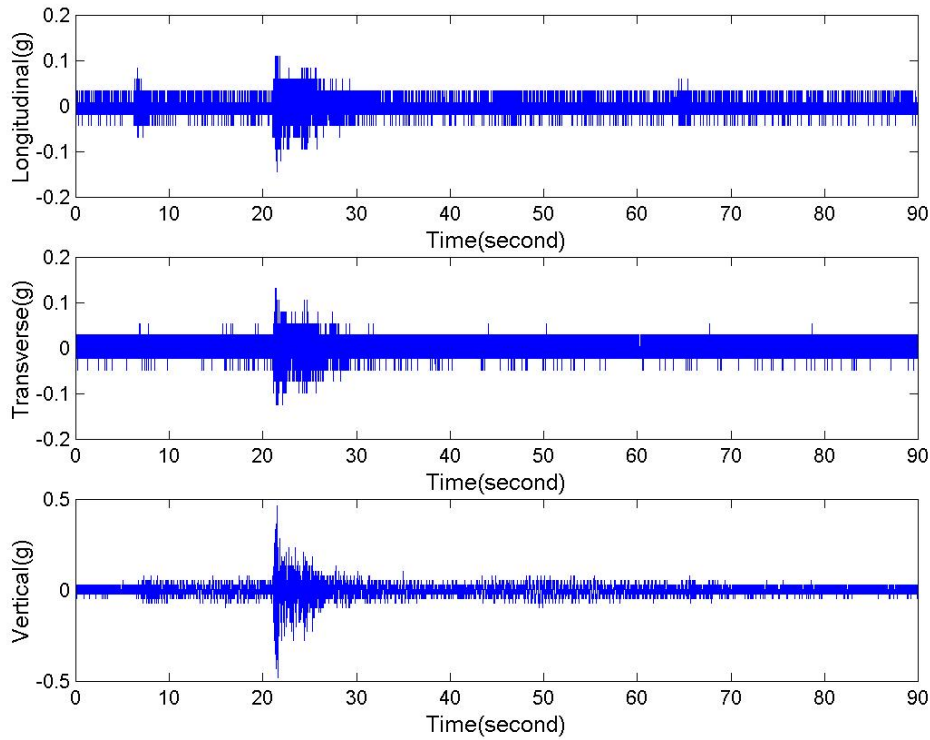


Figure 2.1 Measurement Instrumentation Plan



High-speed test



Bump-and-brake test

Figure 2.2 Typical Acceleration Time Histories at Location U20

Table 2.1 Instrumentation Per Setup

Setup	Points measured
1	D1, D2, U1, U2, U16, D22, U33
2	D3, D4, U3, U4, U16, D22, U33
3	D5, D6, U5, U6, U16, D22, U33
4	D7, D8, U7, U8, U16, D22, U33
5	D9, D10, U9, U10, U16, D22, U33
6	D11, D12, U11, U12, U16, D22, U33
7	D13, D14, U13, U14, U16, D22, U33
8	D15, D16, U15, U16, U16, D22, U33
9	D17, D18, U17, U18, U16, D22, U33
10	D19, D20, U19, U20, U16, D22, U33
11	D21, D22, U21, U22, U16, D22, U33
12	D23, D24, U23, U24, U16, D22, U33
13	D25, D26, U25, U26, U16, D22, U33
14	D27, D28, U27, U28, U16, D22, U33
15	D29, D30, U29, U30, U16, D22, U33
16	D31, D32, U31, U32, U16, D22, U33
17	D33, D34, U33, U34, U16, D22, U33

18	D35, D36, U35, U36, U16, D22, U33
19	D37, D38, U37, U38, U16, D22, U33
20	D39, D40, U39, U40, U16, D22, U33

U refers to upstream and D stands for downstream.

2.3. Peak Picking (PP) System Identification

The raw data from the output only testing displays a series of data that show the acceleration of the bridge in one of the three axial directions with respect to time, creating a time-history record of accelerations for the bridge. The raw data is not particularly useful for the dynamic analysis of the bridge and therefore must be transformed from the time domain into the frequency domain. The manner by which this was accomplished was the implementation of the Fourier Transform, which is mathematically defined using the transform equation:

$$F(\omega) = \int_{-\infty}^{\infty} f(t)e^{i\omega t} dt$$

where $f(t)$ is a function of time, $F(\omega)$ is amplitude as a function of frequency, and ω is circular frequency (radians per second). The inverse of the Fourier Transform is defined by the equation:

$$f(t) = \frac{1}{2\pi} \int_{-\infty}^{\infty} F(\omega)e^{-i\omega t} d\omega.$$

Using the equations above, any function that is a function of time can be converted into a function of frequency or vice versa. The only drawback associated with using these equations is that $f(t)$ must be a continuous function, which does not fit the description of the piecewise nature of digitally sampled data such as obtained in the bridge testing. For this reason, a different form of Fourier Transform must be used, known as the Discrete Fourier Transform (DFT), which is useful when data point values are known at regularly spaced intervals, which lends itself nicely to the problem at hand. The Discrete Fourier Transform is defined by the equation:

$$F_n = \sum_{k=0}^{N-1} f_k e^{2\pi i k n / N} \quad (n = 0, 1, \dots, N-1).$$

where N is the number of sampled points and f_k is a set of N sampled points. The inverse form of the Discrete Fourier Transform is given by the equation:

$$f_k = \frac{1}{N} \sum_{n=0}^{N-1} F_n e^{-2\pi i k n / N} \quad (k = 0, 1, \dots, N-1).$$

This set of equations is extremely useful for engineering applications such as this, but there are still some problems. These equations require N^2 complex mathematical operations which, even with modern computing power, can take quite some time even for small data sets. There is one other method that can reduce the computing time significantly.

The Fast Fourier Transform (FFT), a numerical operation, can exploit the periodic and symmetric nature of trigonometric functions to greatly improve efficiency in comparison to the Discrete Fourier Transform. The number of computations for the Fast Fourier Transform is reduced to $N \log_2(N)$, which is approximately 100 times faster than the Discrete Fourier Transform for a set of 1000 data points.

The peak picking method is initially based on the fact that the frequency response function (FRF) goes through an extreme around the natural frequencies. In the context of vibration measurements, only the FRF is replaced by the auto spectra of the output-only data. In this way the natural frequencies are simply determined from the observation of the peaks on the graphs of the average response spectra. The average response spectra are basically obtained by converting the measured accelerations to the frequency domain by a Discrete Fourier Transform (DFT). The coherence function computed for two simultaneously recorded output signals has values close to one at the natural frequency. This fact also helps to decide which frequencies can be considered as natural.

The peak picking algorithm, however, involves averaging temporal information, thus discarding most of their details. It has some theoretical drawbacks such as (1) picking the peaks is always a subjective task, (2) operational deflection shapes are obtained instead of mode shapes, (3) only real modes or proportionally damped structures

can be deduced by the method, and (4) damping estimates are unreliable. In spite of these drawbacks, this method is most often used in civil engineering practice for ambient vibration measurements because it is fast and easy to apply.

The data processing and modal identification are carried out by a piece of software known as DADiSP (Data Analysis and Display Software) version 2000 by DSP Development Corporation, Cambridge, Massachusetts, (DADiSP 2000). The time-history data was imported into the software. This software is useful for displaying, analyzing and manipulating large pieces of data, such as the 90,000+ points contained in each of the data files obtained. The software was also used to perform Fast Fourier Transforms on the imported data files.

After picking the peaks from the combined spectral plot, the magnitudes of the FFT spectra from the moveable stations were divided by the magnitudes of the FFT spectra from the base stations at each frequency to create a relative-magnitude plot for the bridge, relating the magnitudes at the moveable stations to those at the base station. The relative magnitudes for each point along the bridge were plotted at each of the picked-peak frequencies to determine the mode shapes of the bridges. The mode shapes predicted by the field data were then compared to a preliminary finite-element model for verification. This sequence was repeated for all records in each of the vertical, transverse, and longitudinal direction.

The average response spectra for all measurement data of the vertical, transverse and longitudinal directions are shown in Figures 2.3-2.8. The possible frequencies (peaks) of the vertical data, transverse data and longitudinal data are summarized in Tables 2.2 and 2.3 for the high-speed test and bump-and-brake test, respectively. It can be seen that the bump-and-brake test does not improve the identified results. It means that the ambient vibration measurements induced by normal traffics and natural winds are good enough to identify the modal parameters of a large cable-stayed bridge. Ambient vibration testing provides a convenient, fast and cheap way to perform the bridge dynamic testing.

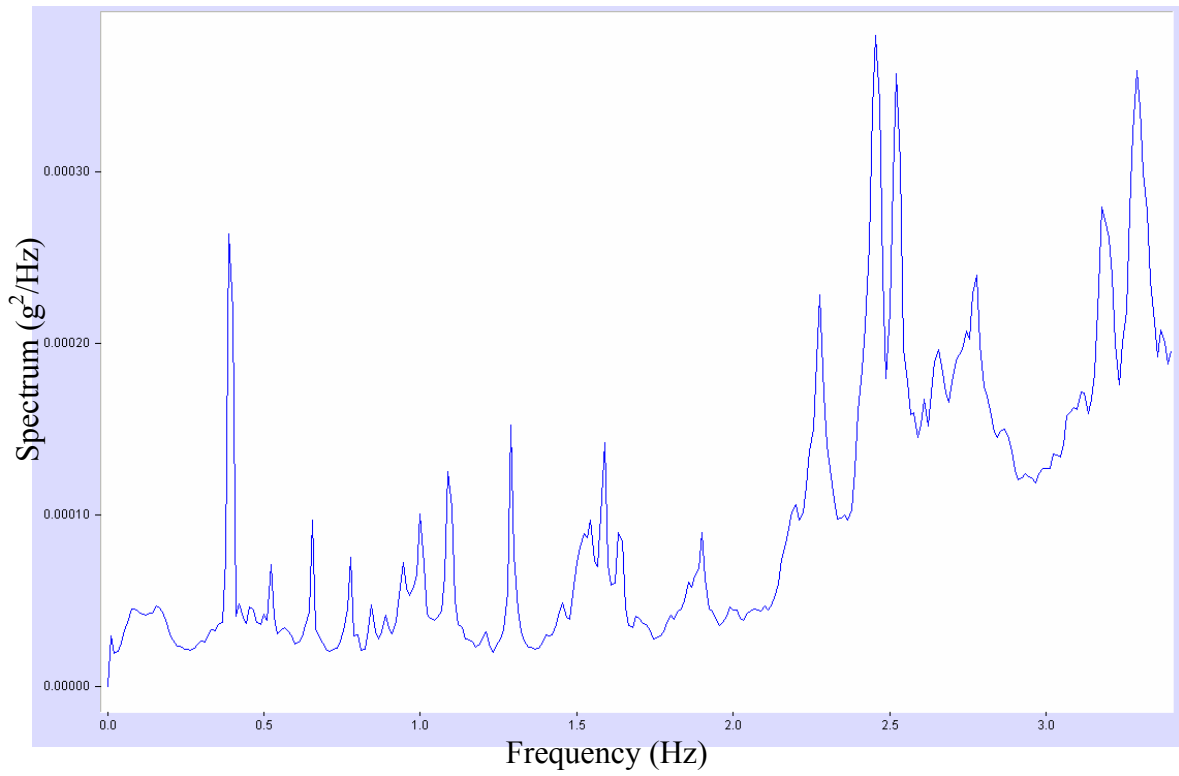


Figure 2.3 Full Data Averaged Vertical Response Spectra (High-speed Test)

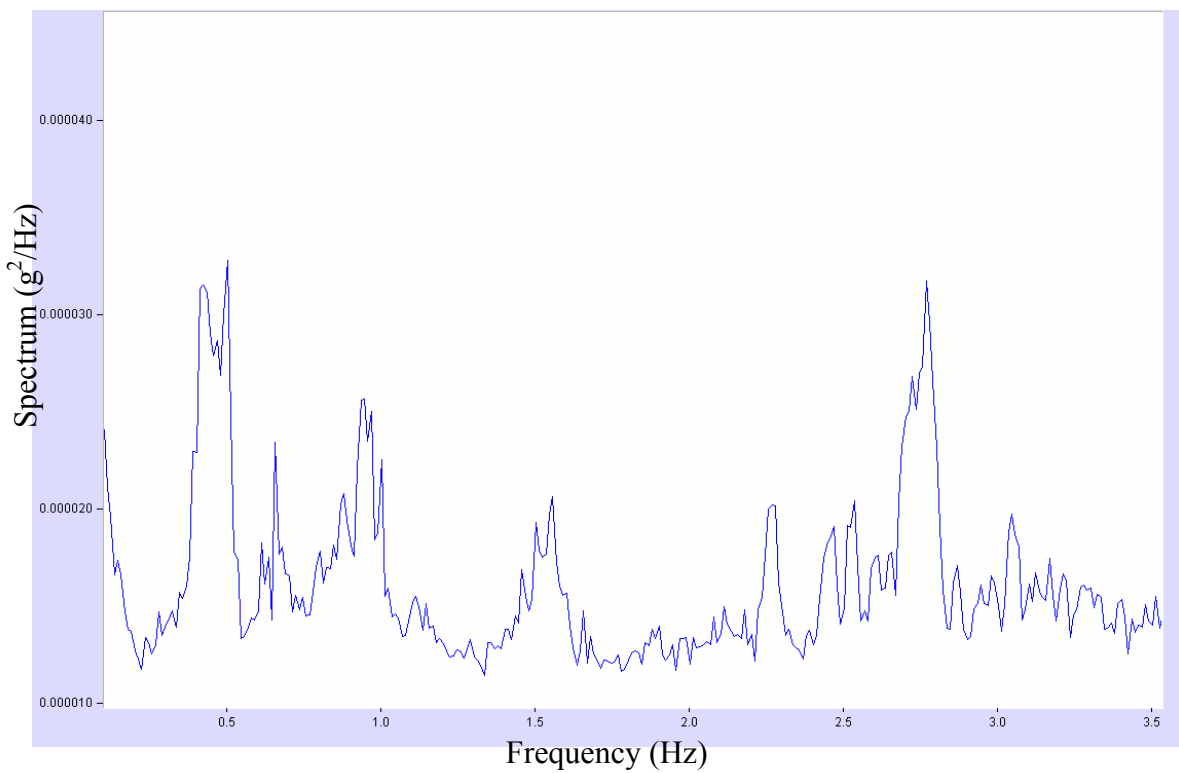


Figure 2.4 Full Data Averaged Transverse Response Spectra (High-speed Test)

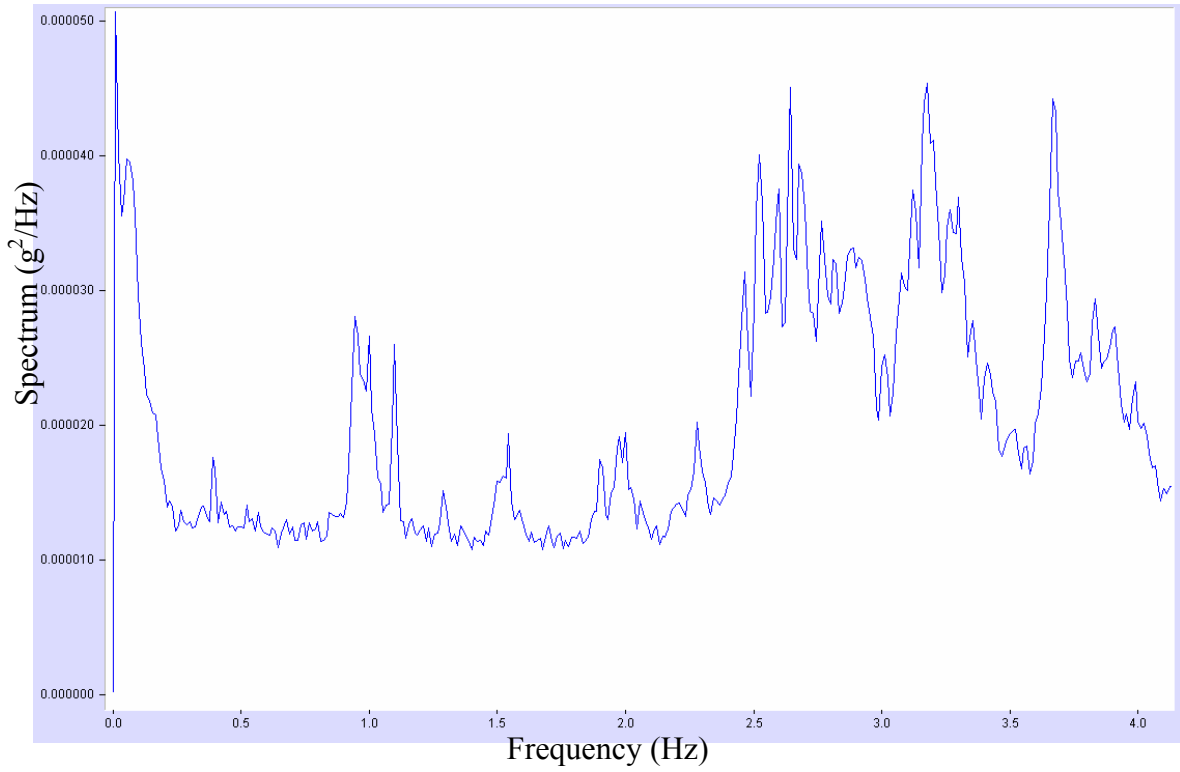


Figure 2.5 Full Data Averaged Longitudinal Response Spectra (High-speed Test)

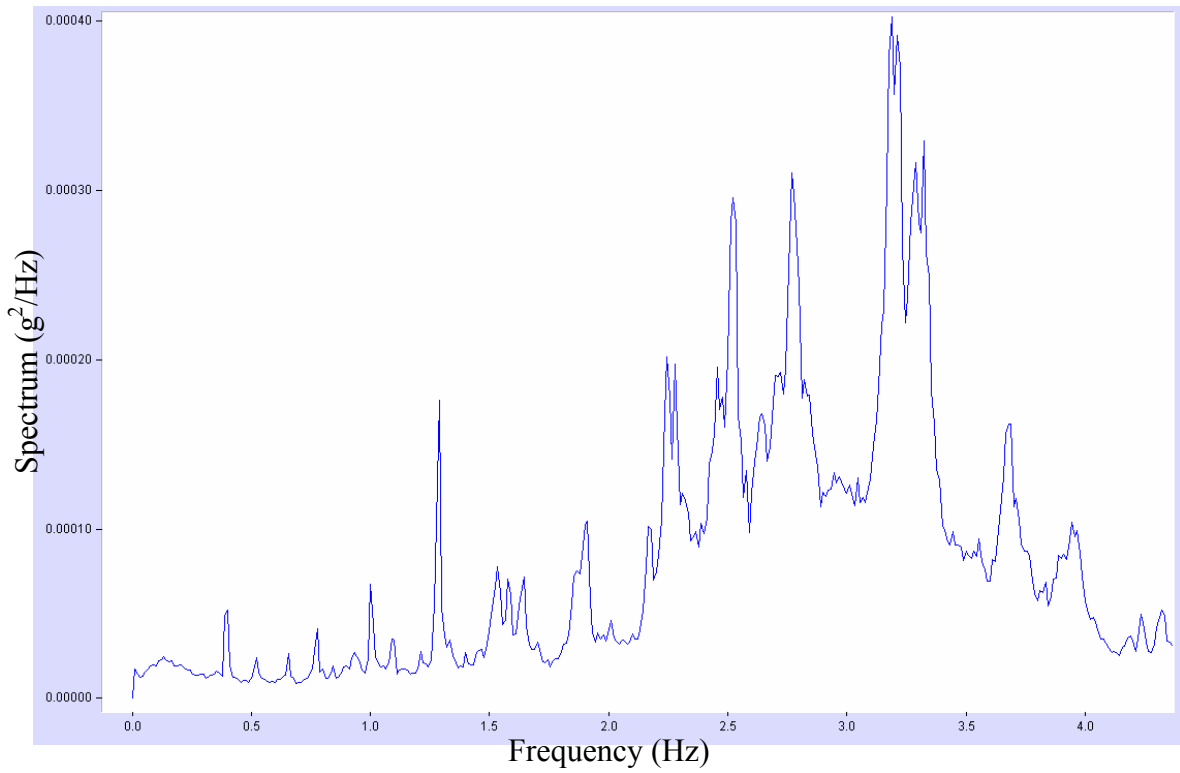


Figure 2.6 Full Data Averaged Vertical Response Spectra (Bump-and-brake Test)

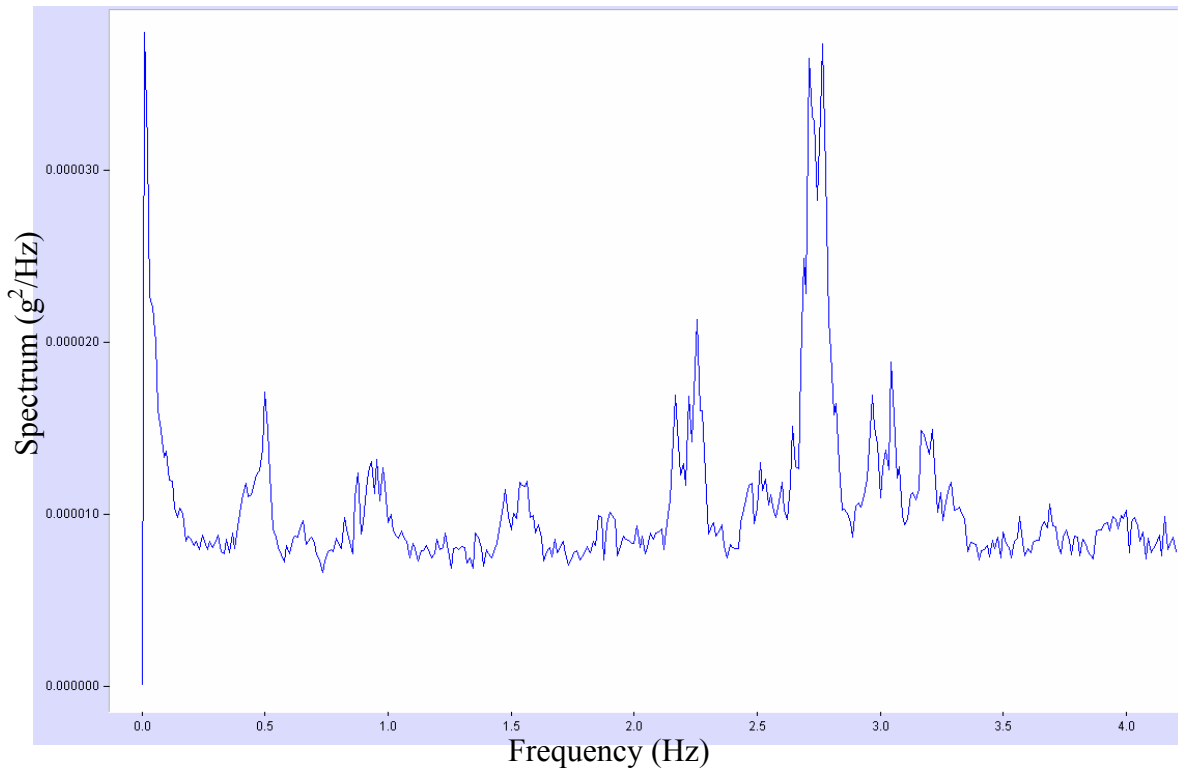


Figure 2.7 Full Data Averaged Transverse Response Spectra (Bump-and-brake Test)

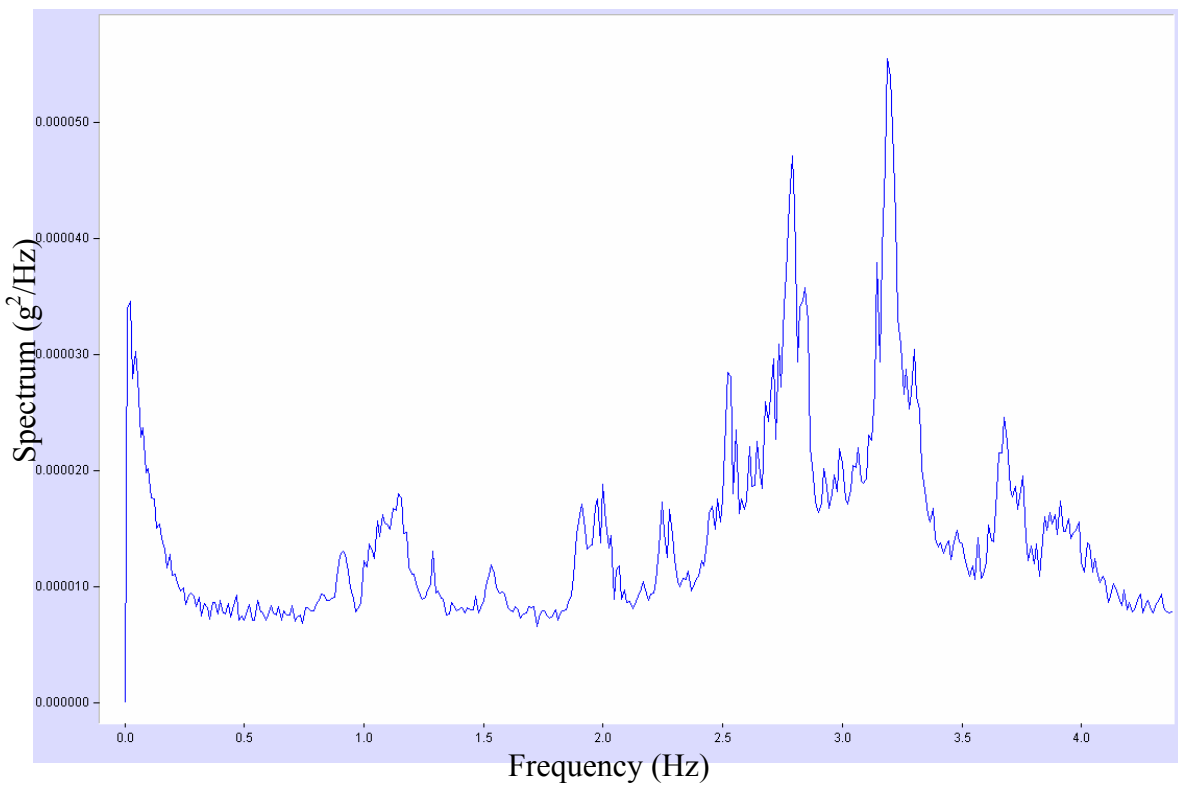


Figure 2.8 Full Data Averaged Longitudinal Response Spectra (Bump-and-brake Test)

Table 2.2 Possible Frequencies of High-speed Test (Hz)

Vertical	Transverse	Longitudinal
0.388889	0.5	0.388889
0.522222	0.655556	0.944444
0.655556	0.944444	1
0.777778	1.555556	1.1
0.844444	2.266667	1.288889
1	2.766667	1.544444
1.088889		1.9
1.288889		2.277778
1.588889		2.522222
1.9		2.644444
2.277778		2.777778
2.455556		
2.522222		
2.777778		

Table 2.3 Possible Frequencies of Bump-and-Brake Test (Hz)

Vertical	Transverse	Longitudinal
0.4	0.5	0.922222
0.522222	0.655556	1.144444
0.655556	0.955556	1.288889
0.777778	1.555556	1.544444
1	2.255556	1.911111
1.088889	2.766667	2.277778
1.288889		2.522222
1.577778		2.777778
1.911111		
2.244444		
2.277778		
2.522222		
2.766667		

The identified frequencies are summarized in Table 2.4 for both high-speed and bump-and-brake test. Good mode shapes have also been extracted by the peak picking system identification method. It has been demonstrated that the bump-and-brake test does not improve the system identification results. The identified the first vertical and the first transverse mode shapes are given in Figures 2.9 and 2.10, respectively.

Table 2.4 Summary of Identified Frequencies (Hz)

High-speed test	Bump-and-brake test	Mean value	Modes
0.3889	0.4	0.3945	First vertical
0.5	0.5	0.5	First transverse
0.5222	0.5222	0.5222	Second vertical
0.6556	0.6556	0.6556	Transverse + torsion
0.7778	0.7778	0.7778	Torsion
0.8444	-	0.8444	Third vertical
0.9444	0.9222	0.9333	First longitudinal
1	1	1	Fourth vertical

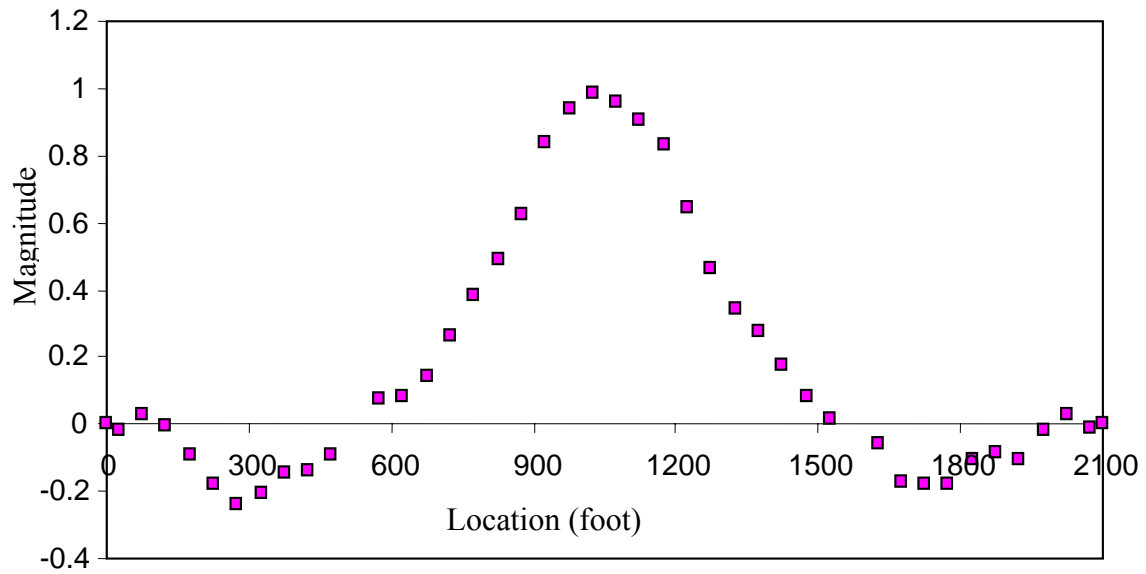


Figure 2.9 Identified First1 Vertical Mode Shape of Maysville Bridge
($f = 0.3889 \text{ Hz}$)

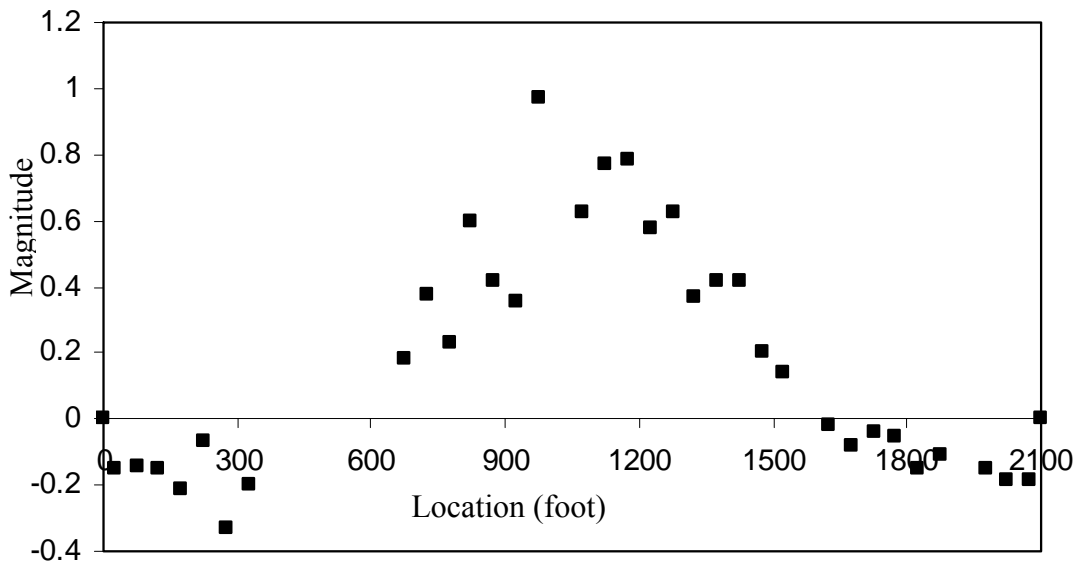


Figure 2.10 Identified First Transverse Mode Shape of Maysville Bridge
($f = 0.5 \text{ Hz}$)

2.4. Remarks

The following remarks can be made from the output-only dynamic testing of the Maysville cable-stayed bridge:

1. The modal parameters can be effectively extracted from output-only dynamic testing by using the frequency domain based peak picking (PP) method.
2. The peak picking identification is very fast and efficient since no model has to be fitted to the data. For real applications, the peak picking method could be used on site to verify the quality of the measurements.
3. The bump-and-brake test does not improve the identified results. It means that the ambient vibration measurements induced by normal traffics and natural winds are good enough to identify the modal parameters of a large cable-stayed bridge.

4. Ambient vibration testing provides a convenient, fast and cheap way to perform the bridge dynamic testing.

3. FINITE ELEMENT MODELING AND CALIBRATION

3.1. General

Modern cable-stayed bridges have been experiencing a revival since the mid-1950s, while the concept of supporting a bridge girder by inclined tension stays can be traced back to the seventh century (Podolny and Fleming 1972). The increasing popularity of contemporary cable-stayed bridges among bridge engineers can be attributed to: (1) the appealing aesthetics; (2) the full and efficient utilization of structural materials; (3) the increased stiffness over suspension bridges; (4) the efficient and fast mode of construction; and (5) the relatively small size of the bridge elements.

For the cable-stayed bridges, it was difficult to do accurate structural analysis. The commonly used classical theories for static analysis of cable-stayed bridges are the elastic theory and the deflection theory. The elastic theory is basically a linearized approximate theory, as it does not take into account the deformed configuration of the structure. Though the values of bending moment and shear yielded by the elastic theory are too high, it satisfies more safe design but not economy. This method is quite expeditious and convenient for preliminary designs and estimates. Basically, the elastic theory is sufficiently accurate for shorter spans or for designing relatively deep rigid stiffening systems that limit the deflections to small amounts. However, the elastic theory does not suite the designing of cable-stayed bridges with long spans, or large dead loads. The deflection theory, in contrast, is a more “exact” theory that takes into account the deformed configuration of the structure and results in a more economical and slender bridge.

Nowadays, it is no longer a problem to accurately predict both the static and dynamic structural behavior of cable-stayed bridges. The finite element method of structural continua provides a convenient and reliable idealization of the structure and is particularly effective in digital-computer analysis. The finite element type of idealization

is applicable to structures of all types. Thanks to rapid computer developments and the accumulation of matrix analysis studies on nonlinear problems. The finite deformation theory with a discrete finite element model has been the most powerful tool used in the nonlinear analysis of cable-supported bridges. The applications of the finite deformation theory can include the effect of all nonlinear sources of cable-stayed bridges such as cables, large deflections, axial force and bending moment interaction.

An important advantage of the finite element method is that structural complexities such as tower movements, cable extensibility, and support conditions, etc. can be considered effectively. The finite element method can also be used to analyze the effect of changes in different parameters, i.e., the parameter design. Two- or three-dimensional finite element models with beam and truss elements are often used to model both the superstructure and the substructure of cable-supported bridges (Nazmy and Abdel-Ghaffar 1990, Wilson and Gravelle 1991, Lall 1992, Ren 1999, Spyrakos et al. 1999). Another advantage of the finite element method lies in its capability to do in-depth dynamic analysis. The dynamic characteristics of cable-supported bridges have been of particular interest since the collapse of the Tacoma Narrows Bridge in the State of Washington on November 7, 1940, as a result of wind action. Parametric studies on natural frequencies and modes (West et al. 1984) using a finite element formulation demonstrate the variation of the modal parameters of stiffened cable-supported bridges. The finite element method has been a unique way to do the dynamic response analysis of cable-supported bridges under the loadings of winds, traffics and earthquakes (Boonyapinyo et al. 1999, Abdel-Ghaffar and Rubin 1983, Abdel-Ghaffar and Nazmy 1991, Ren and Obata 1999).

This chapter describes the structural evaluation effort for the Maysville cable-stayed bridge by using finite element method. Details of a three-dimensional finite element model are presented. The analytical model of the Maysville cable-stayed bridge is constructed in ANSYS, which is one of the most powerful engineering design and analysis software (ANSYS 5.7). The ANSYS is chosen because of the program's significant capability to account for the cable stress stiffening and the pre-stressed modal

analysis capability. This model will be used for both static and dynamic analyses of the Maysville cable-stayed bridge.

In the finite element analysis, the influence of the dead load is considered by the static analysis under dead loads prior to application of the live loads or a dynamic analysis is carried out. The objective of the static analysis process is to achieve the deformed equilibrium configuration of the bridge under dead loads where the structural members are “pre-stressed”. A cable-stayed bridge is indeed a highly pre-stressed structure. Starting from the deformed equilibrium configuration, the modal analysis is followed. Consequently, the dead load effect on the stiffness can be included in the modal analysis; thereby, the modal analysis will be a “pre-stressed” modal analysis.

Hence, the modal analysis of a cable-stayed bridge must include two steps: static analysis due to dead load and “pre-stressed” modal analysis. For a completed cable-stayed bridge, the initial position of the cable and bridge is unknown. Only the final geometry of the bridge due to the dead load can be known by referring to the bridge plan. The initial geometry of the ideal finite element model of a cable-stayed bridge should be such that the geometry of a bridge does not change when a dead load is applied, since this is indeed the final geometry of the bridge as it stands. In other words, the deformed configuration of the bridge under the self-weight dead load should be close to the initial geometry input. In addition, the geometric nonlinear effect has been studied by including the stress stiffening and large deflection. All possible frequencies and mode shapes can be provided performing the pre-stressed modal analysis. A coupled mode can be included to give a comprehensive understanding of the dynamic behavior of the cable-stayed bridges. Finite element (FE) model calibration, i.e., parametric studies, is also performed. The parameters include self-weight of the deck, the stiffness of cables, and bending stiffness of edge girders and sub-stringers. The results of the modal analysis will be compared later with *in-situ* free vibration measurements to calibrate or update the initial finite element model.

3.2. Initial Finite Element Model

Since modern cable-stayed bridges involve a variety of decks, towers and cables that are connected together in different ways, the finite element method (FEM) is generally regarded as the most proper way for conducting the dynamic analysis. In FEM connection, the single-girder beam element model, the double-girder beam element model, the triple-girder beam element model, the shell element model and the thin-walled element model have been developed to model the bridge deck (Yang and McGuire 1986a, Yang and McGuire 1986b, Boonyapinyo et al.1994, Wilson and Gravelle 1991 and Zhu et al. 2000). Referring to Zhu et al.'s work, we choose the triple-girder beam element model to model the bridge deck.

3.2.1. Primary Assumption

A completely three-dimensional finite element model was established by using the finite element analysis software ANSYS version 5.7. The software ANSYS was able to account for the cable stress stiffening and the pre-stressed modal analysis. This model would be used for static and dynamic analyses of the Maysville cable-stayed bridge. Due to the complexity and variations of such a cable-stayed bridge, there are too many uncertainties in both geometry and material. Some primary assumptions are made in establishing the initial finite element model of the Maysville cable-stayed bridge:

- Towers: Only eight section properties are assumed for the lower tower leg, although the tower lower leg is actually variable sections along its height.
- Edge girders: Assumed that two edge girders are completely continuous, although they are composed of eleven different section properties.

3.2.2. The Geometry of the Bridge

After selecting an appropriate modeling methodology, serious considerations must be given to proper representation of the bridge geometry. These geometric issues

are directly related to the structural behavior. The consideration must include not only the global geometry of the bridge, but also local geometric characteristics of individual bridge members. The geometry and member details are extracted from the plan of the Maysville cable-stayed bridge. The plan referred is Kentucky Department of Highways, Ohio Department of Transportation; Mason County, Kentucky – Brown County, Ohio; U.S. 62 & 68 over the Ohio River; Maysville, Kentucky to Aberdeen, Ohio prepared by the American Consulting Engineers, P.L.C. (1996). The drawing number is 23172. Table 3.1 shows the member details extracted from the plan.

Table 3.1 Member Details Extracted from the Plan

Member	Reference
Towers	Sheets C11-C35
Piers 4 & 7	Sheets C9, C10, C36 and C37
Cables	Sheets D70-D73
Edge Girders	Sheets C1, D1-D35, D38-D40
Sub-stringers	Sheets D1-D23, D45
Baffles	Sheets D8-D16, D45
Floor beams	Sheets D1-D23, D41-D44
Wind lock struts	Sheets D1, D2, D22, D23, D51-D53
Decks	Sheets D36, D37, D81-D90

3.2.3. Element Types

A cable-stayed bridge is a complex structural system. Each member of the bridge plays a different role. Different element types are therefore needed. In this FE model, three types of elements were chosen for modeling the different structural members. They are the 3-D elastic beam element (BEAM4), 3-D tension-only truss element (LINK10), and 3-D structural solid element (SOLID45). The theoretical background of each type of elements is briefly described below.

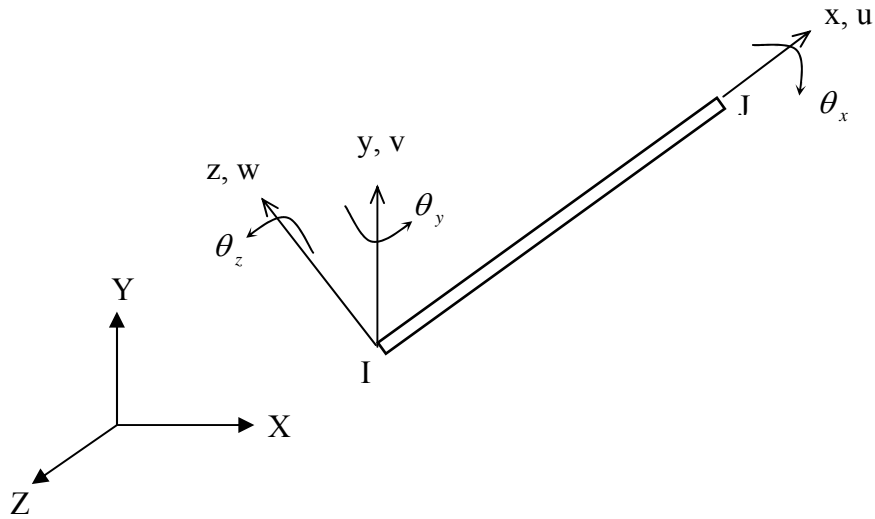


Figure 3.1 BEAM4 3-D Elastic Beam Element

3.2.3.2. LINK10 Element

LINK10 element is a uniaxial 3-D elastic truss element with tension-only (or compression-only) capability. With the tension-only option used here, the stiffness is removed if the element goes into compression (simulating a slack cable or slack chain condition). The feature is unique to model the cables of the Maysville cable-stayed bridge. The element has three degrees of freedom at each node: translations in x, y and z directions of the nodal. No bending of the element is considered. LINK10 3-D truss element is defined by the cross-sectional area, initial strain and material property of two nodes. The geometry, node locations and the coordinate system for this element are shown in Figure 3.2.

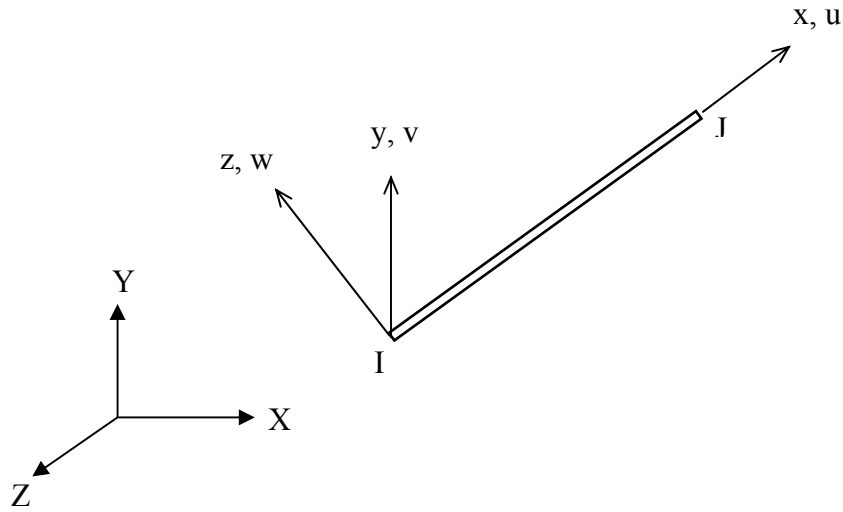


Figure 3.2 3-D Tension-only Truss Element

The stiffness matrix of tension-only truss element in the local coordinate system is

$$[k_l] = \frac{AE}{L} \begin{bmatrix} C_1 & 0 & 0 & -C_1 & 0 & 0 \\ 0 & 0 & 0 & 0 & 0 & 0 \\ 0 & 0 & 0 & 0 & 0 & 0 \\ -C_1 & 0 & 0 & C_1 & 0 & 0 \\ 0 & 0 & 0 & 0 & 0 & 0 \\ 0 & 0 & 0 & 0 & 0 & 0 \end{bmatrix}$$

where

A = element cross-sectional area

E = Young's modulus

L = element length

$C_1 = 1.0$ when tension; 1.0×10^6 when compression.

The consistent mass matrix of LINK10 element in the local coordinate system is

$$[m_i] = \frac{\rho AL(1 - \varepsilon^{in})}{6} \begin{bmatrix} 2 & 0 & 0 & 1 & 0 & 0 \\ 0 & 2 & 0 & 0 & 1 & 0 \\ 0 & 0 & 2 & 0 & 0 & 1 \\ 1 & 0 & 0 & 2 & 0 & 0 \\ 0 & 1 & 0 & 1 & 2 & 0 \\ 0 & 0 & 1 & 0 & 0 & 2 \end{bmatrix}$$

where

ρ = mass density

ε^{in} = initial strain (as an input)

An important input property of the LINK10 elements that are aimed at modeling cable behavior is the initial strain. The initial strain is used for calculating the stress stiffness matrix for the first cumulative iteration. Stress stiffening should always be used for cable problems to provide numerical stability. The initial strain in the element is given by δ / L , where δ is the difference between the element length L and the zero strain length L_0 .

3.2.3.3. SOLID45 Element

SOLID45 element is a 3-D structural solid element having membrane stiffness. It is intended for any solid structures. The element has three degrees of freedom at each node: translations in the nodal x, y, and z directions. SOLID45 3-D structural solid element is defined by eight nodes and material properties. The geometry, node locations, and the coordinate system for 3-D 8-node brick solid element are shown in Figure 3.3. The implicit expressions of shape function, stiffness matrix and mass matrix can be found in the standard book of finite element method (Bathe 1982, etc.).

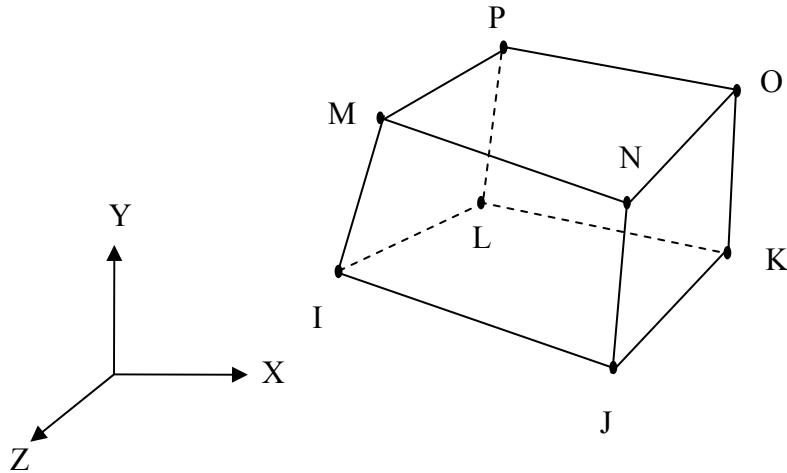


Figure 3.3 3-D structural solid element

3.2.4. Material Properties and Real Constants

The basic materials used in the Maysville cable-stayed bridge are the structural steel, concrete and high strength steel. The preliminary material constants used in the finite element model are shown in Table 3.2; furthermore, they follow the typical values of ASMT standards.

Table 3.2 Preliminary Material Properties

Group No.	Young's modulus (lb/ft ²)	Poisson's ratio	Mass density (lb/ft ³)	Structural member
1	4.176×10^9	0.3	490	Edge girders, Floor beams, Sub-stringers, Baffles
2	4.176×10^9	0.3	490	Edge girders
3	4.176×10^9	0.3	490	Cables
4	6.087×10^8	0.2	150	Tower columns & struts
5	4.856×10^8	0.2	150	Tower footing & stem
6	5.191×10^8	0.2	150	Piers 4 & 7
7	6.867×10^8	0.2	150	Decks

The real constants consist of all necessary geometric properties of the cross-section and initial strain if necessary. Depending on the element type, different real constants are considered as the input. All preliminary real constants used in the current

model are summarized in Table 3.3. Real constants are based on the following facts of the main structural members.

Edge Girder

The edge girders are of the continuous type with an expansion bearing at each end, two fixed bearings at each tower, and two tie-down linkages at each pier. Each edge girder consists of type I beams of eleven different cross-sections. There are floor beams and wind-locks between two edge girders.

Cables

The cables are composed of 31 - 55 strands of high strength steel wire, each strand being 0.6 inches in diameter. These strands are parallel to each other, which are surrounded by PE pipe forming a single cable. The initial strains are obtained from the axial force of the bridge plans.

Towers

The towers are composed of upper legs, middle legs, lower legs, upper strut, lower strut, stem and footing. The tower lower strut is connected with the edge girders by two fixed bearings.

Piers

Each pier is composed of two columns and a top strut. The pier top strut is connected with the edge girders by two tie-down linkages.

Floor Beams and Sub-stringers

In the cable-stayed spans, the reinforced concrete grid decks are supported by the frames which are composed of edge girders, floor beams and sub-stringers. The floor beams are the type I structures with variable cross-sections. The sub-stringer is a standard type I cross-sectional beam (W18×76).

Table 3.3 Preliminary Real Constants

Type	Cross-section Area: (ft ²)	Inertia moment: (ft ⁴)		Initial strain	Structural member
		I _{zz}	I _{yy}		
1	1.375	8.4503	0.098706	-	Edge girder
2	1.1875	8.16068	0.132278	-	Edge girder
3	1.59375	10.4443	0.259513	-	Edge girder
4	1.01389	3.81433	0.190475	-	Edge girder
5	0.90972	3.5355	0.190245	-	Edge girder
6	1.08681	4.07368	0.223557	-	Edge girder
7	1.11111	4.15438	0.234585	-	Edge girder
8	1.04167	3.90729	0.231048	-	Edge girder
9	1.09722	4.0791	0.329942	-	Edge girder
10	1.30556	4.64581	0.3307634	-	Edge girder
11	1.22222	8.41951	0.190663	-	Edge girder
12	0.65174	0.152822	1.901718	-	Floor beam
13	0.90139	0.152922	7.800261	-	Floor beam
14	0.65924	0.152823	2.056549	-	Floor beam
15	0.64431	0.15282	1.754162	-	Floor beam
16	0.15486	0.06414	0.00733	-	Sub-stringer
17	0.11722	0.217014	0.00011	-	Baffle
18	0.8125	0.152893	4.777927	-	Wind-lock
19	171	1154.25	5144.25	-	Tower (upper & middle)
20	182.875	1760.865	5501.4896	-	Tower (lower)
21	206.625	2974.094	6215.97	-	Tower (lower)
22	230.375	4187.32	6930.45	-	Tower (lower)
23	254.125	5400.55	7644.93	-	Tower (lower)
24	277.875	6613.78	8359.41	-	Tower (lower)
25	301.625	7827.01	9073.89	-	Tower (lower)
26	325.375	9040.24	9788.36	-	Tower (lower)
27	349.125	10253.47	10502.84	-	Tower (lower)
28	96	1152	512	-	Tower (upper strut)
29	96	2048	288	-	Tower (lower strut)
30	44.18	155.32	155.32	-	Piers 4 & 7

31	56.25	263.67	263.67	-	Piers 4 & 7
32	0.107986	-	-	2.4994E-03	Cables 1 & 40
33	0.107986	-	-	2.3801E-03	Cables 2 & 39
34	0.107986	-	-	2.0588E-03	Cables 3 & 38
35	0.0844444	-	-	2.7425E-03	Cables 4 & 37
36	0.0844444	-	-	1.8055E-03	Cables 5 & 36
37	0.0844444	-	-	1.9745E-03	Cables 6 & 35
38	0.060868	-	-	2.2645E-03	Cables 7 & 34
39	0.060868	-	-	2.7142E-03	Cables 8 & 33
40	0.060868	-	-	1.8101E-03	Cables 9 & 32
41	0.060868	-	-	2.2299E-03	Cables 10 & 31
42	0.060868	-	-	2.2503E-03	Cables 11 & 30
43	0.060868	-	-	2.1284E-03	Cables 12 & 29
44	0.060868	-	-	2.1988E-03	Cables 13 & 28
45	0.060868	-	-	2.3176E-03	Cables 14 & 27
46	0.0844444	-	-	2.05E-03	Cables 15 & 26
47	0.0844444	-	-	2.221E-03	Cables 16 & 25
48	0.0844444	-	-	2.4733E-03	Cables 17 & 24
49	0.107986	-	-	2.3295E-03	Cables 18 & 23
50	0.107986	-	-	2.3907E-03	Cables 19 & 22
51	0.107986	-	-	2.4428E-03	Cables 20 & 21

3.2.5. Details of the Model

A detailed 3-D finite element model of the bridge is developed. This model was used for both the static and dynamic analysis of the bridge. The main structural members of the Maysville cable-stayed bridge are the edge girders, cables, floor beams, sub-stringers, decks and towers that are discretized by different finite elements. The finite elements used for modeling the bridge are described below.

Modeling of the cable is possible in the ANSYS by employing the tension-only truss elements and utilizing its stress stiffening capability. The element is nonlinear and requires an iteration solution. All cable members of the Maysville cable-stayed bridge are designed to sustain the tension force only and hence modeled by 3-D tension-only truss elements (LINK10) but the section properties are different. Each cable between the edge girder and the tower are modeled as a single finite element. The stiffness is removed with this element if the element goes into compression. Both stress stiffening and large

displacement capability are available. The stress stiffening capability is needed for analysis of structures with a low or non-existing bending stiffness as is the case with cables. Hence, an important feature input for this element is the initial strain in the element. This initial strain is used in calculating the stress stiffness matrix for the first cumulative iteration. In the model, initial strains are the final stay tension that is from the part 4 in this report.

The columns and struts of the towers are modeled as 3-D elastic beam elements (BEAM4), whereas the stem and footing of the towers are modeled as 8-node brick membrane solid elements (SOLID45). Large deflection capability of 3-D elastic beam elements and 8-node brick solid elements is available.

The edge girders and sub-stringers are modeled as 3-D elastic beam elements (BEAM4) because of their continuous nature across many panels. The piers, floor beams and baffles are also modeled as 3-D elastic beam elements (BEAM4) to provide tension, compression, bending and torsion stiffness.

The aforementioned bridge deck is presented with a triple-girder model. In the triple-girder model, a central girder, i.e. the sub-stringer, is located at the centroid of the original bridge deck. Two side girders, i.e., the edge girders, of the same section properties are symmetrically located at the corresponding cable planes. The decks may be distributed over these three girders in the model. For the triple-girder model, we may obtain the equivalent mass and stiffness of the central girder and two side girders by referring to Zhu et al.'s work (2000). In the triple-girder model, the transverse connection between the central girder and the side girder is generally simplified as the rigid link. In the current model, the stiffness of the floor beam and the wind-lock may be properly raised by increasing the elastic modulus.

In addition, the fixed bearings and tie-down linkages that connect the edge girders and towers and piers, are modeled as 3-D elastic beam elements (BEAM4) with larger bending stiffness. For the purpose of latter parametric study and model calibration

through *in-situ* dynamic testing, all material properties and real constants that reflect effectively the properties of individual structural members are listed in Tables 3.4 and 3.5, respectively. The initial strains in Table 3.5 are obtained by considering the initial tension forces in the cables listed in Table 3.7.

Table 3.4 Material Properties

Group No.	Young's modulus (lb/ft ²)	Poisson's ratio	Mass density (lb/ft ³)	Structural member
1	4.176×10^9	0.3	953.1	Edge girders
2	4.176×10^9	0.3	973.77	Edge girders
3	4.176×10^9	0.3	932.12	Edge girders
4	4.176×10^9	0.3	995.67	Edge girders
5	4.176×10^9	0.3	1010.33	Edge girders
6	4.176×10^9	0.3	986.11	Edge girders
7	4.176×10^9	0.3	983.04	Edge girders
8	4.176×10^9	0.3	991.96	Edge girders
9	4.176×10^9	0.3	984.79	Edge girders
10	4.176×10^9	0.3	960.42	Edge girders
11	4.176×10^9	0.3	969.72	Edge girders
12	4.176×10^9	0.3	1210.55	Sub-stringer
13	4.176×10^9	0.3	490	Cables
14	4.176×10^9	0.3	490	Baffles
15	4.176×10^{12}	0.3	1	Floor beams & Wind lock
16	6.087×10^8	0.2	150	Tower columns & struts
17	4.856×10^8	0.2	150	Tower footing & stem
18	5.191×10^8	0.2	150	Piers 4 & 7
19	4.176×10^{11}	0.3	10	Tie-down linkages
20	4.176×10^{10}	0.3	10	Fixed bearings

Table 3.5 Real Constants

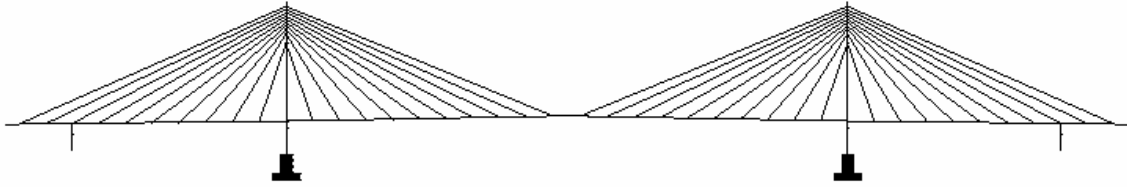
Type	Cross-section Area: (ft ²)	Inertia moment: (ft ⁴)		Initial strain	Structural member
		I _{zz}	I _{yy}		
1	2.875	9.4503	0.0987	-	Edge girder
2	2.6875	9.161	0.1323	-	Edge girder
3	3.094	11.44	0.2595	-	Edge girder
4	2.514	4.8143	0.1905	-	Edge girder
5	2.4097	4.5355	0.1903	-	Edge girder
6	2.587	5.074	0.2236	-	Edge girder
7	2.6111	5.1544	0.2346	-	Edge girder
8	2.542	4.9073	0.2311	-	Edge girder
9	2.5972	5.0791	0.3299	-	Edge girder
10	2.8056	5.6458	0.3308	-	Edge girder
11	2.7222	9.4195	0.1907	-	Edge girder
12	0.6517	0.01528	0.01902	-	Floor beam
13	0.9014	0.01529	0.01801	-	Floor beam
14	0.6592	0.01528	0.01056	-	Floor beam
15	0.6443	0.01528	0.01754	-	Floor beam
16	6.1549	24.0641	2572	-	Sub-stringer
17	0.1172	0.217	0.00011	-	Baffle
18	0.8125	0.01529	0.01778	-	Wind-lock
19	87	902.25	3772.25	-	Tower (upper & middle)
20	182.88	1760.87	5501.49	-	Tower (lower)
21	206.63	2974.09	6215.97	-	Tower (lower)
22	230.38	4187.32	6930.45	-	Tower (lower)
23	254.13	5400.55	7644.93	-	Tower (lower)
24	277.88	6613.78	8359.41	-	Tower (lower)
25	301.63	7827.01	9073.89	-	Tower (lower)
26	325.38	9040.24	9788.36	-	Tower (lower)
27	349.13	10253.47	10502.84	-	Tower (lower)
28	36	652	332	-	Tower (upper strut)
29	40	1133.33	213.33	-	Tower (lower strut)
30	44.18	155.32	155.32	-	Piers 4& 7
31	56.25	263.67	263.67	-	Piers 4& 7
32	0.107986	-	-	2.1262E-03	Cables 1 & 41
33	0.107986	-	-	1.8326E-03	Cables 2 & 42
34	0.107986	-	-	1.6459E-03	Cables 3 & 43
35	0.0844444	-	-	2.0857E-03	Cables 4 & 44
36	0.0844444	-	-	1.7162E-03	Cables 5 & 45
37	0.0844444	-	-	1.6586E-03	Cables 6 & 46
38	0.060868	-	-	2.1422E-03	Cables 7 & 47
39	0.060868	-	-	2.0084E-03	Cables 8 & 48

40	0.060868	-	-	1.6019E-03	Cables 9 & 49
41	0.060868	-	-	1.7491E-03	Cables 10 & 50
42	0.060868	-	-	1.2892E-03	Cables 11 & 51
43	0.060868	-	-	1.7298E-03	Cables 12 & 52
44	0.060868	-	-	1.5544E-03	Cables 13 & 53
45	0.060868	-	-	1.9069E-03	Cables 14 & 54
46	0.0844444	-	-	1.6722E-03	Cables 15 & 55
47	0.0844444	-	-	1.7613E-03	Cables 16 & 56
48	0.0844444	-	-	1.8118E-03	Cables 17 & 57
49	0.107986	-	-	1.7829E-03	Cables 18 & 58
50	0.107986	-	-	1.6813E-03	Cables 19 & 59
51	0.107986	-	-	2.1393E-03	Cables 20 & 60
52	0.107986	-	-	2.1674E-03	Cables 21 & 61
53	0.107986	-	-	1.6563E-03	Cables 22 & 62
54	0.107986	-	-	1.8539E-03	Cables 23 & 63
55	0.0844444	-	-	1.9873E-03	Cables 24 & 64
56	0.0844444	-	-	1.8475E-03	Cables 25 & 65
57	0.0844444	-	-	1.7891E-03	Cables 26 & 66
58	0.060868	-	-	2.1052E-03	Cables 27 & 67
59	0.060868	-	-	1.7566E-03	Cables 28 & 68
60	0.060868	-	-	1.2943E-03	Cables 29 & 69
61	0.060868	-	-	1.7255E-03	Cables 30 & 70
62	0.060868	-	-	1.9745E-03	Cables 31 & 71
63	0.060868	-	-	1.3029E-03	Cables 32 & 72
64	0.060868	-	-	1.8542E-03	Cables 33 & 73
65	0.060868	-	-	1.8609E-03	Cables 34 & 74
66	0.0844444	-	-	1.7777E-03	Cables 35 & 75
67	0.0844444	-	-	1.7752E-03	Cables 36 & 76
68	0.0844444	-	-	2.0219E-03	Cables 37 & 77
69	0.107986	-	-	1.7405E-03	Cables 38 & 78
70	0.107986	-	-	1.6893E-03	Cables 39 & 79
71	0.107986	-	-	2.1729E-03	Cables 40 & 80
72	1.0	0.1	0.1	-	Tie-down linkages
73	5.5	2.47	2.47	-	Fixed bearings

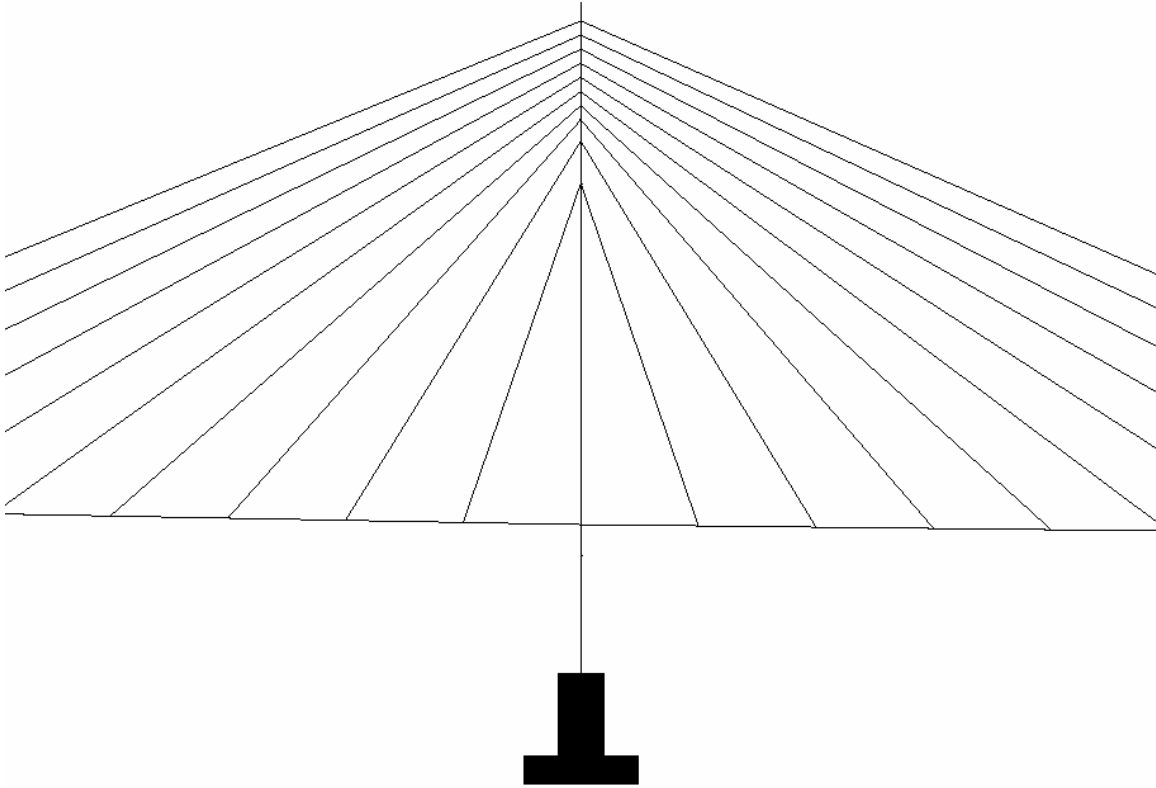
The finite element model of the Maysville cable-stayed bridge totally consists of 994 nodes and 1321 finite elements that include 1161 BEAM4 elements, 80 LINK10 elements and 80 SOLID45 elements. As a result, the number of active degree of freedom (DOF) is 5168. The details of the model such as element types, material types and real constant types are summarized in Table 3.6 for individual structural members. The detailed 3-D finite element models are shown in Figures 3.4-3.6.

Table 3.6 Details of the Model

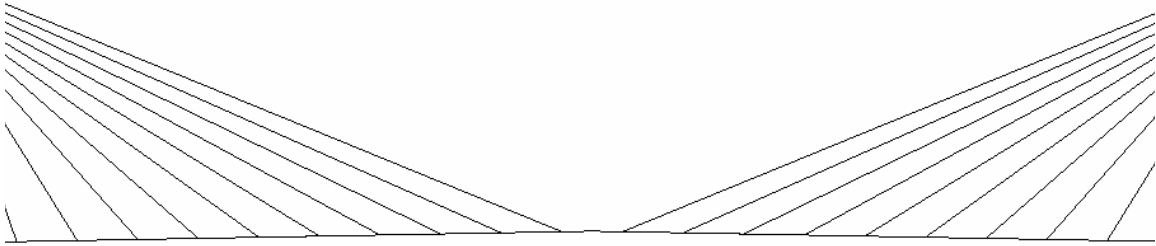
Member	Element Type	Material Type	Real Constant Type
Edge girder	BEAM4	1,2,9-17	1 - 11
Floor beam	BEAM4	19	12 - 15
Sub-stringer	BEAM4	18	16
Baffle web plate	BEAM4	20	17
Wind lock	BEAM4	19	18
Tower upper & middle legs	BEAM4	4	19
Tower lower leg	BEAM4	4	20 - 27
Tower upper strut	BEAM4	4	28
Tower lower strut	BEAM4	4	29
Pier	BEAM4	6	30, 31
Cable	LINK10	3	32 - 71
Tower stem & footing	SOLID45	5	-
Tie-down linkage	BEAM4	7	72
Fixed bearing	BEAM4	8	73



Full Elevation



Part Elevation – Tower and Cables

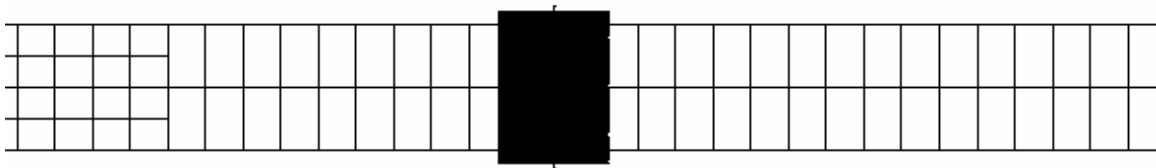


Part Elevation – Central Span

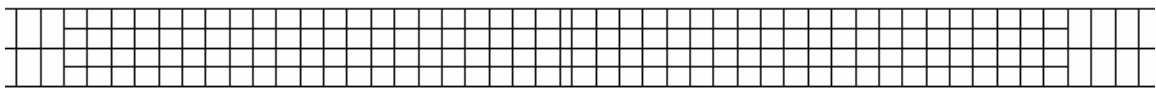
Figure 3.4 Elevation of Finite Element Model



Full Plan

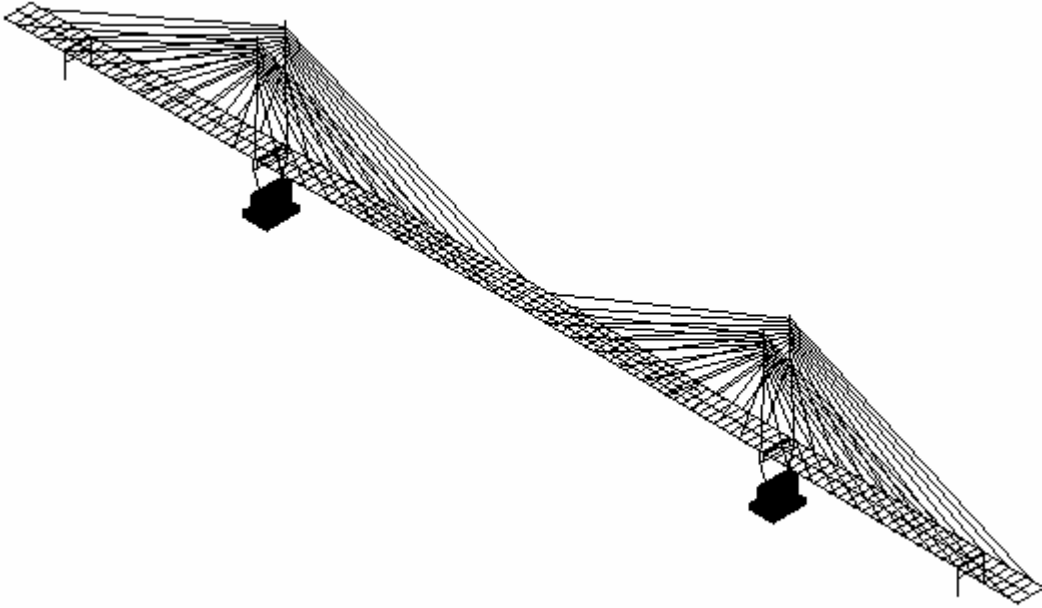


Part Plan – Tower, Edge Girders, Substringer, Baffles and Floor Beams

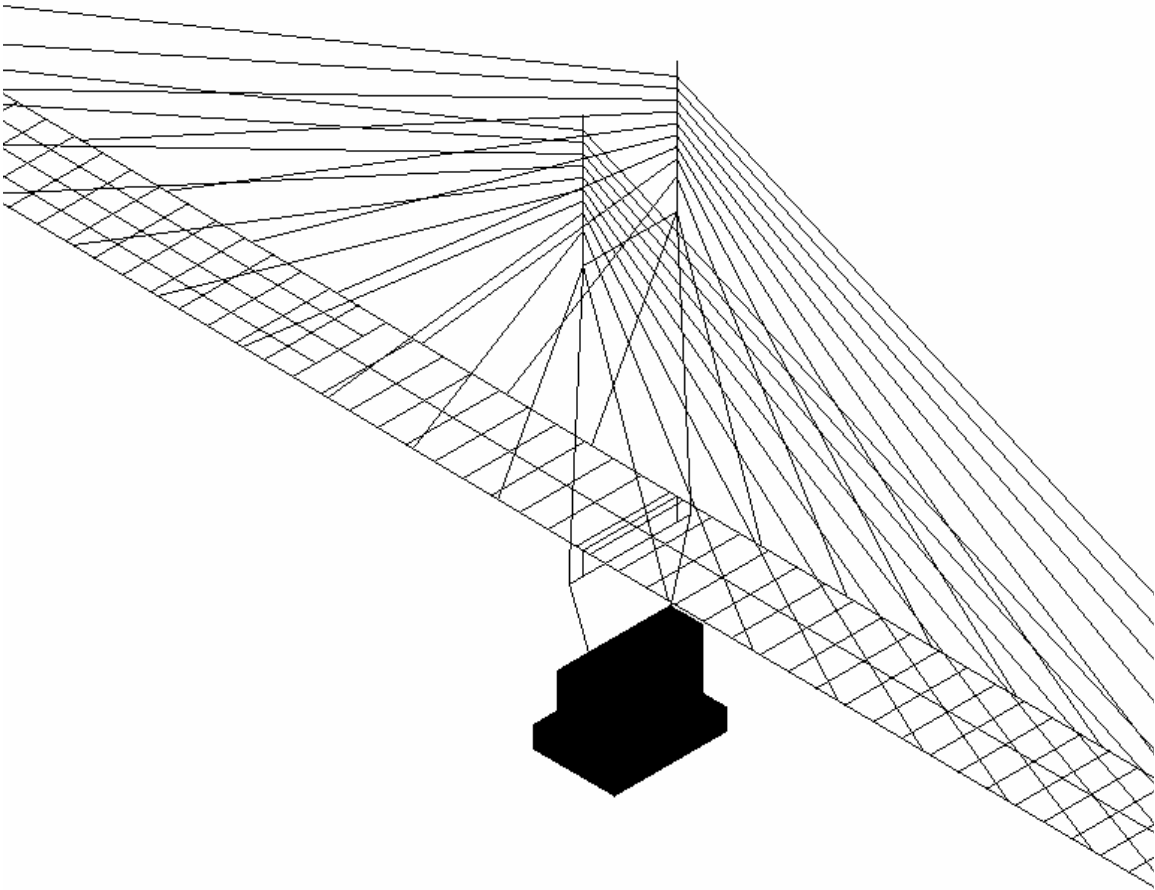


Part Plan – Central Span, Edge Girders, Substringer, Baffles and Floor Beams

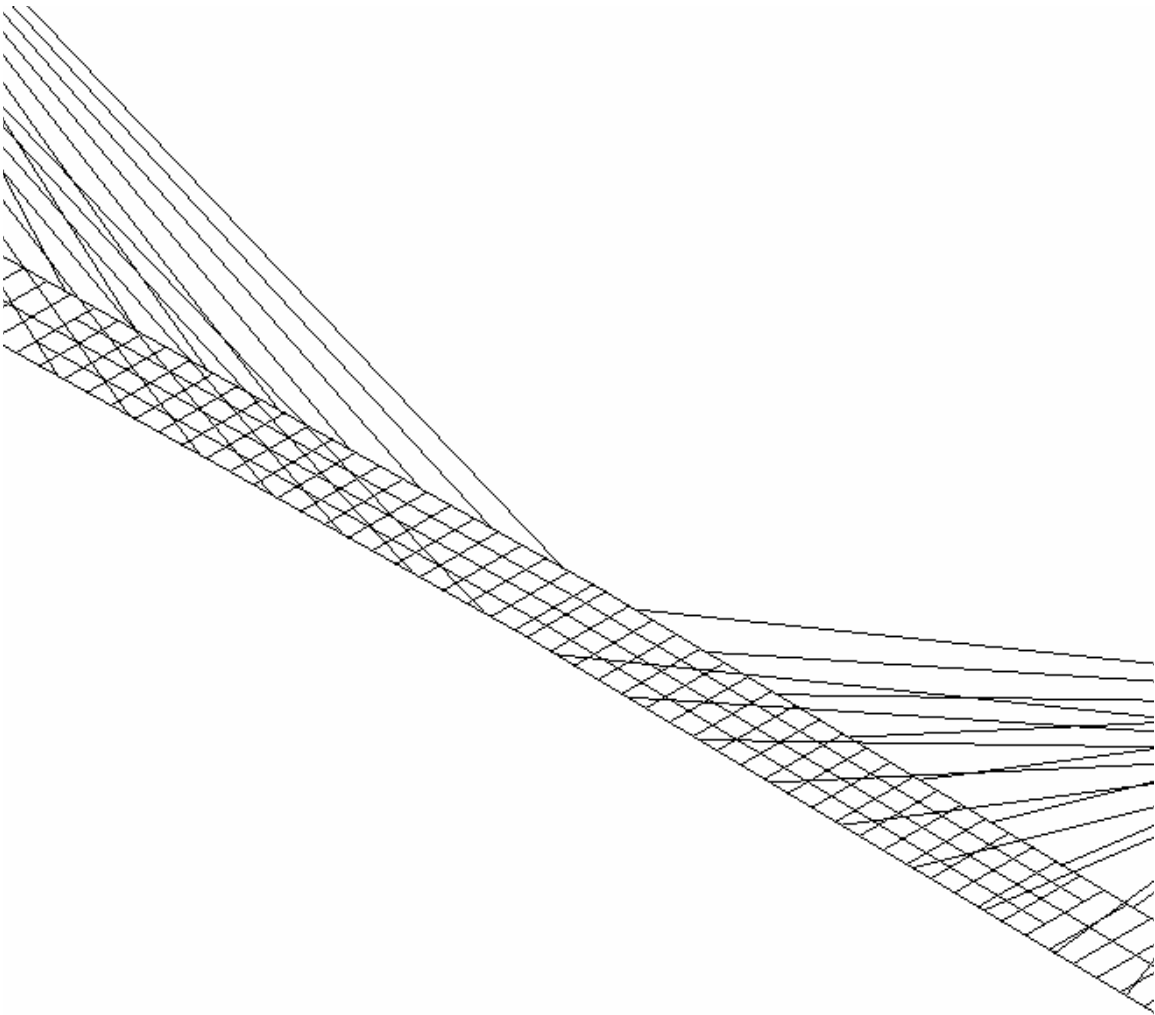
Figure 3.5 Plan of Finite Element Model



Full Elevation – Isotropic



Part Elevation – Tower and Cables



Part Elevation – Central Span

Figure 3.6 Isotropic Elevation of Finite Element Model

3.2.6. Boundary Conditions

The boundary conditions of an actual bridge are always complex but are often idealized as fixes, hinges and rollers in the analytical model. In current model, the towers and piers of the Maysville cable-stayed bridge are treated as being fixed in all degrees-of-freedom at the bases. The north and south ends of the deck are connected to the piers by a tension-link mechanism that permits the end of the deck to rotate freely about the vertical (y) and transverse (z) axes. Rotation about the longitudinal axis (x) and all three translational degree of freedom are modeled as fixed at each end of the deck.

The connection of the deck to the towers and the piers presented a special challenge to the development of the finite element model. For the connection of the deck to the towers, the deck-tower bearings are simulated using two rigid vertical links. These two links are used to connect two edge girders to the lower tower strut. In order to restrain the relative motions between deck and tower, the relative three translational motions and two rotations about longitudinal (x) and vertical (y) axes between deck and tower are coupled; the only relative motion possible is a free rotation of the deck with respect to the tower cross-beam, about the z axis. For the connection of the deck to the piers, the girder linkages are modeled using two rigid vertical links. The relative vertical (y) and transverse (z) displacements between girder and pier are coupled.

3.3. Static Analysis under Dead Load

In the design of cable-stayed bridges, the dead load often contributes most of bridge loads. The dead load has a significant influence on the stiffness of a cable-stayed bridge. In the finite element analysis, this influence can be considered by the static analysis under dead loads before the live load or dynamic analysis is carried out. The objective of the static analysis process is intended to achieve the deformed equilibrium configuration of the bridge due to dead loads in which the structural members are “pre-stressed”. After doing the deformed equilibrium configuration, the real analysis is followed. Consequently, the dead load effect on the stiffness is included in the analysis.

For the static analysis of the Maysville cable-stayed bridge under dead loads, the dead load value of the deck can be given by considering the volume of the deck and the density of the concrete. Actually, the deck loads are transferred from the edge girders, sub-stringers and floor-beams to the stayed cables and towers. Thus in the finite element analysis, the dead load is equivalently distributed to the sub-stringer and the two edge girders.

The capabilities of the static analysis procedure in the ANSYS include large deflections (geometrically nonlinear analysis) and stress stiffening. Since the structure involves non-linearity, an iterative solution associated with the Newton-Raphson solution procedure is required.

3.3.1. Initial Tension in the Cables

A cable-stayed bridge directly derives its stiffness from the cable tension. The final geometry of the bridge due to the dead load is known from the drawing of the Maysville cable-stayed bridge plans. Referring to the drawing, we have modeled the initial geometry of the bridge, which is really the shape of the bridge under the dead load. Actually, the bridge deck was stayed piece by piece from the cable. And thus the cable stretched and deflected down until almost all of the deck was stayed from the cables, resting on each end on the towers.

It turns out that the ideal finite element model of a cable-stayed bridge should be such that on application of the dead load, the geometry of the bridge does not change; this is indeed the final geometry of the bridge. In other words, the deformed configuration of the bridge under the self-weight should be as close to the initial geometry. This can be approximately realized by manipulating the initial tension force in the cables that is specified as an input quantity (pre-strain) in the cable elements. Hence, the bridge can be modeled in the final geometry with a pre-tension force in the cables. In such a way, the initial tension force in the cables plays an important role. The initial tension force in the cables can be achieved by the testing. The initial tension forces in the cables of the model are listed in the table 3.7 from the chapter 4, Cable Testing and Modeling.

Table 3.7 Initial Tension Forces in the Cables

Cable Number	Cable Designs' Axial Force (kips)	Final Stay Tension Dead Load Only Upstream Cable (kips)	Final Stay Tension Dead Load Only Downstream Cable (kips)
1	1127.1	958.8	974.3
2	1073.3	826.4	847.9
3	928.4	742.2	828.0
4	967.1	735.5	799.9
5	636.7	605.2	583.8
6	696.3	584.9	563.4
7	575.6	544.5	526.5
8	689.9	510.5	502.9
9	460.1	407.2	301.0
10	566.8	444.6	437.7
11	572.0	327.7	327.7
12	541.0	439.7	439.7
13	558.9	395.1	480.9
14	589.1	484.7	484.7
15	722.9	589.7	546.7
16	783.2	621.1	700.3
17	872.2	638.9	681.8
18	1050.5	804.0	782.5
19	1078.1	758.2	822.6
20	1101.6	964.7	964.7
21	1101.6	977.4	965.6
22	1078.1	746.9	758.3
23	1050.5	836.0	824.4
24	872.2	700.8	697.3
25	783.2	651.5	630.8
26	722.9	630.9	566.9
27	589.1	535.1	501.5
28	558.9	446.5	403.6
29	541.0	329.0	337.4
30	572.0	438.6	431.7
31	566.8	501.9	495.0
32	460.1	331.2	331.2
33	689.9	471.3	439.1
34	575.6	473.0	483.7
35	696.3	626.9	627.5
36	636.7	626.0	626.6
37	967.1	713.0	735.3
38	928.4	784.9	720.5
39	1073.3	761.8	783.3
40	1127.1	979.9	969.3

3.3.2. Geometric Non-linearity

For the static analysis, it is well known that a long span cable-stayed bridge exhibits geometrically nonlinear characteristics that are reflected in the nonlinear load-deflection behavior under any load conditions. These geometrically nonlinear sources may come from

- The large deflection effect due to changes in geometry;
- The combined axial load and bending moment interaction effect;
- The sag effect due to changes in cable tension load levels.

In the structural analysis for small deflection, the geometric change of the structure is always assumed to be small and can be neglected so that all quantities, such as force and deformation, are determined by the original configuration of the structure. In such a case, the overall stiffness of the structure in the deformed configuration is assumed to be equal to the stiffness of the undeformed configuration, in order to make the analysis simpler. However, a large deflection solution is required whenever the displacements are large enough so that the structural stiffness matrix based on the initial geometry does not characterize the deformed structure. Since cable-stayed bridges are highly flexible structural system, the displacements under normal working loads are deemed to be large enough to warrant a nonlinear analysis that accounts for the rigid body motion of the structure. The geometric change can be no longer neglected. In this case, the bridge stiffness must be always updated in the simultaneous deformed configuration. Due to this simultaneous deformed configuration is also an unknown, the iteration techniques should be used.

In the ANSYS, the capability for large deflection analysis is available for most of the structural element types. The large deflection is accounted for by reorienting the stiffness into its new configuration through updating the nodal locations. In the geometrically nonlinear analysis, the deformations are characterized by the large

displacements and large rotations, but small strains. This is consistent with the fact that most of structures behave. The total Lagrange (T.L.) formulation is employed in which the basic working variable is the total displacement vector rather than the incremental displacement vector as the updated Lagrange (U.L.) formulation does.

The main girders and towers of a cable-stayed bridge are often the structural members subjected to both the axial force and the bending moment. In the linear structural analysis, the axial stiffness and the flexural stiffness are considered to be uncoupled. However, if the deformations are no longer small, these structural members are subjected to an interaction between the axial force (tension or compression) and the bending moment. The additional bending moment would be caused by a simultaneously axial force applied due to the lateral deformation of a bending member and the flexural stiffness of the member would be altered. As a result, the effective bending stiffness of the member will decrease for a compressive axial force and increase for a tensile axial force. On the other hand, the presence of bending moments will affect the axial stiffness of the member due to an apparent shortening of the member caused by bending deformations. For the case of cable-stayed bridges, the large deformation may occur. The interaction between the axial force and the bending moment might be significant and should be considered. This effect can be included in the geometric stiffness matrix by using geometrically nonlinear analysis.

For a cable, supported at its ends and subjected to its own weight and an externally applied axial force, it sags into the shape of a catenarian. The axial stiffness of the cable varies nonlinearly as a function of cable tension force, which in turn changes with the distance of cable ends. For conventional truss members the sag due to self-weight can be ignored but for cable members this sag should be considered for the accurate analysis. Indeed, the sag phenomenon of individual cables results in geometrically nonlinear behavior of cable-stayed bridges. The sagging cable problem needs an explicit stress stiffness matrix included in the mathematical formulation to provide numerical stability. Basically, the cable sag effect can be included by introducing

axial strains in the cables and running a static stress-stiffening analysis to determine an equilibrium configuration where the cables are “pre-stressed”.

The cable sag can be accounted for in the ANSYS by employing the tension-only truss element and utilizing its stress-stiffening capability in conjunction with a large deflection analysis. The stress stiffening is an effect that causes a stiffness change in the element due to the loading or stress within the element. The stress-stiffening capability is needed for the analysis of structures with a low or non-existent bending stiffness as is the case with cables. Physically, the stress-stiffening represents the coupling between the in-plane and transverse deflections within the structure. This coupling is the mechanism used by thin flexible structures to carry the lateral loads. As the in-plane tensile force increases, the capacity to assume the lateral loads increases. In other words, the transverse stiffness increases as the tensile stress increases. More details can be found in the ANSYS references.

The finite element model described previously is used here to reveal the large deflection effect on the structural behavior of the Maysville cable-stayed bridge due to the dead load. Table 3.8 shows the comparison of the maximum deck deflection between small deflection analysis and large deflection analysis. It is clearly shown that the large deflection has almost no effect on the deck deflection due to dead load alone. This is consistent with the observation that the maximum deck deflection of the bridge is very limited (about 0.06 feet) due to introducing the pre-strain in the cables in which the bridge becomes quite stiffening. Further comparison between small deflection analysis and large deflection analysis without introducing the cable pre-strain, as shown in Table 3.8 too, has demonstrated that the large deflection does not change the deck deflection significantly even though the maximum deck deflection of the bridge is about 4.4 feet. Therefore, the large deflection analysis is not necessary in determining the initial equilibrium configuration of the bridge due to dead load and the small deflection analysis is enough in the current finite element model. But the stress stiffening must be always included in the static analysis of cable-supported bridges and hence the static analysis of a cable-stayed bridge is always geometrically nonlinear.

Table 3.8 Comparison of Maximum Deflections (absolute value, foot)

Analysis type	With cable pre-strain	Without cable pre-strain
Small deformation	0.063517	4.452
Large deformation	0.060901	4.471

In the finite element modeling of a cable-stayed bridge, it is quite natural to discretize the cable between the tower and the girder into a single tension-only truss element (cable element). But two node cable elements, as we know, are relatively weak elements. However, since two end nodes of the cable element are connected with the beam elements of the tower and the girder, the nonlinear static analysis or the modal analysis can be carried out. Another key feature in the nonlinear structural analysis is the choice of convergence criterion to control the iteration procedure. The defaulted force convergence criterion in the ANSYS cannot provide an efficient iteration solution in the large deflection analysis of the Maysville cable-stayed bridge. Sometimes the force convergence criterion results in the divergence especially when the structural deflection reaches slightly large. Instead, the displacement convergence criterion is very effective and always results in the convergent solution. In addition, as mentioned previously the stress stiffening plays an important role in the static analysis of cable-stayed bridges. The sagging of the cable requires the stress part in the stiffness matrix and results in the nonlinear analysis. Stress stiffening must be always used for sagging cable problem to provide numerical stability. Using a large deformation solution without the stress stiffening capability leads to an aborted run due to divergent oscillation.

3.4. Modal Analysis

Cable-stayed bridges are more flexible than other structures because of large spans. One important aspect of such a flexible structure is a large displacement response of the deck when subject to dynamical loads. As a result, considerable amount of work has been conducted to study the dynamic behavior of cable-stayed bridges as a part of the design of wind and seismic resistance. The dynamic characteristics of a structure can be effectively analyzed in terms of natural frequencies and mode shapes. Modal analysis is needed to determine the natural frequencies and mode shapes of the entire cable-stayed

bridge. The natural frequencies and mode shapes of the Maysville cable-stayed bridge are studied by using the current finite element model. Since the established model is a 3-D finite element model, a general modal analysis is capable to provide all possible modes of the bridge (transverse, vertical, torsion and coupled).

The modal analysis needs to solve the eigenvalue problem. The eigenvalue and eigenvector extraction technique used in the analysis is the Block Lanczos method. The Block Lanczos eigenvalue extraction method is available for large symmetric eigenvalue problems. Typically, this solver is applicable to the type of problems solved using the Subspace eigenvalue method, however, at a faster convergence rate. The Block Lanczos algorithm is basically a variation of the classic Lanczos algorithm, where the Lanczos recursions are performed using a block of vectors as opposed to a single vector. Additional theoretical details on the classic Lanczos method can be found in any textbooks on eigenvalue extraction.

3.4.1. Effect of Initial Equilibrium Configuration

As mentioned previously, the modal analysis of a cable-stayed bridge should include two steps: the static analysis loaded by the dead load and then followed by pre-stressed modal analysis. This kind of pre-stressed modal analysis is available in the ANSYS. In order to investigate the effect of initial equilibrium configuration due to the dead load and the pre-strain in the cables on the dynamic properties of the Maysville cable-stayed bridge, the following three cases are considered:

- Case 1: the regular modal analysis without dead load effect where the modal analysis is starting from the undeformed configuration;
- Case 2: the pre-stressed modal analysis where the modal analysis follows a dead-load linear static analysis without the pre-strain in the cables;
- Case 3: the pre-stressed modal analysis where the modal analysis follows a dead-load linear static analysis with a pre-strain in the cables.

Table 3.9 Comparison of Frequencies (Hz)

Mode Order	Case 1	Case 2	Case 3
1	0.42822	0.42695	0.43238
2	0.51145	0.51259	0.51667
3	0.54743	0.54258	0.55814
4	0.67755	0.67728	0.67984
5	0.69939	0.70067	0.71077
6	0.82175	0.80945	0.82744
7	0.96813	0.95713	0.97172
8	0.97909	0.97413	0.98676
9	1.0119	1.0100	1.0101
10	1.0178	1.0166	1.0170
11	1.0546	1.0460	1.0576
12	1.1248	1.1199	1.1306
13	1.1421	1.1270	1.1466
14	1.1791	1.1749	1.1822
15	1.2395	1.2324	1.2453
16	1.3139	1.2877	1.3173
17	1.3712	1.3564	1.3762
18	1.5161	1.4896	1.5144
19	1.5233	1.5031	1.5291
20	1.5897	1.5731	1.5838

The comparison results of frequencies among above three cases are summarized in Table 3.9. It is clearly shown that the beneficial effect of self-weight is used in improving stiffness. The cable-stayed bridge with sufficient amount of pre-strain in the cables is a highly pre-stressed structure. In the current case of the Maysville cable-stayed bridge, the dead load effect will increase the natural frequency due to the stiffening of the structure. Therefore, the regular modal analysis without a dead-load static analysis will result in the under-estimation of the cable-stayed bridge capacity and consequently provides more safe evaluation of the bridge capacity.

Furthermore, compared with Case 2 and Case 3, the pre-strain in the cables increases the natural frequencies of the cable-stayed bridge if the pre-stressed modal analysis is used. It implies that it is the self-weight not the initial equilibrium configuration starting the vibration contributes the stiffness improvement because the pre-strain in the cables changes the initial equilibrium configuration and the distribution

of the pre-stress due to dead load. But the initial equilibrium configuration to start the vibration is obviously essential to the dynamic responses under wind or seismic loadings.

3.4.2. Modal Analysis Results

To make the results close to the real situation, the pre-stressed modal analysis starting from the dead-load deformed equilibrium configuration with a pre-strain in the cables is performed here to evaluate the modal properties of the Maysville cable-stayed bridge. The natural frequencies, mass distribution percentages and modal participation factors are summarized in Tables 3.10-11, respectively. The participation factor of particular mode demonstrates the importance of that mode. The mass fraction expresses the whole mass participation percentages before that mode. The table of the participation factor and mass distribution percentage is available in the ANSYS to provide the list of participation factors, mode coefficients and mass distribution percentages for each mode extracted. The participation factors and mode coefficients are calculated based on an assumed unit displacement spectrum in each of the global Cartesian directions.

In general, several modes of vibration contribute to the total dynamic response of the structure. For the purpose of directional uncertainty and the simultaneous occurrence of forces in the three orthogonal directions, coupling effects within each mode of vibration should be considered. Coupling effects, however, make it difficult to categorize the modes into simple vertical, transverse, or torsion, thus making comparisons with experimental measurements difficult. Most of studies are aimed to analyze the modal behavior of cable-stayed bridges in terms of pure vertical, transverse and torsion modes of vibration. Since the Maysville cable-stayed bridge is modeled as a complete 3-D structure, all possible coupled modes can be obtained. It provides the full understanding of the dynamic behavior of the bridge.

The first ten sets of mode shapes are shown in Figures 3.7-3.16, respectively. All mode shapes are normalized to unity instead of mass matrix in order to check with the corresponding mode shapes obtained from the ambient vibration tests. The mode

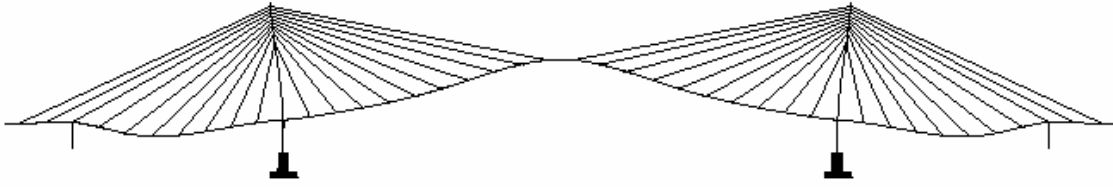
classification can be identified by observing the mass distribution percentage, the modal participation factor and the animated mode shape and is listed in Table 3.11. It can be found that one dominated mode is always coupled with other modes. The vibration modes of the Maysville cable-stayed bridge are complicated and coupled.

Table 3.10 Natural Frequencies (Hz) and Mass Fraction

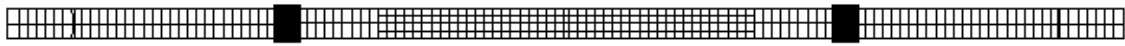
Frequency (Hz)	Mass Fraction					
	X	Y	Z	ROTX	ROTY	ROTZ
0.432382	0.260E-08	0.244372	0.546E-19	0.554E-20	0.374E-19	0.199699
0.516669	0.260E-08	0.244372	0.134066	0.265E-01	0.115612	0.199699
0.558143	0.505E-01	0.244372	0.134066	0.265E-01	0.115612	0.202260
0.679844	0.505E-01	0.244372	0.478464	0.365E-01	0.412584	0.202260
0.710774	0.505E-01	0.244372	0.478464	0.365E-01	0.412585	0.202260
0.827436	0.505E-01	0.266012	0.478464	0.365E-01	0.412585	0.219965
0.971719	0.120565	0.266012	0.478464	0.365E-01	0.412585	0.301822
0.986763	0.120565	0.266012	0.522047	0.719E-01	0.450167	0.301822
1.01009	0.120565	0.266012	0.522049	0.719E-01	0.586955	0.301822
1.01698	0.120565	0.266012	0.995998	0.964224	0.995417	0.301822
1.05762	0.120565	0.782893	0.995998	0.964224	0.995417	0.724139
1.13061	0.120565	0.782893	0.995998	0.964224	0.995420	0.724139
1.14657	0.123567	0.782893	0.995998	0.964224	0.995420	0.805311
1.18224	0.123567	0.782893	0.996005	0.986833	0.995426	0.805311
1.24527	0.123567	0.782893	0.996005	0.986833	0.995453	0.805311
1.31735	0.123567	0.915299	0.996005	0.986833	0.995453	0.913457
1.37622	0.123567	0.915299	0.996557	0.995955	0.995925	0.913457
1.51437	0.303394	0.915299	0.996557	0.995955	0.995925	0.915697
1.52913	0.303394	0.915299	0.996557	0.995955	0.995963	0.915697
1.58377	0.303395	0.943610	0.996557	0.995955	0.995963	0.939036

Table 3.11 Natural Frequencies (Hz) and Participation Factors

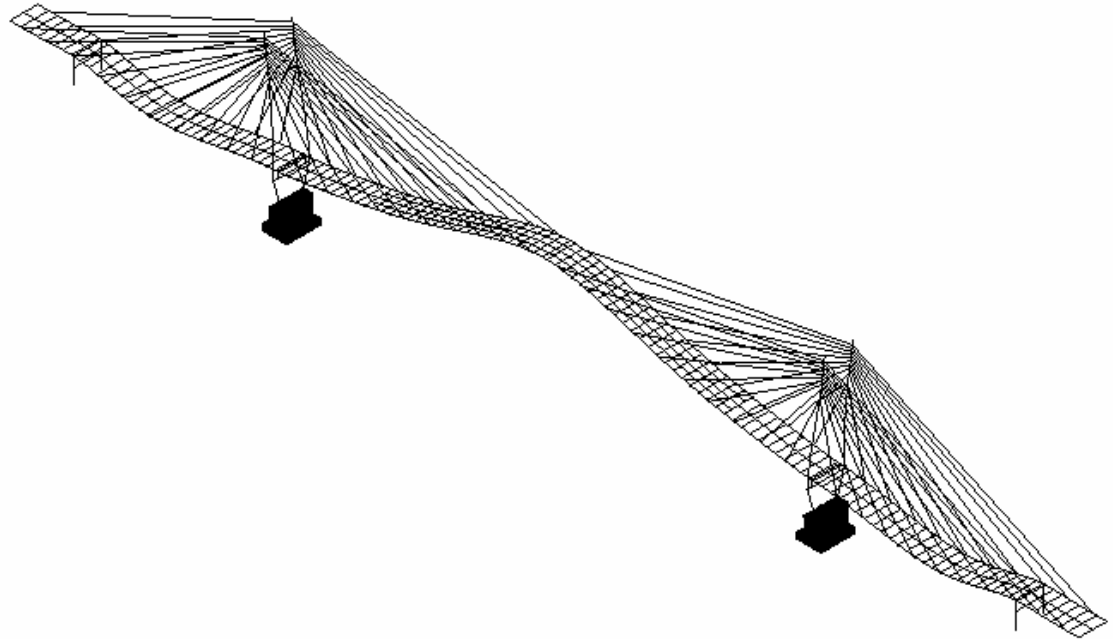
Frequency (Hz)	Participation Factor						Mode
	X	Y	Z	ROTX	ROTY	ROTZ	Classification
0.432382	0.037	381.68	-0.19E-6	-0.65E-5	0.17E-3	0.40E+6	Vertical
0.516669	0.28E-6	0.12E-6	301.37	14315.	-0.31E+6	0.25E-4	Transverse + Torsion
0.558143	-163.36	0.069	-0.11E-7	0.21E-5	0.20E-6	45388.	Vertical
0.679844	0.12E-6	0.49E-7	483.03	8771.5	-0.51E+6	0.98E-4	Transverse + Torsion
0.710774	0.79E-9	0.19E-6	0.035	1.7706	1183.3	0.20E-3	Torsion
0.827436	-0.071	113.58	-0.18E-6	-0.32E-5	0.23E-3	0.12E+6	Vertical
0.971719	-192.14	0.25327	-0.53E-6	-0.53E-4	0.48E-3	0.25E+6	Vertical
0.986763	0.50E-6	0.38E-7	-171.83	-16520.	0.18E+6	-0.33E-3	Torsion
1.01009	0.24E-7	-0.17E-6	1.2841	162.80	-0.34E+6	-0.24E-3	Tower Sway
1.01698	-0.11E-6	0.75E-7	566.64	82971.	-0.59E+6	0.23E-3	Tower Sway
1.05762	0.065	555.09	-0.11E-7	-0.96E-5	-0.11E-3	0.58E+6	Vertical
1.13061	-0.83E-9	0.91E-6	-0.041	-7.0631	1684.2	0.87E-3	Torsion
1.14657	39.798	-0.171	-0.29E-7	0.31E-4	0.16E-4	0.25E+6	Vertical
1.18224	0.77E-7	0.18E-7	-2.1783	13207.	2245.3	-0.87E-3	Torsion
1.24527	-0.41E-8	0.27E-6	-0.022	3.8318	4826.4	0.27E-3	Torsion
1.31735	-0.025	280.95	0.31E-7	-0.74E-7	0.33E-5	0.29E+6	Vertical
1.37622	-0.21E-6	-0.34E-7	19.337	-8389.2	-20217.	-0.72E-4	Torsion
1.51437	-308.00	0.35716	0.10E-6	0.13E-4	-0.89E-4	-42445.	Vertical
1.52913	0.25E-6	0.11E-8	-0.064	-2.1273	-5717.5	0.17E-4	Torsion
1.58377	0.73138	129.91	-0.27E-7	-0.22E-5	-0.55E-4	0.13E+6	Vertical



Elevation

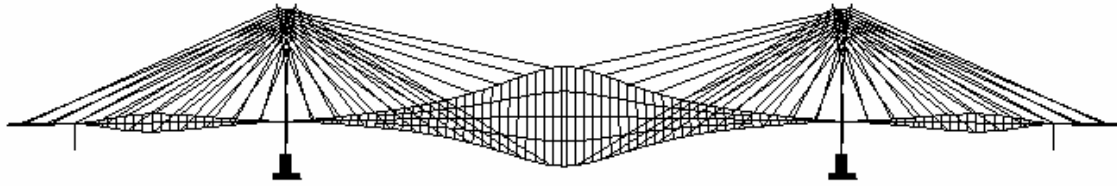


Plan



3-D View

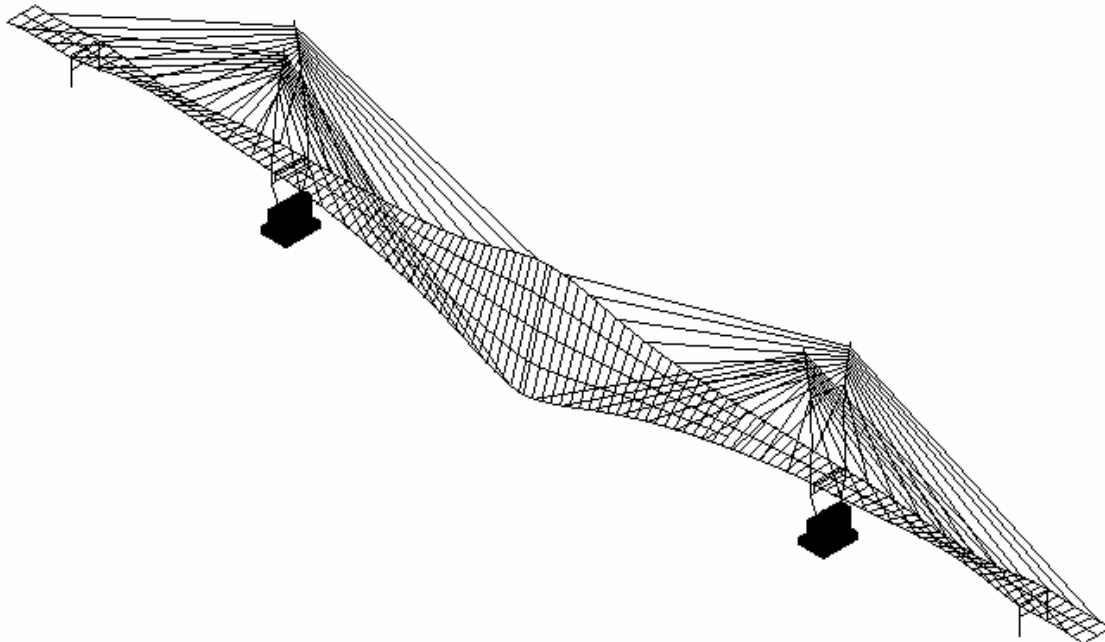
Figure 3.7 1st Mode Shape ($f = 0.432\text{Hz}$, Vertical)



Elevation

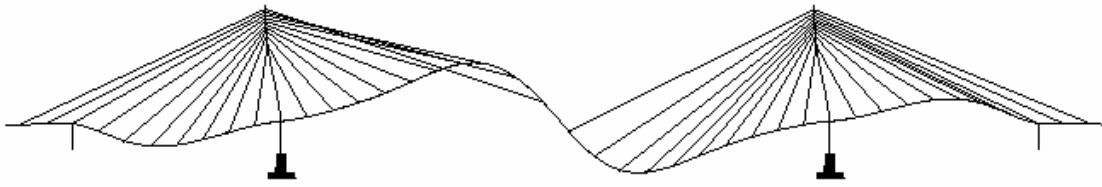


Plan

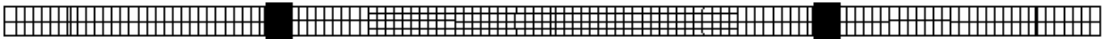


3-D View

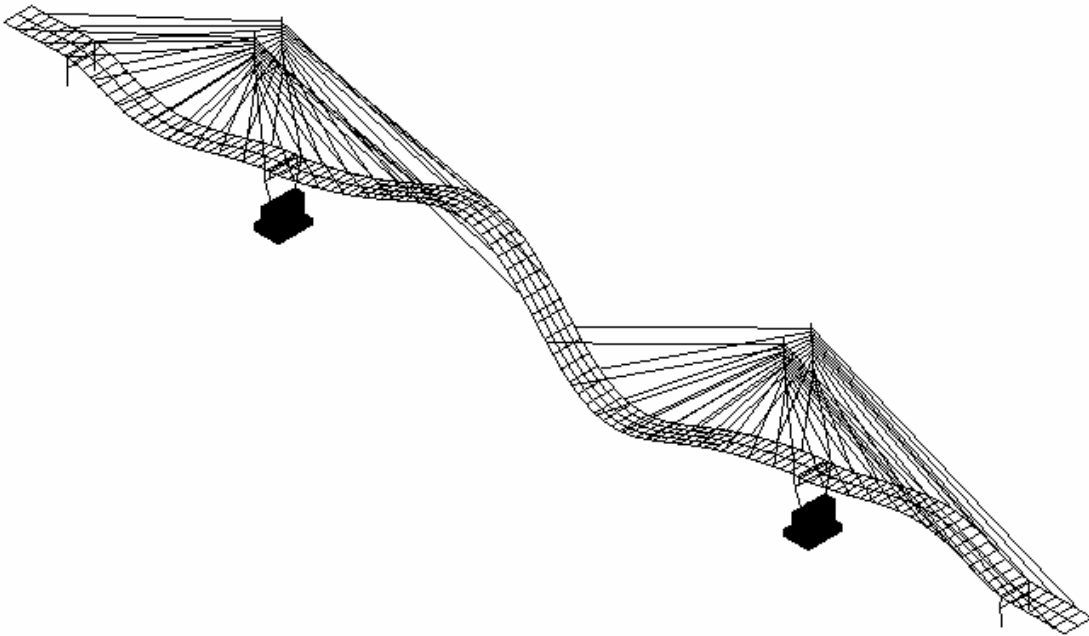
Figure 3.8 2nd Mode Shape ($f = 0.517\text{Hz}$, Transverse + Torsion)



Elevation

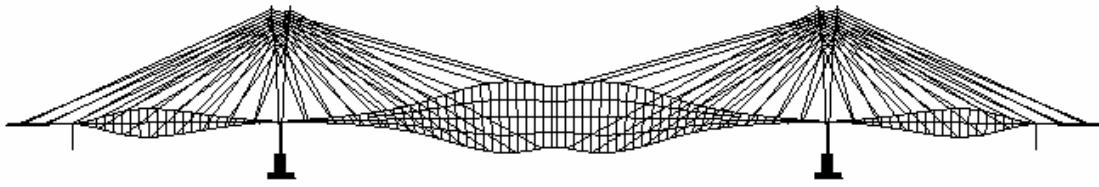


Plan



3-D View

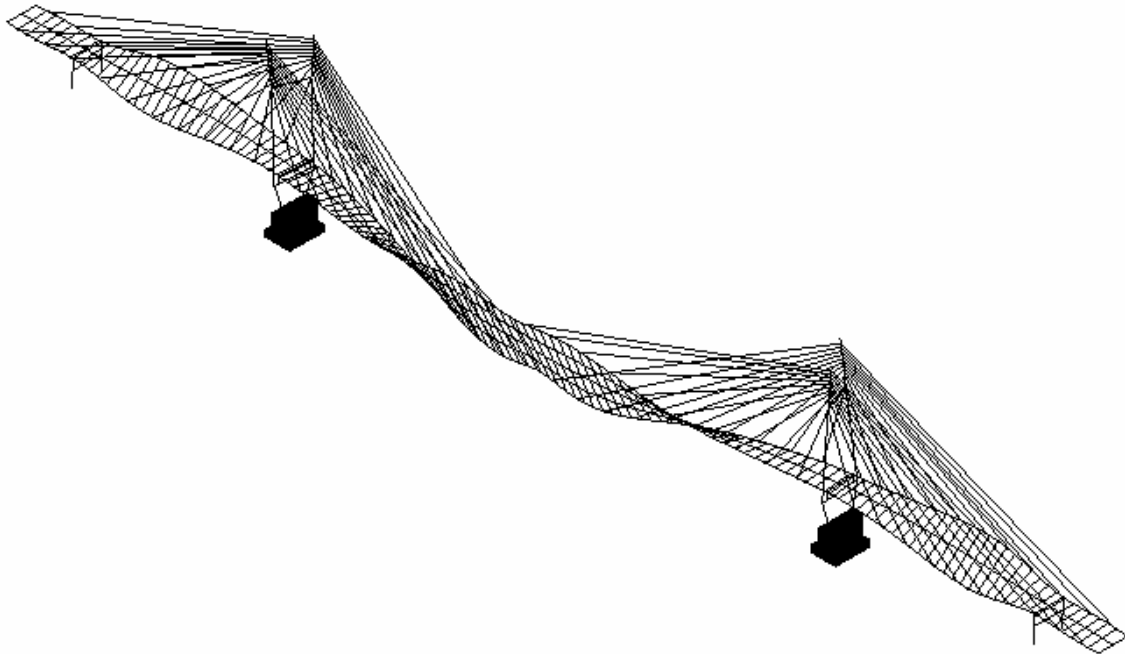
Figure 3.9 3rd Mode Shape ($f = 0.558\text{Hz}$, Vertical)



Elevation

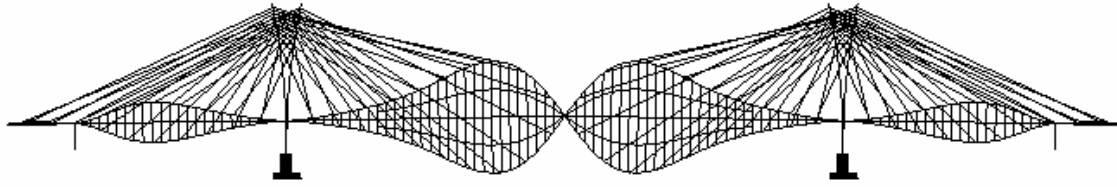


Plan



3-D View

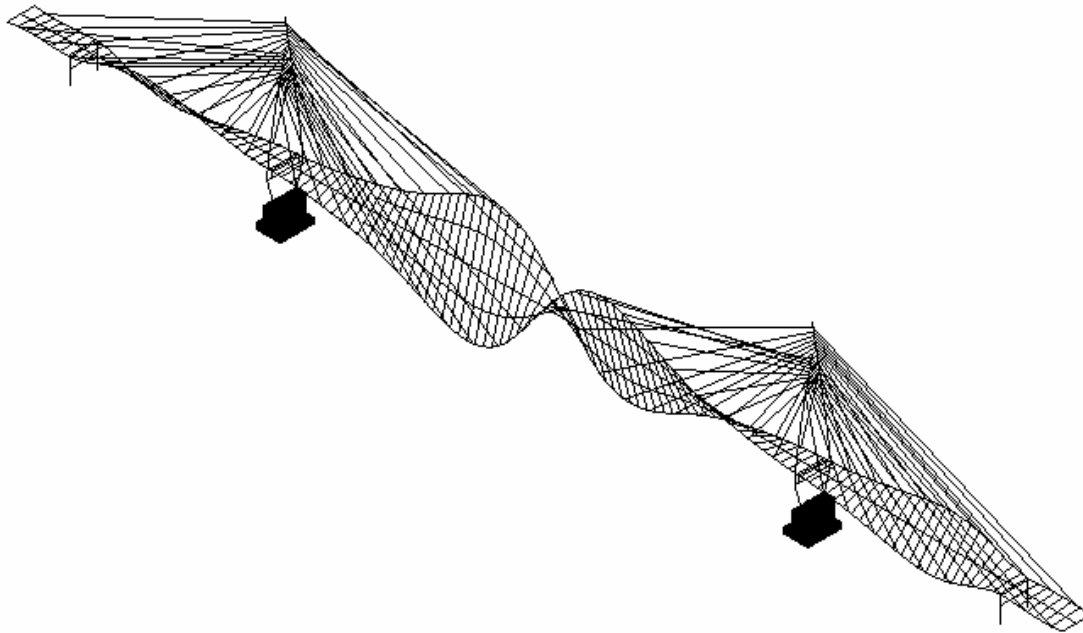
Figure 3.10 4th Mode Shape ($f = 0.679\text{Hz}$, Transverse + Torsion)



Elevation

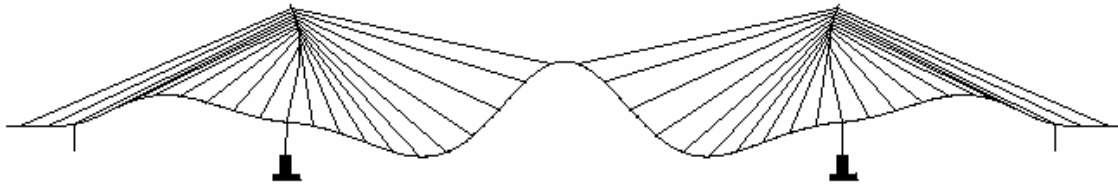


Plan

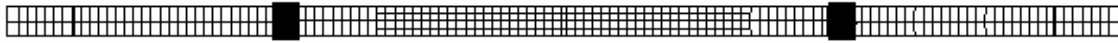


3-D View

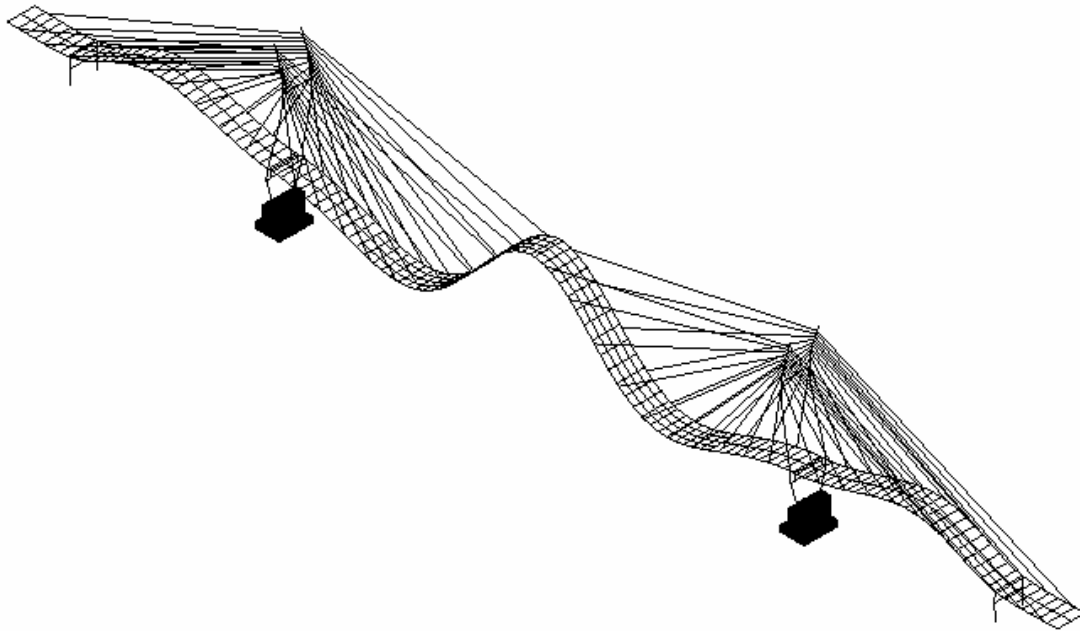
Figure 3.11 5th Mode Shape ($f = 0.711\text{Hz}$, Torsion)



Elevation

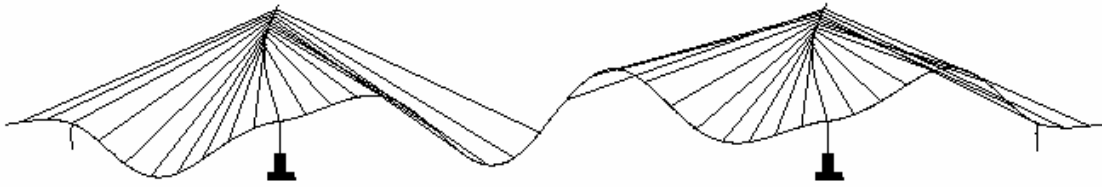


Plan



3-D View

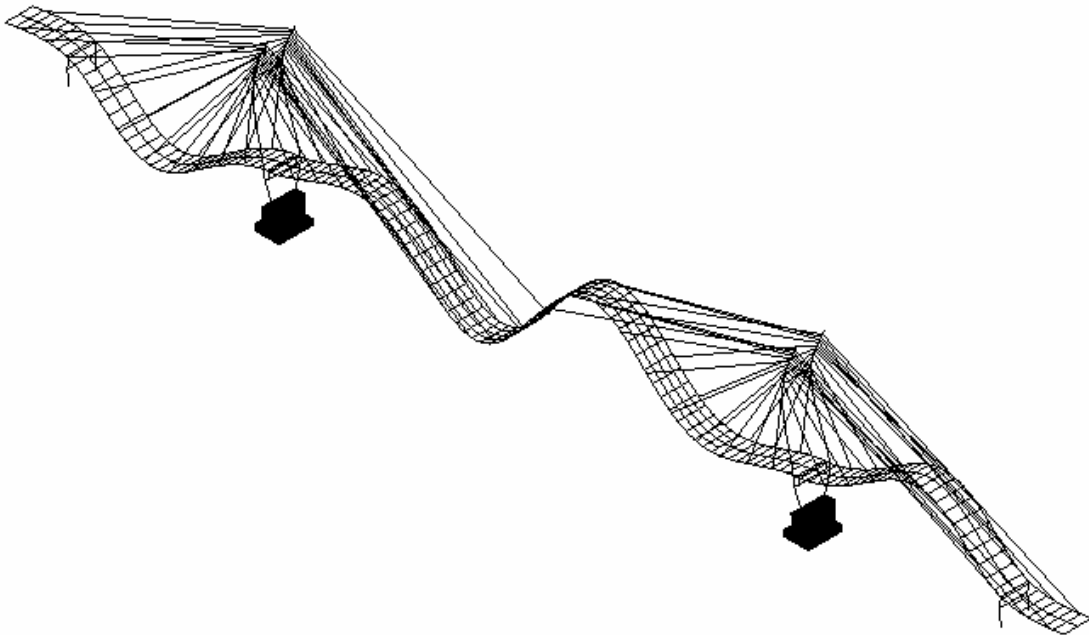
Figure 3.12 6th Mode Shape ($f = 0.827\text{Hz}$, Vertical)



Elevation

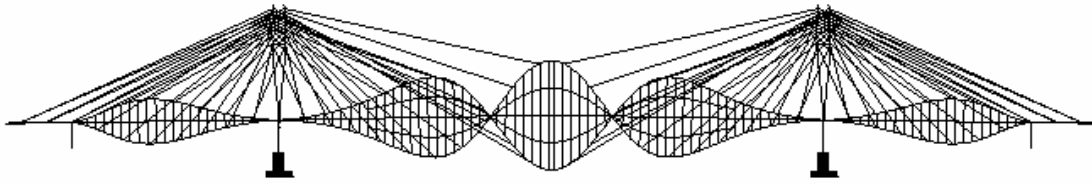


Plan



3-D View

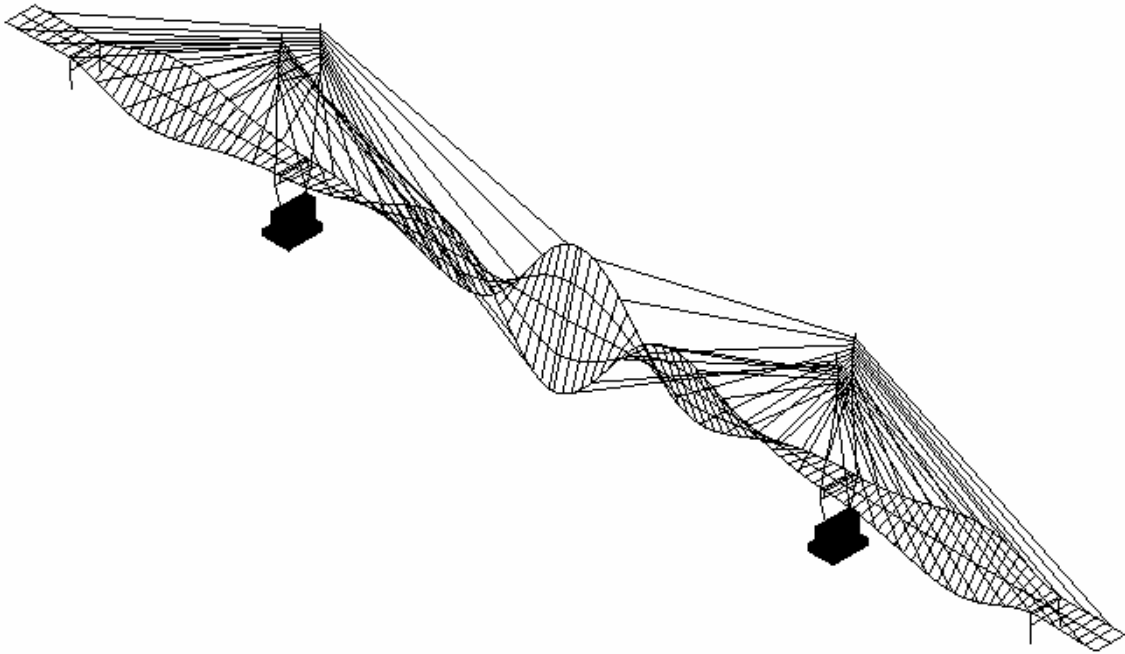
Figure 3.13 7th Mode Shape ($f = 0.972$ Hz, Vertical)



Elevation



Plan

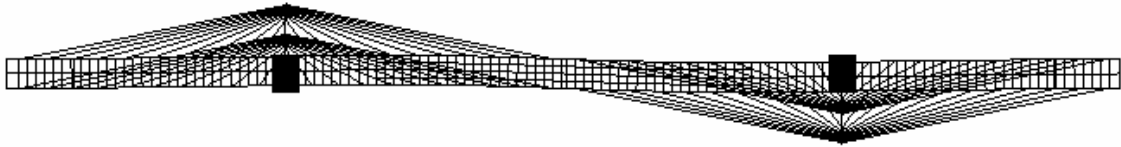


3-D View

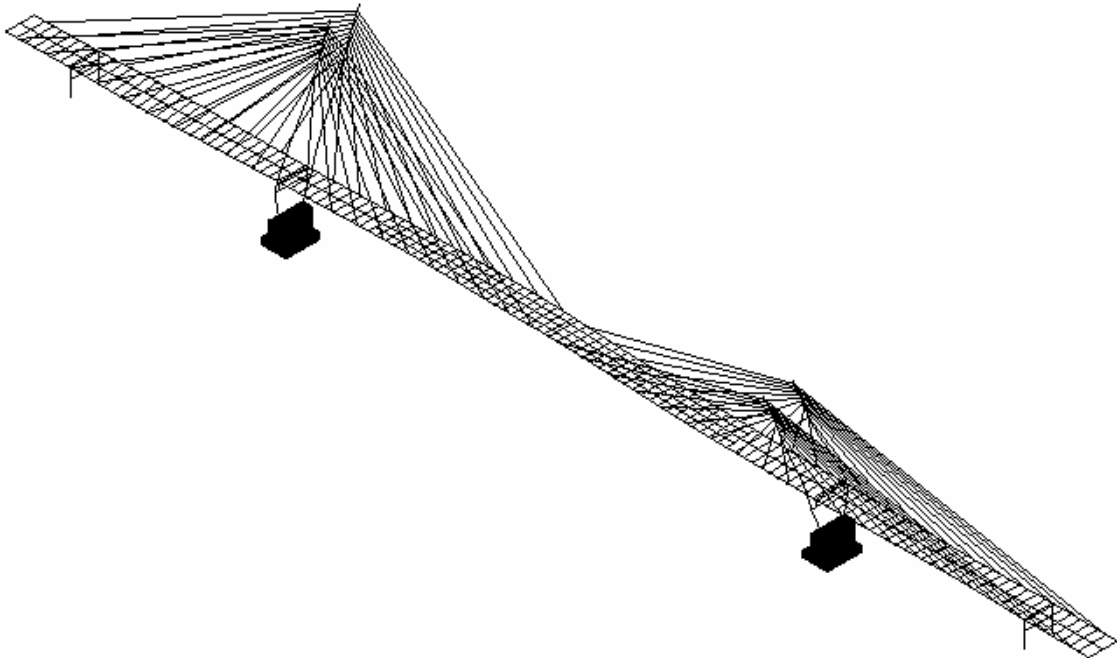
Figure 3.14 8th Mode Shape ($f = 0.987$ Hz, Torsion)



Elevation

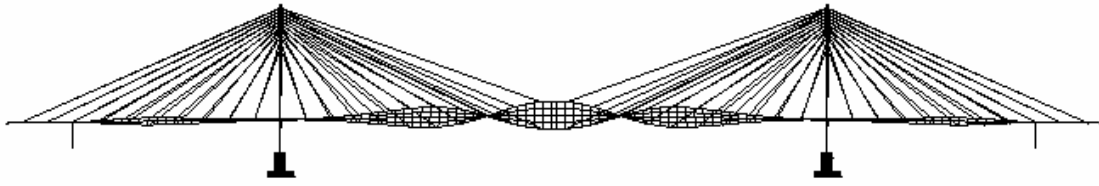


Plan

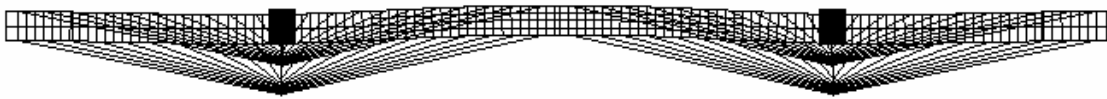


3-D View

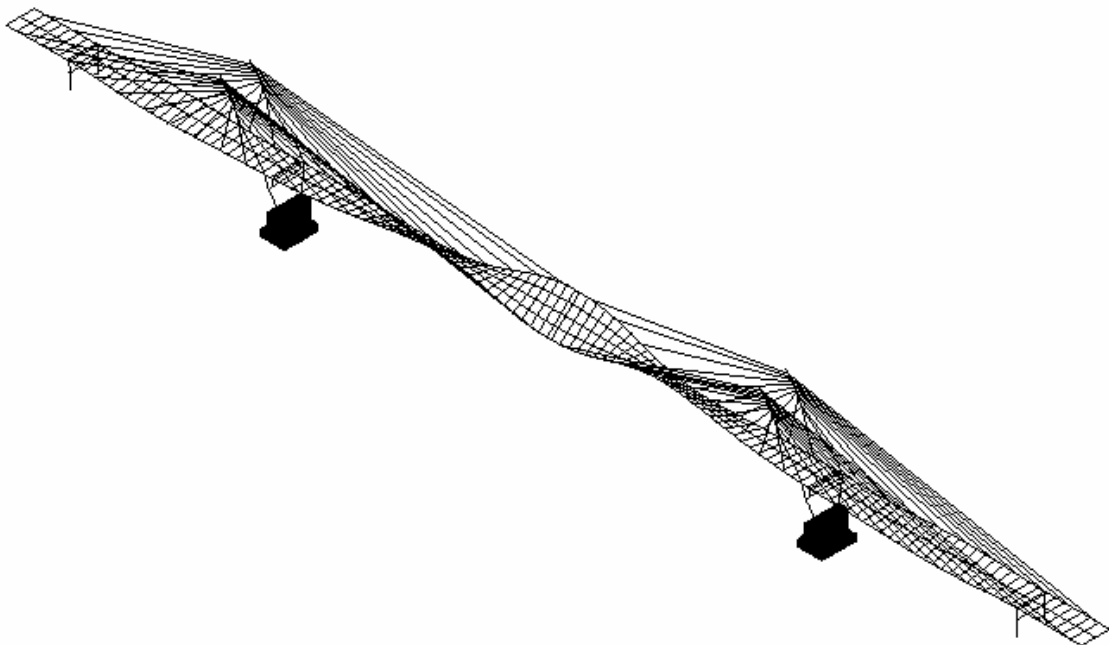
Figure 3.15 9th Mode Shape ($f = 1.010$ Hz, Tower Sway)



Elevation



Plan



3-D View

Figure 3.16 10th Mode Shape ($f = 1.017$ Hz, Tower Sway)

3.5. Parametric Studies

In order to calibrate the FEM model of the Maysville cable-stayed bridge with *in-situ* free vibration measurements in the sense of modal parameters, the structural and material parameters that may largely affect the modal properties of the bridge are supposed to be identified. This can be realized by the parametric studies. As mentioned previously, one of the most advantages of finite element modeling and analysis is to make the parametric studies possible. The parametric studies reported here not only prove the efficiency of the finite element methodology, but also demonstrate the extent and nature of variation in modal properties that a variation in the input parameters can cause. The FE model calibration can be conducted by adjusting these parameters to match the frequencies and mode shapes between testing and modeling. The calibrated FE model will be served as the base line for future structural evaluations of the bridge.

There are several structural and material parameters that would affect the modal behavior of the Maysville cable-stayed bridge, such as the mass, the cable tension stiffness, the vertical and transverse bending stiffness of the deck. The effects of these parameters on the modal properties of the bridge are studied as follows.

3.5.1. Deck Weight

The change of deck self weights is reflected by the relative mass density of edge girders and sub-stringers that is defined by

$$\bar{\rho} = \frac{\rho}{\rho_0}$$

where ρ_0 is the standard mass density of edge girders and sub-stringers listed in Table 3.4. Frequencies for different deck mass density are summarized in Table 3.12. The variation of the first two frequencies with the relative mass density for the edge girders

and sub-stringers is shown in Figure 3.17. From the Table 3.12 and Figure 3.17, it can be seen that the frequencies increase steadily with decreasing in the deck self weight.

Table 3.12 Frequencies (Hz) for Different Deck Mass Densities

Mode order	Relative mass density $\bar{\rho} = \frac{\rho}{\rho_0}$ for the deck					
	0.0	0.25	0.5	1.0	1.5	2.0
1	1.01171	0.7719	0.58855	0.43238	0.35738	0.31127
2	1.01352	0.94648	0.70965	0.51667	0.42634	0.37143
3	1.22042	0.95654	0.75121	0.55814	0.46199	0.40204
4	1.29195	1.01216	0.92656	0.67984	0.56062	0.48791
5	1.69098	1.01282	0.96244	0.71077	0.58911	0.51425
6	1.81431	1.24967	1.01209	0.82744	0.68272	0.59202
7	2.10219	1.26837	1.02769	0.97172	0.80196	0.69609
8	2.36746	1.38644	1.11149	0.98676	0.81272	0.70563
9	2.40301	1.60638	1.30268	1.01009	0.86481	0.74811
10	2.66564	1.77411	1.35547	1.01698	0.93023	0.80521
11	3.51727	1.98032	1.47549	1.05762	0.93405	0.8078
12	3.58382	1.98173	1.54769	1.13061	0.96946	0.84081
13	3.68853	2.18368	1.60871	1.14657	1.00755	0.88067
14	3.68862	2.18999	1.64129	1.18224	1.01402	0.9248
15	3.7085	2.19237	1.74587	1.24527	1.01785	0.97016
16	3.95994	2.30302	1.77593	1.31735	1.07463	1.00288
17	4.32194	2.41695	1.85663	1.37622	1.12406	1.01308
18	4.39223	2.47055	1.91597	1.51437	1.2487	1.07755
19	4.39707	2.4956	2.00153	1.52913	1.25635	1.08591
20	4.4961	2.66895	2.09444	1.58377	1.30747	1.1323

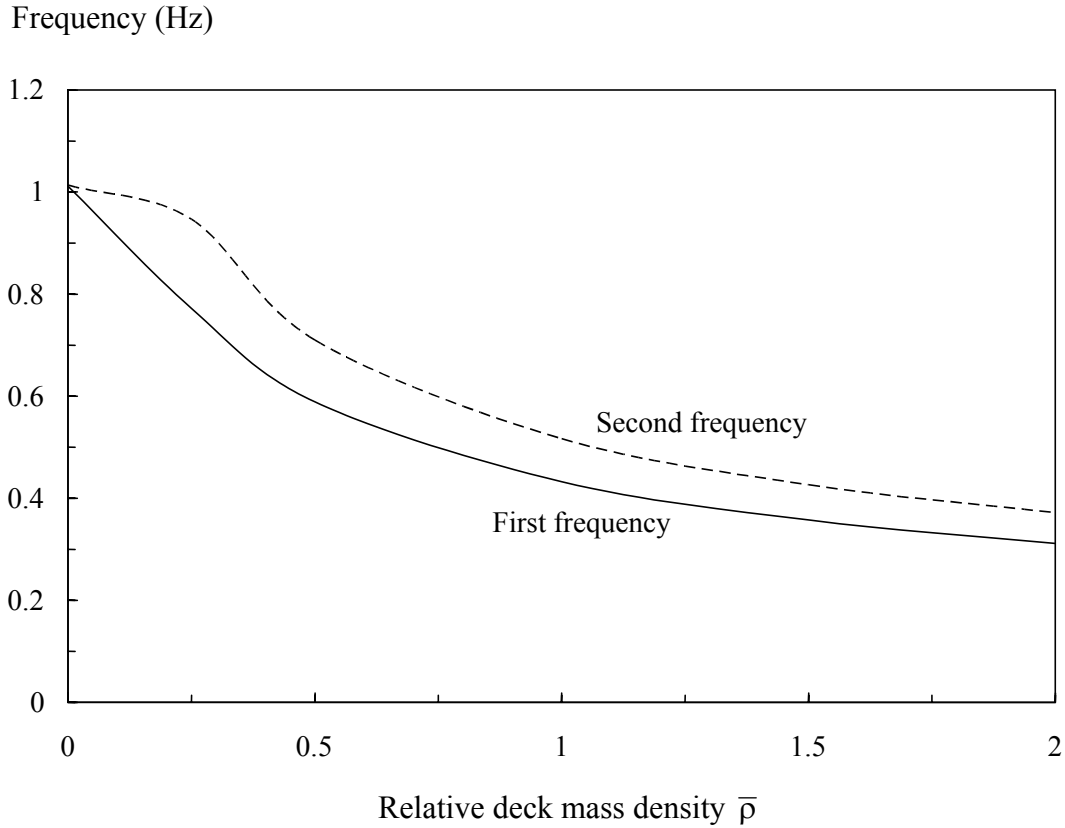


Figure 3.17 Frequencies vs Deck Mass Density

3.5.2. Cable Stiffness

The tension stiffness of cables depends on the sectional area A , the elastic modulus E and the pre-strain. Because the initial tension force has been given in Table 3.7, we only study the effect of the sectional area A and elastic modulus E on the modal properties of the bridge, respectively in the following.

3.5.2.1. Cable Sectional Area

The change of cable sectional areas is represented by the relative sectional area of cables that is defined by

$$\bar{A} = \frac{A}{A_0}$$

where A_0 is the standard sectional area of cables given in Table 3.5. Frequencies for different cable area ratios are summarized in Table 3.13. The variation of the first two frequencies with the relative cable area is shown in Figure 3.18. It has been found that the increasing the cable sectional area results in the increment of frequency values. Increasing the cable areas does result in larger tension stiffness, which is supposed to increase the frequencies, but at the same time cable weight increases with the increasing cable area, which results in reducing the frequencies. These two effects tend to compensate for each other resulting in the less increment of frequencies. It should be noted that the variation of cable areas does cause a reordering of the dominated mode shapes as they relate to the sequential natural frequency orders.

Table 3.13 Frequencies (Hz) for Different Cable Areas

Mode order	Relative sectional area $\bar{A} = \frac{A}{A_0}$ for the cables					
	0.25	0.5	0.75	1.0	1.5	2.0
1	0.24269	0.32753	0.38572	0.43238	0.50672	0.56572
2	0.30932	0.42651	0.47911	0.51667	0.56249	0.58381
3	0.3438	0.43133	0.50387	0.55814	0.63928	0.69973
4	0.46104	0.5783	0.65317	0.67984	0.71177	0.75017
5	0.48747	0.65121	0.66661	0.71077	0.79906	0.8664
6	0.58751	0.65354	0.75367	0.82744	0.93357	0.9787
7	0.6044	0.77301	0.88668	0.97172	0.99404	0.98621
8	0.62577	0.79531	0.9024	0.98676	1.0005	1.00781
9	0.6745	0.81282	0.94878	1.01009	1.09234	1.17408
10	0.68198	0.89254	1.01787	1.01698	1.11881	1.21684
11	0.70288	0.89298	1.02397	1.05762	1.22798	1.35951
12	0.71069	0.9144	1.0273	1.13061	1.28605	1.39844
13	0.74635	0.96628	1.0339	1.14657	1.32635	1.47001
14	0.87662	1.02703	1.06321	1.18224	1.36804	1.51034
15	0.8868	1.03183	1.12061	1.24527	1.44449	1.60063
16	1.03572	1.07928	1.2128	1.31735	1.48027	1.60788
17	1.04054	1.10325	1.25419	1.37622	1.57349	1.68702
18	1.04302	1.26192	1.41134	1.51437	1.64986	1.73328
19	1.12207	1.3044	1.42354	1.52913	1.68474	1.75254
20	1.12794	1.34597	1.48059	1.58377	1.71941	1.85779

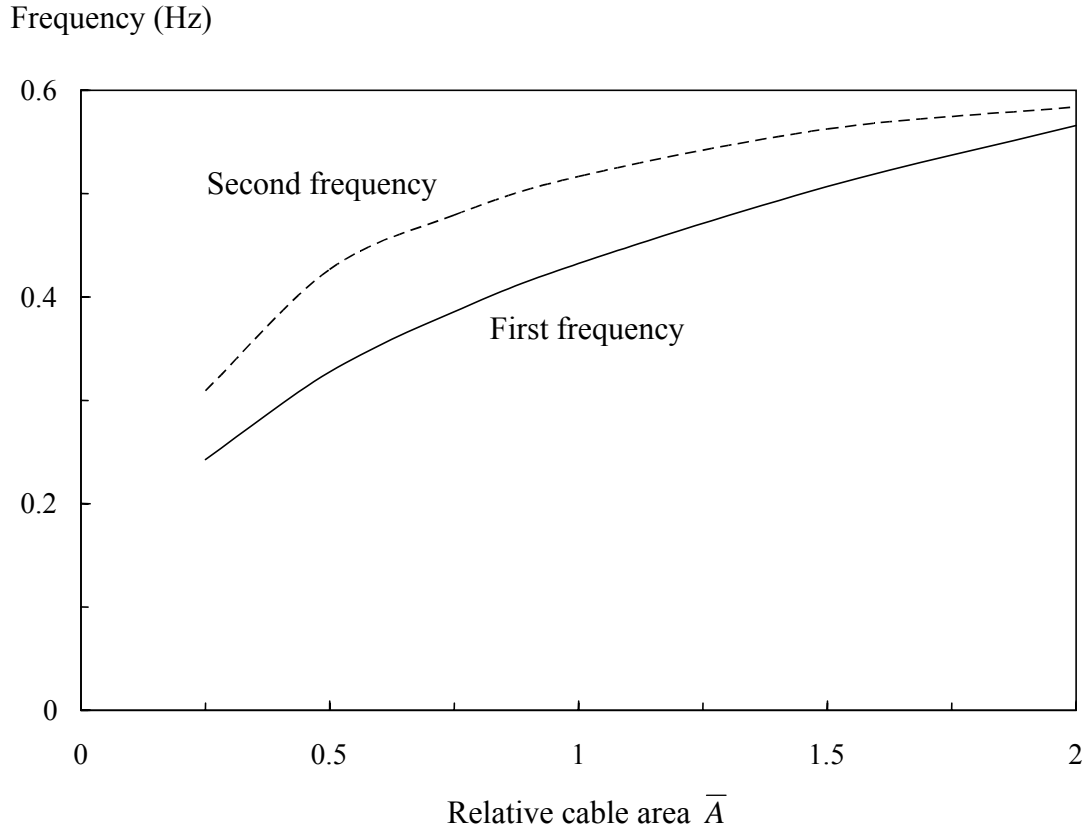


Figure 3.18 Frequencies vs Cable Section Area

3.5.2.2. Cable Elastic Modulus

The variation of cable elastic modulus is represented by the relative cable elastic modulus that is defined by

$$\bar{E} = \frac{E}{E_0}$$

where E_0 is the standard elastic modulus of cables defined in Table 3.4. Frequencies for different cable elastic modulus ratios are summarized in Table 3.14. The variation of the first two frequencies with the relative cable elastic moduli is shown in Figure 3.19. It has been observed that a variation in cable elastic modulus (cable tension stiffness) causes a reordering of the dominated mode shapes as they relate to the sequential order of natural

frequencies, especially for higher modes. The frequencies increase smoothly as the elastic modulus of cables increases in most cases.

Table 3.14 Frequencies (Hz) for Different Cable Moduli

Mode order	Relative elastic modulus $\bar{E} = \frac{E}{E_0}$ for the cables						
	0.1	0.25	0.5	1.0	1.5	2.0	4.0
1	0.20049	0.23969	0.32527	0.43238	0.50995	0.57283	0.62024
2	0.23705	0.30494	0.42285	0.51667	0.56655	0.59159	0.75175
3	0.29449	0.33913	0.42858	0.55814	0.64267	0.70695	0.87161
4	0.35179	0.45543	0.57392	0.67984	0.71711	0.76223	0.93291
5	0.38391	0.48165	0.64713	0.71077	0.80508	0.87941	1.01034
6	0.44748	0.5814	0.64983	0.82744	0.93801	1.01029	1.01773
7	0.45407	0.59995	0.76978	0.97172	1.01019	1.01623	1.08178
8	0.47675	0.62207	0.78989	0.98676	1.01589	1.01711	1.19587
9	0.5208	0.66777	0.80988	1.01009	1.09685	1.18373	1.37224
10	0.52134	0.67594	0.88838	1.01698	1.12632	1.23299	1.50104
11	0.57682	0.6977	0.88871	1.05762	1.23263	1.37016	1.67365
12	0.58447	0.70597	0.91014	1.13061	1.29344	1.41465	1.72515
13	0.67194	0.73933	0.96103	1.14657	1.33113	1.48065	1.74383
14	0.76714	0.86833	1.01012	1.18224	1.37524	1.52679	1.91006
15	0.84821	0.87809	1.01567	1.24527	1.45207	1.61731	1.93633
16	0.90673	1.01006	1.07443	1.31735	1.48548	1.61879	1.99873
17	0.91809	1.01596	1.09726	1.37622	1.5814	1.69898	2.07571
18	0.93702	1.03257	1.25497	1.51437	1.65531	1.75069	2.10449
19	0.93724	1.11159	1.29867	1.52913	1.69089	1.76358	2.22891
20	0.98504	1.12133	1.34102	1.58377	1.72731	1.86811	2.24509

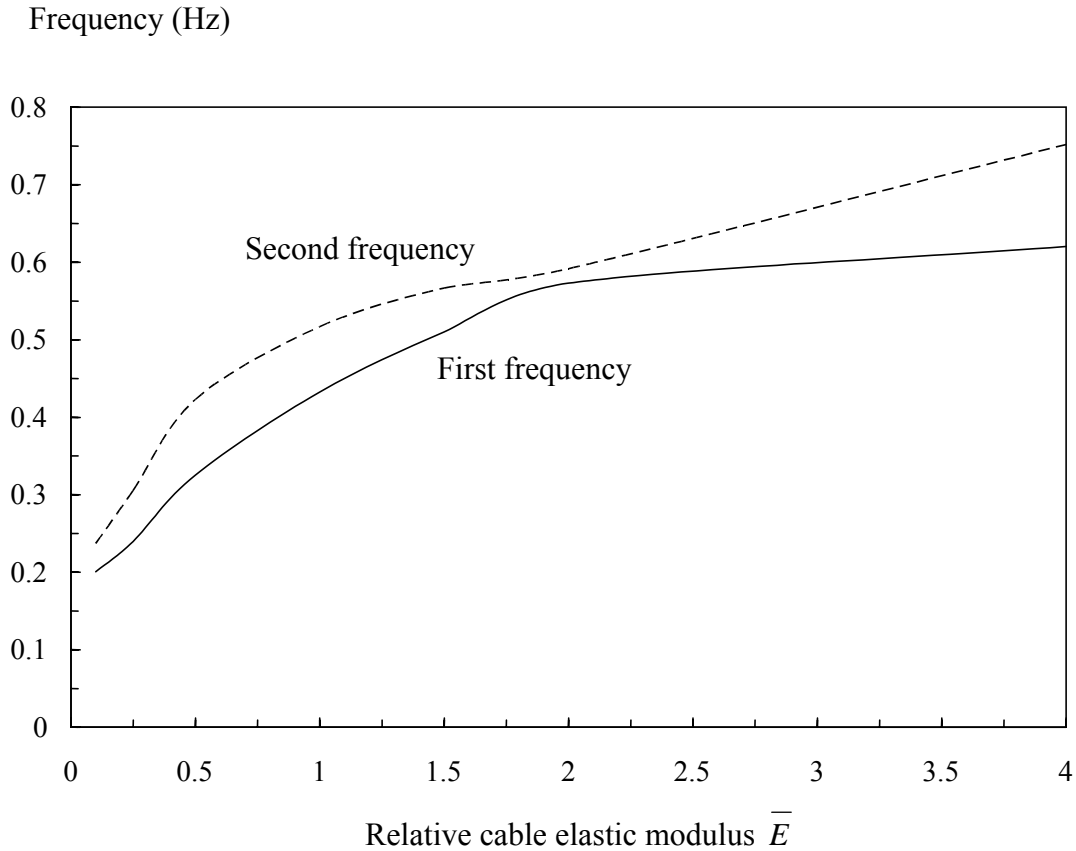


Figure 3.19 Frequencies vs Cable Elastic Modulus

3.5.3. Deck Bending Stiffness

The deck system of the Maysville cable-stayed bridge is modeled by the edge girders and sub-stringers. A variation in the deck bending stiffness is then represented by the relative inertia moment of edge girders and sub-stringers. They are changed by the same ratio. The vertical bending stiffness and lateral bending stiffness of edge girders and sub-stringers are studied, respectively.

3.5.3.1. Deck Vertical Bending Stiffness

The variation of the deck vertical bending stiffness is represented by the relative vertical inertia moment of edge girders and sub-stringers that is defined by

$$\bar{I}_z = \frac{I_z}{I_{z0}}$$

where I_{z0} is the standard vertical inertia moment of edge girders and sub-stringers defined in Table 3.5. Frequencies for different deck vertical bending stiffnesses are summarized in Table 3.15. The variation of the first two frequencies with the relative deck vertical bending stiffness is shown in Figure 3.20. The results show that the vertical frequencies increase smoothly as the deck vertical bending stiffness increases. However, the deck vertical bending stiffness is a little effect on both transverse and torsion frequencies.

Table 3.15 Frequencies (Hz) for Different Deck Vertical Stiffnesses

Mode order	Relative vertical bending stiffness $\bar{I}_z = \frac{I_z}{I_{z0}}$ for the deck					
	0.1	0.5	1.0	2.0	3.0	4.0
1	0.38498	0.41843	0.43238	0.4485	0.4594	0.46789
2	0.46003	0.51024	0.51667	0.52317	0.5271	0.52993
3	0.4944	0.52293	0.55814	0.60373	0.63691	0.66398
4	0.65175	0.67476	0.67984	0.68443	0.6869	0.68856
5	0.66149	0.69017	0.71077	0.73659	0.755	0.76979
6	0.70953	0.77866	0.82744	0.89695	0.95131	0.99767
7	0.81565	0.90738	0.97172	1.01013	1.01015	1.01017
8	0.87472	0.95893	0.98676	1.01436	1.01565	1.0159
9	0.91873	0.98771	1.01009	1.03002	1.05991	1.08582
10	0.92142	1.01004	1.01698	1.06034	1.12705	1.18277
11	0.98733	1.01649	1.05762	1.14767	1.21606	1.26953
12	1.00974	1.05903	1.13061	1.18842	1.23259	1.27543
13	1.0161	1.0895	1.14657	1.24299	1.28674	1.32209
14	1.0302	1.13631	1.18224	1.27056	1.36534	1.40797
15	1.03572	1.17519	1.24527	1.31437	1.37199	1.46199
16	1.0675	1.19258	1.31735	1.48554	1.57352	1.65036
17	1.08212	1.30339	1.37622	1.5272	1.6835	1.6943
18	1.10546	1.32195	1.51437	1.69002	1.69347	1.78096
19	1.11302	1.38732	1.52913	1.70463	1.77625	1.80385
20	1.16913	1.41103	1.58377	1.71421	1.83863	1.95523

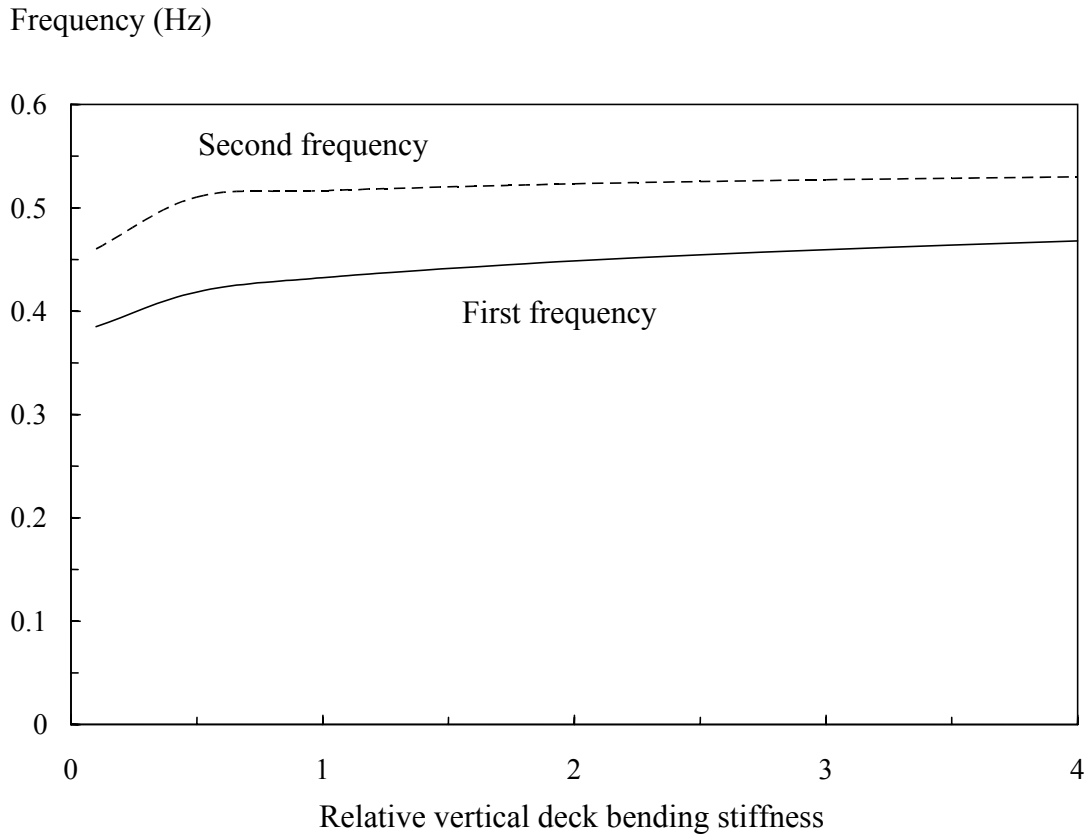


Figure 3.20 Frequencies vs Deck Vertical Bending Stiffness

3.5.3.2. Deck Lateral Bending Stiffness

The variation of the deck lateral bending stiffness is represented by the relative lateral inertia moment of edge girders and sub-stringers that is defined by

$$\bar{I}_y = \frac{I_y}{I_{y0}}$$

where I_{y0} is the standard lateral inertia moment of edge girders and sub-stringers defined in Table 3.5. Frequencies for different deck lateral bending stiffnesses are summarized in Table 3.16. The variation of the first two frequencies with the relative deck lateral

bending stiffness is shown in Figure 3.21. The results show that the increment of the deck lateral bending stiffness does affect on the transverse and torsion frequencies but does not contribute to the vertical frequencies. It has been noted that increasing the deck lateral bending stiffness results in the warping of the deck and the variation of the deck lateral bending stiffness causes a reordering of the dominated mode shapes as they relate to the sequential order of natural frequencies.

Table 3.16 Frequencies (Hz) for Different Lateral Deck Stiffnesses

Mode order	Relative lateral bending stiffness $\bar{I}_y = \frac{I_y}{I_{y0}}$ for the deck						
	0.1	0.25	0.5	0.75	1.0	1.5	2.0
1	0.43232	0.43234	0.43235	0.43237	0.43238	0.43241	0.43243
2	0.48619	0.50459	0.52275	0.52564	0.51667	0.48642	0.45628
3	0.5581	0.55811	0.55812	0.55813	0.55814	0.55816	0.55818
4	0.72635	0.70255	0.67756	0.6715	0.67984	0.64714	0.59794
5	0.82742	0.82742	0.79753	0.75046	0.71077	0.71227	0.74025
6	0.89497	0.85452	0.82742	0.82743	0.82744	0.82745	0.82746
7	0.97167	0.97168	0.9717	0.97171	0.97172	0.90481	0.8504
8	1.00801	1.00877	1.00943	1.00982	0.98676	0.97174	0.94841
9	1.01347	1.01386	1.01439	1.01438	1.01009	1.01023	0.97176
10	1.05756	1.05757	1.05759	1.04186	1.01698	1.0179	0.98864
11	1.14653	1.14654	1.10494	1.05761	1.05762	1.02809	1.01091
12	1.23763	1.18246	1.14655	1.14656	1.13061	1.05765	1.01985
13	1.28781	1.31731	1.2706	1.19476	1.14657	1.07277	1.03925
14	1.3173	1.35123	1.31732	1.25116	1.18224	1.12844	1.05768
15	1.43191	1.38558	1.33359	1.31733	1.24527	1.1466	1.14662
16	1.50669	1.43442	1.40484	1.31883	1.31735	1.24971	1.15407
17	1.51434	1.51435	1.49817	1.45627	1.37622	1.31737	1.27966
18	1.58373	1.52166	1.51435	1.51436	1.51437	1.38817	1.31739
19	1.59945	1.58374	1.55219	1.58376	1.52913	1.49694	1.38008
20	1.62908	1.62909	1.58375	1.59488	1.58377	1.502	1.38399

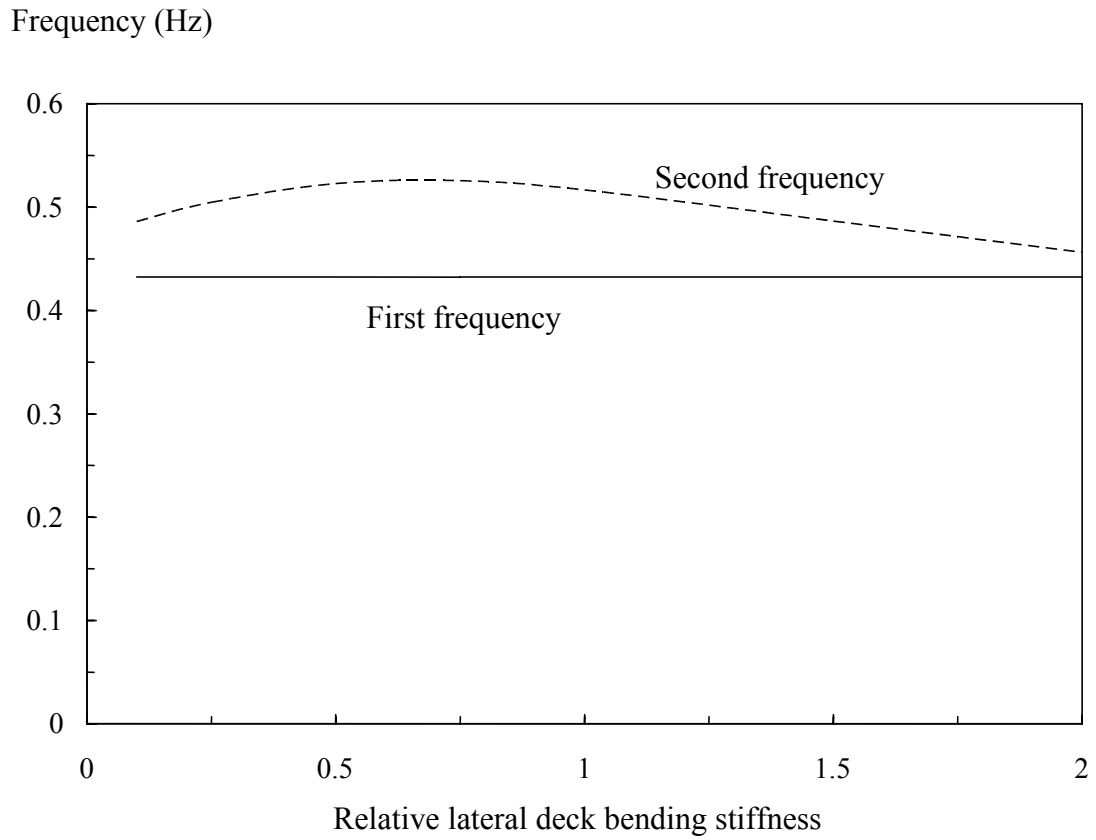


Figure 3.21 Frequencies vs Deck Lateral Bending Stiffness

3.6. Finite Element Model Calibration

A realistic computation model, calibrated with the help of experimental measurements, can be a valuable tool in the efforts to preserve the bridge structural evaluation using dynamic-based methods. The process is required to combine the bridge analyses and experimental measurements. Confidence in using FE models for dynamic performance predictions of a structure is lacking owing to a relatively difference between experimental and analytical modes. The differences are not only from the modeling errors resulting from simplifying assumptions made in modeling the complicated structures but also from parameter errors due to structural defect and uncertainties in the material and geometric properties. Dynamic-based evaluation is therefore based on a comparison of the experimental modal analysis data obtained *in-situ* field tests with the finite element predictions. The FE model of a real structure is then calibrated by using dynamic measurement results.

We have known the real dynamic properties of the bridge through field free vibration testing. And we have already known the structural or material parameters that may largely affect the modal properties of the bridge through parametric studies. The original finite element model can be calibrated by adjusting these parameters to match the frequencies and mode shapes best between testing and modeling. The updated structural and material parameters are summarized in Table 3.17 and Table 3.18, respectively.

Table 3.17 Calibrated Real Constants

Type	Cross-section Area: (ft ²)	Inertia moment: (ft ⁴)		Initial strain	Structural member
		I _{zz}	I _{yy}		
1	2.715	9.4503	0.0987	-	Edge girder
2	2.5275	9.161	0.1323	-	Edge girder
3	2.934	11.44	0.2595	-	Edge girder
4	2.354	4.8143	0.1905	-	Edge girder
5	2.2497	4.5355	0.1903	-	Edge girder
6	2.427	5.074	0.2236	-	Edge girder
7	2.4511	5.1544	0.2346	-	Edge girder
8	2.382	4.9073	0.2311	-	Edge girder
9	2.4372	5.0791	0.3299	-	Edge girder

10	2.6456	5.6458	0.3308	-	Edge girder
11	2.5622	9.4195	0.1907	-	Edge girder
12	0.6517	0.01528	0.01902	-	Floor beam
13	0.9014	0.01529	0.01801	-	Floor beam
14	0.6592	0.01528	0.01056	-	Floor beam
15	0.6443	0.01528	0.01754	-	Floor beam
16	5.51486	24.0641	2572	-	Sub-stringer
17	0.1172	0.217	0.00011	-	Baffle
18	0.8125	0.01529	0.01778	-	Wind-lock
19	87	902.25	3772.25	-	Tower (upper & middle)
20	182.88	1760.87	5501.49	-	Tower (lower)
21	206.63	2974.09	6215.97	-	Tower (lower)
22	230.38	4187.32	6930.45	-	Tower (lower)
23	254.13	5400.55	7644.93	-	Tower (lower)
24	277.88	6613.78	8359.41	-	Tower (lower)
25	301.63	7827.01	9073.89	-	Tower (lower)
26	325.38	9040.24	9788.36	-	Tower (lower)
27	349.13	10253.47	10502.84	-	Tower (lower)
28	36	652	332	-	Tower (upper strut)
29	40	1133.33	213.33	-	Tower (lower strut)
30	44.18	155.32	155.32	-	Piers 4& 7
31	56.25	263.67	263.67	-	Piers 4& 7
32	0.107986	-	-	2.1262E-03	Cables 1 & 41
33	0.107986	-	-	1.8326E-03	Cables 2 & 42
34	0.107986	-	-	1.6459E-03	Cables 3 & 43
35	0.0844444	-	-	2.0857E-03	Cables 4 & 44
36	0.0844444	-	-	1.7162E-03	Cables 5 & 45
37	0.0844444	-	-	1.6586E-03	Cables 6 & 46
38	0.060868	-	-	2.1422E-03	Cables 7 & 47
39	0.060868	-	-	2.0084E-03	Cables 8 & 48
40	0.060868	-	-	1.6019E-03	Cables 9 & 49
41	0.060868	-	-	1.7491E-03	Cables 10 & 50
42	0.060868	-	-	1.2892E-03	Cables 11 & 51
43	0.060868	-	-	1.7298E-03	Cables 12 & 52
44	0.060868	-	-	1.5544E-03	Cables 13 & 53
45	0.060868	-	-	1.9069E-03	Cables 14 & 54
46	0.0844444	-	-	1.6722E-03	Cables 15 & 55
47	0.0844444	-	-	1.7613E-03	Cables 16 & 56
48	0.0844444	-	-	1.8118E-03	Cables 17 & 57
49	0.107986	-	-	1.7829E-03	Cables 18 & 58
50	0.107986	-	-	1.6813E-03	Cables 19 & 59
51	0.107986	-	-	2.1393E-03	Cables 20 & 60
52	0.107986	-	-	2.1674E-03	Cables 21 & 61
53	0.107986	-	-	1.6563E-03	Cables 22 & 62
54	0.107986	-	-	1.8539E-03	Cables 23 & 63

55	0.0844444	-	-	1.9873E-03	Cables 24 & 64
56	0.0844444	-	-	1.8475E-03	Cables 25 & 65
57	0.0844444	-	-	1.7891E-03	Cables 26 & 66
58	0.060868	-	-	2.1052E-03	Cables 27 & 67
59	0.060868	-	-	1.7566E-03	Cables 28 & 68
60	0.060868	-	-	1.2943E-03	Cables 29 & 69
61	0.060868	-	-	1.7255E-03	Cables 30 & 70
62	0.060868	-	-	1.9745E-03	Cables 31 & 71
63	0.060868	-	-	1.3029E-03	Cables 32 & 72
64	0.060868	-	-	1.8542E-03	Cables 33 & 73
65	0.060868	-	-	1.8609E-03	Cables 34 & 74
66	0.0844444	-	-	1.7777E-03	Cables 35 & 75
67	0.0844444	-	-	1.7752E-03	Cables 36 & 76
68	0.0844444	-	-	2.0219E-03	Cables 37 & 77
69	0.107986	-	-	1.7405E-03	Cables 38 & 78
70	0.107986	-	-	1.6893E-03	Cables 39 & 79
71	0.107986	-	-	2.1729E-03	Cables 40 & 80
72	1.778	0.26	0.26	-	Tie-down linkages
73	7.1	4.21	4.21	-	Fixed bearings

Table 3.18 Calibrated Material Properties

Group No.	Young's modulus (lb/ft ²)	Poisson's ratio	Mass density (lb/ft ³)	Structural member
1	4.176×10 ⁹	0.3	953.1	Edge girders
2	4.176×10 ⁹	0.3	973.77	Edge girders
3	4.176×10 ⁹	0.3	932.12	Edge girders
4	4.176×10 ⁹	0.3	995.67	Edge girders
5	4.176×10 ⁹	0.3	1010.33	Edge girders
6	4.176×10 ⁹	0.3	986.11	Edge girders
7	4.176×10 ⁹	0.3	983.04	Edge girders
8	4.176×10 ⁹	0.3	991.96	Edge girders
9	4.176×10 ⁹	0.3	984.79	Edge girders
10	4.176×10 ⁹	0.3	960.42	Edge girders
11	4.176×10 ⁹	0.3	969.72	Edge girders
12	4.176×10 ⁹	0.3	1210.55	Sub-stringer
13	4.176×10 ⁹	0.3	490	Cables
14	4.176×10 ⁹	0.3	490	Baffles
15	4.176×10 ¹²	0.3	490	Floor beams & Wind lock
16	6.087×10 ⁸	0.2	150	Tower columns & struts
17	4.856×10 ⁸	0.2	150	Tower footing & stem
18	5.191×10 ⁸	0.2	150	Piers 4 & 7
19	4.176×10 ¹⁰	0.3	490	Tie-down linkages
20	4.176×10 ¹⁰	0.3	150	Fixed bearings

The several frequencies coming out of the system identification through the free vibration measurements and FEM predictions are summarized in Table 3.19. A good agreement of frequencies has been found between FE modeling and in *situ* vibration measurements. Since the floor beams in FEM are modeled as more rigid beams, its mode shape is transverse plus torsion. As mentioned previously, a dominated mode of the Maysville cable-stayed bridge in 3-D FE modeling is always coupled with other mode shapes. The higher the dominated mode is, the more serious the coupling. Because the experimental modal properties of the bridge come from the free vibration measurements, the better matching for higher modes is not expected and not realistic.

Table 3.19 Comparison of Frequencies

Mode	Test (Hz)	FE Model (Hz)	Mode classification
1	0.3945	0.43	Vertical
2	0.5	0.507	Transverse; Transverse + Torsion for FEM
3	0.5222	0.556	Vertical
4	0.6556	0.646	Transverse + torsion
5	0.7778	0.709	Torsion
6	0.8444	0.824	Vertical
7	0.9333	-	Longitudinal
8	1	0.964	Vertical

The first three vertical and the first two transverse mode shapes of both FE modeling and vibration testing are shown in Figures 3.22-3.26. The test mode shapes are directly obtained by picking up the magnitude values of each spectral diagram at the peak points from the moveable stations divided by those of each spectral diagram at the peak points from the base stations. The FE mode shapes have been normalized according to the maximum value (unity) of the test point. In fact, the mode shapes through ambient vibration are not always that good because ambient excitation does not lend itself to frequency response functions (FRFs) or impulse response functions (IRFs) since the input

force can not be measured. Peak picking is always a subjective task. This is one of the drawbacks of structural system identification through ambient measurements.

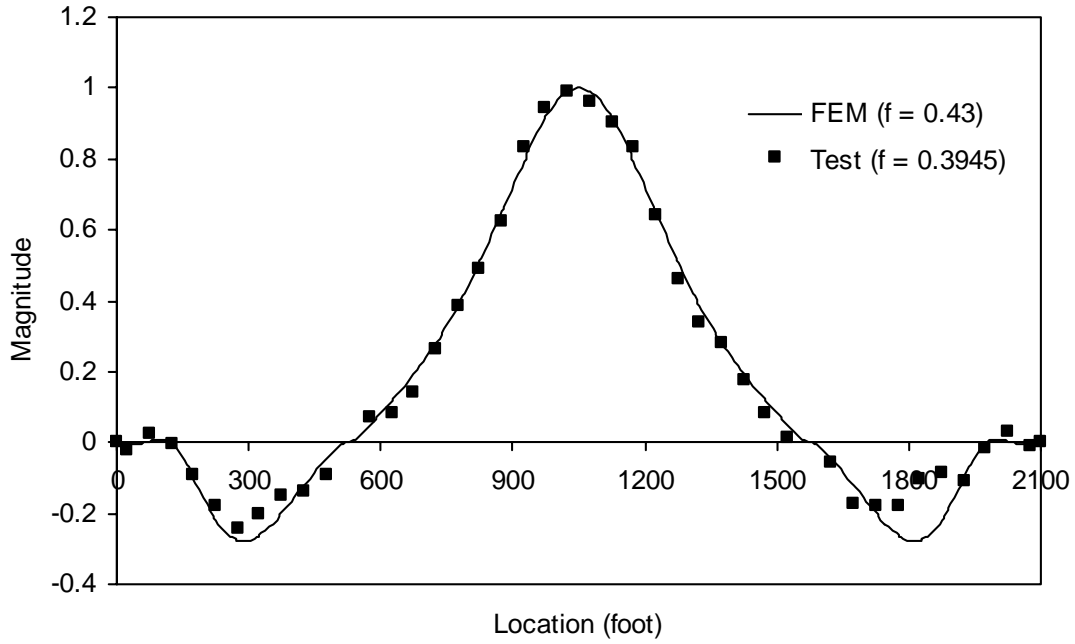


Figure 3.22 Comparison of First Vertical Mode Shape

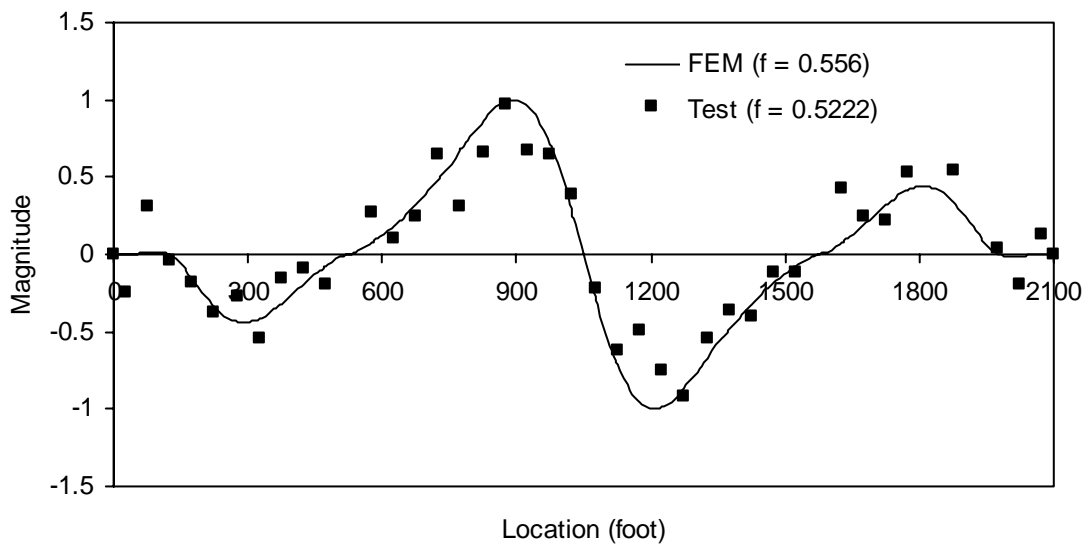


Figure 3.23 Comparison of Second Vertical Mode Shape

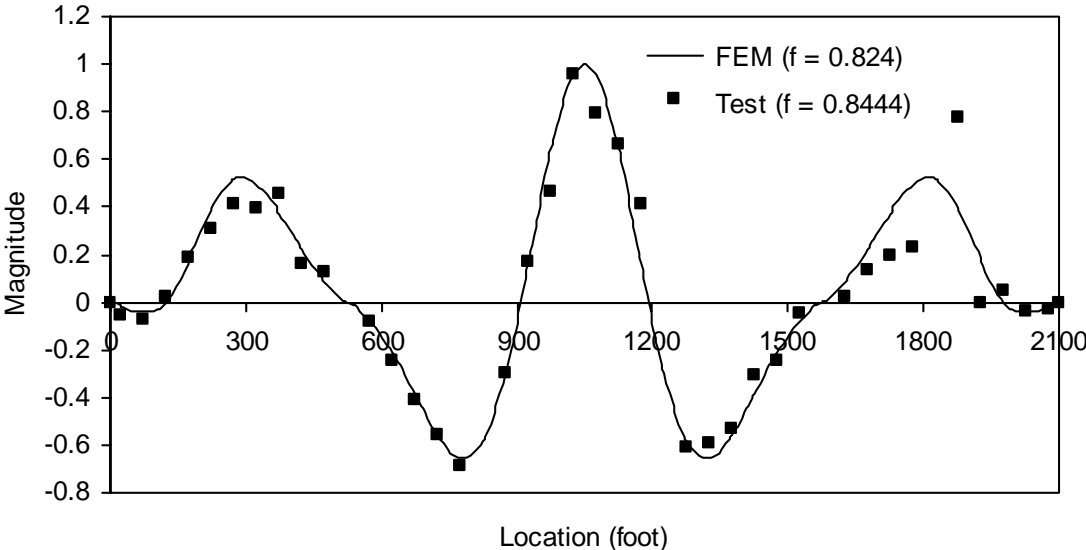


Figure 3.24 Comparison of Third Vertical Mode Shape

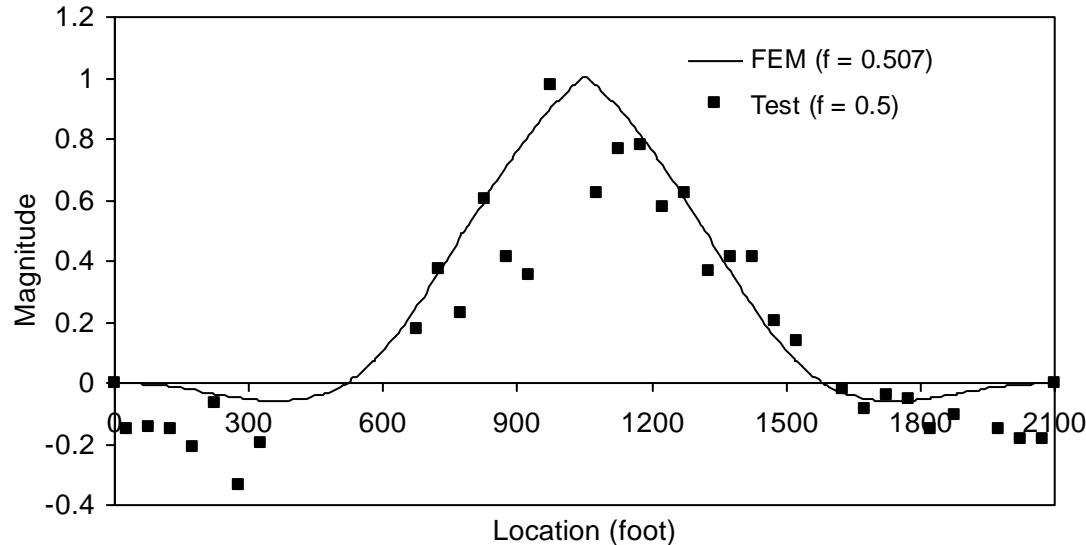


Figure 3.25 Comparison of First Transverse Mode Shape

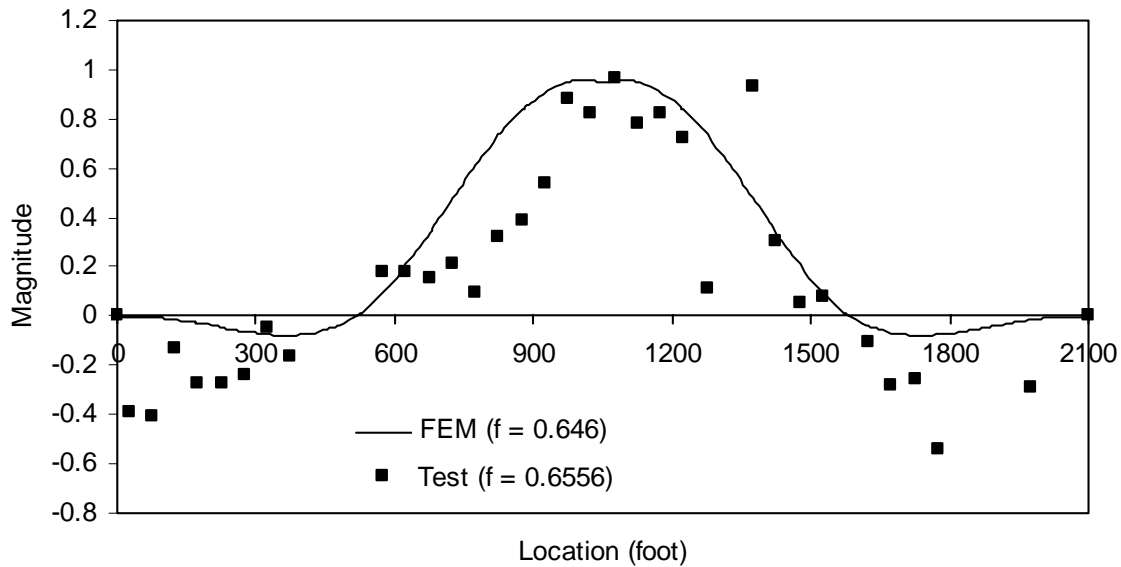


Figure 3.26 Comparison of Second Transverse Mode Shape

3.7. Remarks

A detailed 3-D finite element model has been developed for the Maysville cable-stayed bridge in order to make a start toward the evaluation of this structure. From the static analysis due to dead loads, followed by pre-stressed modal analysis, parametric studies and FE Modeling calibration, the following observations and comments can be made:

1. It is natural to discretize the cable between the tower and the edge girder into a single tension-only truss element (cable element). Two node cable elements, however, are relatively weak elements. But, since two end nodes of the cable element are connected with the beam elements of the tower and the girder, sufficient constraints at each cable node are provided and then the nonlinear static analysis or the modal analysis can be carried out.

2. The completely 3-D nonlinear modeling of a cable-stayed bridge has proved to be difficult. The smaller discretization would be computationally very large and inefficient. Convergence of such a large number of nonlinear elements is not always guaranteed. The choice of convergent criterion to control the iteration procedure becomes essential. The common force convergent criterion defaulted in the ANSYS is not so effective in the nonlinear analysis of a cable-stayed bridge. Instead, the displacement convergence criterion has proved to be effective and often results in the convergent solution.
3. Due to the cable sagging, the static analysis of a cable-stayed bridge is always a geometric nonlinear. The stress stiffening of cable elements (cable sagging effect) plays an important role in both the static and dynamic analysis of a cable-stayed bridge. Nonlinear static analysis without the stress stiffening effect will lead to an aborted run due to the divergent oscillation even though the displacement convergence criterion is used.
4. The large deflection has been demonstrated to be the limited effect on the member forces and the deck deflection of the bridge under dead loads. After introducing enough amount of initial strain in the cables, the static analysis of the Maysville cable-stayed bridge due to dead loads can be elastic and small deflection. The stress stiffening effect, however, is always required to ensure the convergent solution.
5. The initial strain in the cables is the key factor to control the initial equilibrium configuration under the dead load. For a completed bridge, the common fact is that the initial position of the cable and bridge is unknown. The initial geometry of the bridge which was modeled is really the deflected shape of the bridge loaded by the dead load. The initial equilibrium configuration of the bridge due to dead loads can be approximately achieved by referring to the bridge plans.
6. It is demonstrated that a cable-stayed bridge is a highly pre-stressed structure. The modal or any dynamic analysis must start from the initial equilibrium configuration

due to dead loads. This initial equilibrium configuration can be a small deflection static analysis because the large deflection can be ignored. The modal analysis of a cable-stayed bridge should include two steps: small deflection static analysis under the dead load and followed by pre-stressed modal analysis, so that the dead load effect on the stiffness can be included. In other words, the modal analysis of a cable-stayed bridge must be a pre-stressed modal analysis.

7. It is clearly shown that the self-weight can improve the stiffness of a cable-stayed bridge. In the case of the Maysville cable-stayed bridge, the dead load effect increases the natural frequency of the bridge due to the stiffening of the structure. Therefore, the regular modal analysis without a dead-load static analysis will underestimate the stiffness of the cable-stayed bridge and consequently provide the more safe evaluation of the bridge.
8. It is observed that one dominated mode is always coupled with other modes. The dominated mode shapes of the Maysville cable-stayed bridge in the low-frequency (0~1.0 Hz) range are mainly vertical direction. This reveals the fact that the lateral stiffness of the cable stayed bridge is stronger than that of the suspension bridge (Ren and Harik 2001).
9. From the parametric studies, it is found that the key parameters affecting the vertical modal properties are the mass, cable sectional area, cable elastic modulus and deck vertical bending stiffness. The key parameters affecting the transverse and torsion modal properties are the mass, cable sectional area, cable elastic modulus and deck lateral bending stiffness.
10. A good agreement of frequencies has been found between FE modeling and in *situ* free vibration testing. The identified frequencies from the High-speed and Bump-brake measurements are quite stable. But the mode shapes are not too good as output-only measurement does not lend itself to frequency response functions (FRFs) or

impulse response functions (IRFs) since the input force can not be measured. This is also one of the drawbacks of output-only measurements.

11. The better matching for higher modes is not expected and not realistic too, as the experimental modal properties of the bridge come from the output-only measurement.
12. The calibrated finite element model may be serviced as a baseline in the future structural analysis and monitoring of the Maysville cable-stayed bridge.

4. CABLE TESTING AND MODELING

4.1. General

Separate consideration of the cable response is motivated by the occurrence of wind-induced vibrations of bridge stay cables worldwide. Observed and documented since the mid-1980's, a particularly troublesome vibration has been observed in light-to-moderate wind combined with light rain (Hikami, 1988). "Rain-wind" vibrations led to failure of anchor details on many bridges, including the Hartman Bridge in Texas (Johnson, 1999). Researchers worldwide continue to study factors affecting wind-induced stay cable vibration toward the goal of developing design approaches for prevention and mitigation (see, for example, Matsumoto 1992, Yoshimura 1995, Pinto da Costa 1996, Main and Jones 1999, Caetano 2000a, Caetano 2000b and Main and Jones 2001).

The eighty cables of the Maysville cable-stayed bridge are unique flexible structures whose dynamic response characteristics depend on material properties, tension, and possibly temperature. The Maysville cables were constructed according to the plans with modifications as detailed in the as-built information provided by William Caroland. In the original plans, the eighty cables are nominally four sets of twenty cables. Each set is associated with either the Kentucky (South) or Ohio (North) tower and with the upstream (East) or downstream (West) side of the bridge as seen in the aerial photograph (Figure 4.1) and elevation drawing (Figure 4.2). Cables are numbered from 1 to 40 from Kentucky.

To bring the bridge deck into alignment side-to-side as the constructed sections met in the center and to smooth the vertical deck profile, cable design tensions were adjusted from those listed in the original plans. No final dead load tension difference exceeded 36% of the original dead load tension, with some tensions increasing (max 35.7% for both Cables 12E and 12W) and some decreasing (max 34.9% for both Cables 11E and 11W). Changes to all design dead load tensions are presented graphically in Figure 4.3.



Figure 4.1 Aerial View of the Maysville Bridge, January 2001

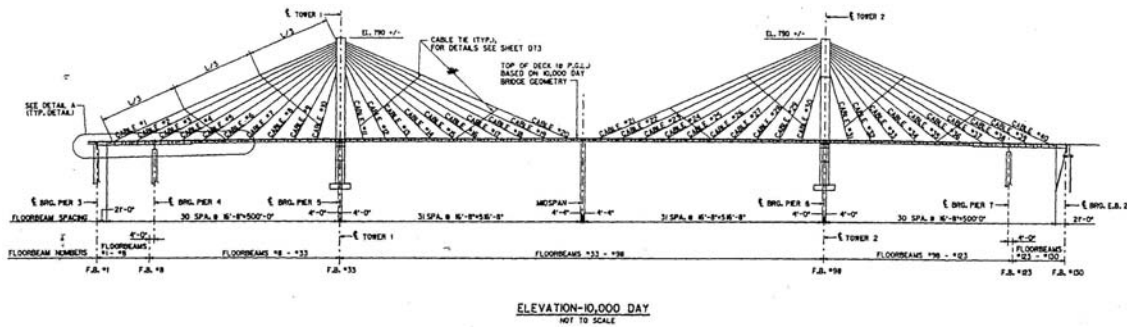


Figure 4.2 Elevation Drawing of the Maysville Bridge

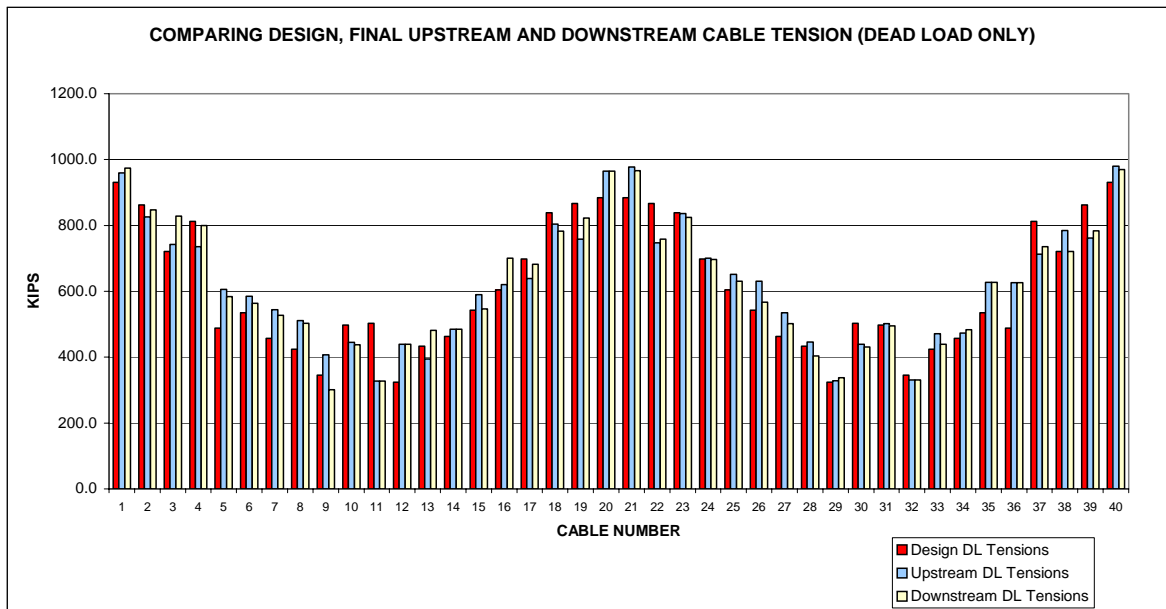


Figure 4.3 Recorded Changes to Design Tensions for Deck Alignment and Profile Adjustment

A typical cable cross section includes a number of 0.6-inch steel strands within a PE pipe (see Figure 4.4). The stands are individually coated in grease and sheathed in a black polyethylene cover. They are each wedged into the template at the deck and run up the PE pipe to the tower and fitted through a matching template. Each strand is parallel inside the stay, installed in a particular order. Theoretically one strand could be removed and replaced individually by pulling it out of its sheath inside the grouting. Cables are adjusted to their final tensions and then grouted with cement having a specific weight twice that of water. Grout is pumped in to the cables in sections from the base to the tower; the maximum section height is approximately 100 ft, the limit of the pump. Helical strikes are molded in the enclosing PE pipe and the longer cables are restrained with stranded steel “cross-ties” (See Figure 4.4) to prevent large amplitude wind-induced vibrations experienced recently on several cable-stayed bridges in North America (Schrader, 1999). Figure 4.5 shows the restrainer design.



Figure 4.4 Steel Strands in Template (left) and Helical Strikes and Cross-ties (right)

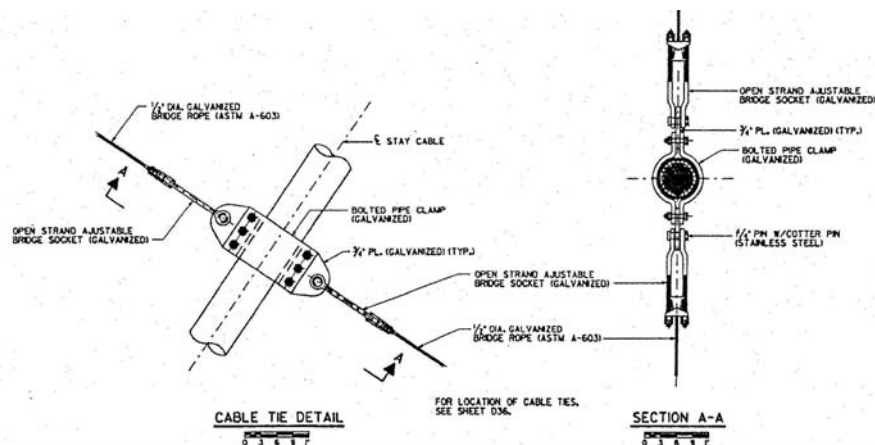


Figure 4.5 Restrainer (Cross-tie) Design Detail

Nominal Maysville cable designs are summarized in Table 4.1. Design lengths range from 164 to 526 feet; diameters range from 6.3 to 8.9 inches; and numbers of steel strands range from 24 to 43. Length, tension and weight determine the taut string frequency.

Table 4.1 Nominal Cable Designs (Cables 21-40 are Symmetric to Cables 1–20)

Cable No.	Length feet	Axial Force kips	Weight kips	Diameter inches	No. Steel Strands
1 & 40	526.26	1127.1	37.46	8.86	43
2 & 39	479.75	1073.3	34.15	8.86	43
3 & 38	433.58	928.4	30.86	8.86	43
4 & 37	387.66	967.1	22.45	7.87	37
5 & 36	344.89	636.7	19.59	7.87	35
6 & 35	301.82	696.3	17.14	7.87	35
7 & 34	261.18	575.6	9.73	6.30	24
8 & 33	224.20	689.9	8.35	6.30	24
9 & 32	192.38	460.1	7.16	6.30	24
10 & 31	164.81	566.8	6.14	6.30	24
11 & 30	164.09	572.0	6.11	6.30	24
12 & 29	190.96	541.0	7.11	6.30	24
13 & 28	222.33	558.9	8.28	6.30	24
14 & 27	258.98	589.1	9.64	6.30	24
15 & 26	299.35	722.9	17.00	7.87	35
16 & 25	342.02	783.2	19.43	7.87	35
17 & 24	386.34	872.2	21.94	7.87	35
18 & 23	432.25	1050.5	30.77	8.86	43
19 & 22	478.55	1078.1	34.06	8.86	43
20 & 21	525.25	1101.6	37.39	8.86	43

Assuming linear response, development of correlated finite element models of the cables requires field tests under a variety of conditions. Three different field tests of the cables were conducted to support development of accurate finite element models. This chapter summarizes the field-testing and test results, the modeling approaches and analysis results and closes with conclusions and recommendations.

4.2. Field Testing of the Maysville Bridge Stay Cables

Three field tests of the Maysville Bridge Stay Cables were conducted as follows:

1) January 10, 2001 – Prior to opening the bridge, loaded trucks were run to excite dynamic response of the bridge, including the cables. The acceleration responses of twenty cables (North tower, downstream side; Cables 21W-40W) and their deck anchors were recorded as trucks drove a fast pass (Figure 4.6 left) and a slower bump-and-break pass (Bump seen in Figure 4.6 right). The tests were conducted in a manner similar to that used for deck and tower response testing on January 11, 2001 described elsewhere in this report. Surface temperatures ranged from 17 to 43 degrees F. Dr. Suzanne Smith, with students Jennie Campbell, Andrew Clem, Philip Hadinata, and Vijay Kulkarni, conducted the test.



Figure 4.6 High-speed (left) and Bump-and-brake (right) tests on January 10, 2001

2) May 22, 2001 – Acceleration responses of the 40 downstream cables (Cables 1W-40W) and their deck anchors were recorded as typical light and moderate traffic traveled the bridge. Air temperatures ranged from 58 to 72 degrees F. Humidity and wind speed were also noted. Rain fell during measurements of the response of the first two cables. Dr. Suzanne Smith, Jennie Campbell and Ryan Dant conducted the test, with Dr. Charles Wang, Lancaster University, Lancaster, England.

3) August 13, 2001 - Acceleration responses of 60 cables (including all cables not tested to date) and their deck anchors were recorded as typical traffic traveled the

bridge as seen in Figure 4.7. Air temperatures ranged from 82 to 86 degrees F. The test was conducted by Dr. Suzanne Smith, Jennie Campbell, Ryan Dant, and Kin Fai Lore.



Figure 4.7 Typical Traffic Including Heavy Trucks During Test on August 13, 2001

4.2.1. First Field Test, January 10, 2001

The first field test and results are summarized in Figures 4.6 and 4.8 through 4.15 and in Table 4.2 (at the end of the field test section). The bridge was closed to traffic for the field tests. Excitation was provided by two loaded trucks, weighing respectively 64,010 and 60,750 lbs. These were driven in tandem from Kentucky to Ohio (lower right to upper left in Figure 4.1) at near 55 miles per hour (Figure 4.6 left). The lead truck traveled alone on the return, hitting a bump set to induce vertical deck motions (Figure 4.6 right) and then further on rapidly braking to a stop to induce longitudinal deck motions. Some of the test runs occurred coincident with those reported in Chapter 2, but differences in testing approaches (record lengths, for example) and no simultaneous measurement capability precluded synchronized testing of the cables with the superstructure.

Cable response measurement proceeded as with previous successful tests of cables of two bridges in Texas (Johnson 1999, Schrader 1999) with cables comparable to these. Two triaxial accelerometers (PCB Piezotronics, Inc. model 3703G3FD3G) were used to measure three-dimensional accelerations of each cable and anchor (representing the motion of the deck); voltage signals were recorded for 60 seconds at a sampling rate of 200 Hz to a notebook PC using Iotech's Wavebook/512 12-bit, 1 MHz Data

Acquisition System. The first accelerometer was placed on the anchor; the second was mounted securely to the cable as far up as could be reached without a lift (Figure 4.8). Both accelerometers were oriented with respect to the cable with the x-axis parallel to the longitudinal axis, the y-axis transverse to the cable horizontally for out-of-plane motion (this is lateral with respect to the bridge deck), and the z-axis transverse to the cable in the vertical plane of static equilibrium. One channel of the anchor accelerometer failed during the test, so its orientation was changed to measure the y- and z-axis directions (note different orientation in Figure 4.8). Simultaneous measurement of tower anchor motion for each cable was not possible. However, note that superstructure testing showed tower motion to be one-to-two orders of magnitude smaller than deck motions.



Figure 4.8 Typical Accelerometer Mounting (top left) and Orientation on Cable (top right) and Anchor (bottom)

Figure 4.9 presents typical anchor measurements for downstream cable number 29, an unrestrained cable about one quarter distance from the Ohio side. The high speed pass is presented on the left; the “bump and brake” pass is presented on the right. In each case, the top plot is the x-direction acceleration response, the second plot is the y-

direction acceleration response and the third subplot is the z-direction acceleration response. Note that significant motion of the anchorage starts when the truck(s) first encounter the bridge deck, at approximately 3 seconds for the high-speed pass and at approximately 7 seconds for the bump and brake test. In Figure 4.9 right, the bump is seen at 17 seconds and the brake and ring-down afterwards start at 22 seconds. Corresponding cable response accelerations are seen respectively in Figures 4.10 left and right. Significant cable accelerations (maximum acceleration of 0.05 g to 0.1 g) were excited in all three directions in both cases.

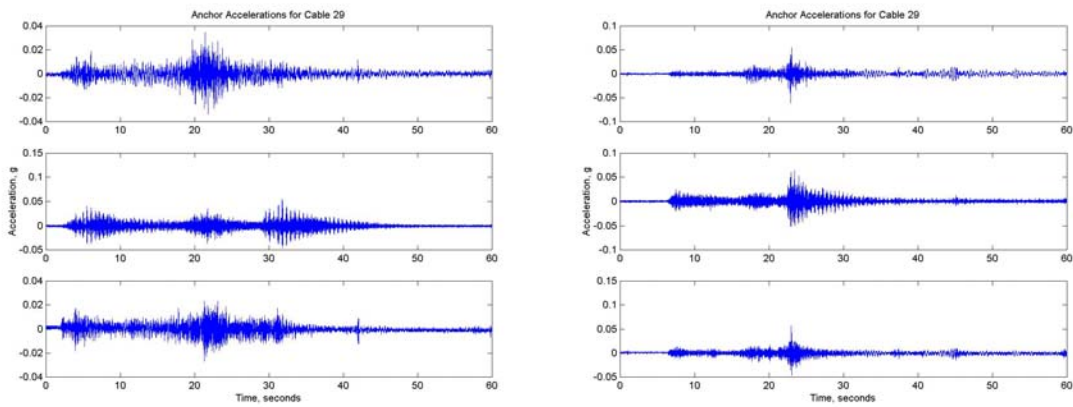


Figure 4.9 Anchor 29W Acceleration Time Histories: Fast (left) and Bump-and-brake (right)

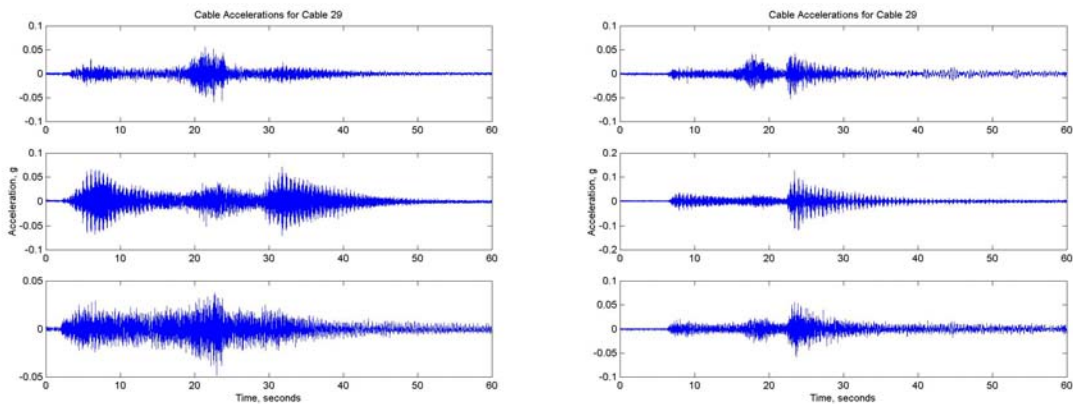


Figure 4.10 Cable 29W Acceleration Time Histories: Fast (left) and Bump-and-brake (right)

The Power Spectral Density (PSD) of an acceleration time history shows the frequency content (the “spectrum”) of the measured signal. PSDs are used to determine the cable fundamental frequency, to understand the response and to correlate models. Examination of the frequency content of the cable response yields the frequency of the

first (fundamental) cable mode as the difference between the excited higher modes (harmonics) (Smith and Johnson 1998, Johnson 1999). PSDs were computed using MATLAB[®] for the anchor and cable accelerations. In each case, overlapping (by 256 points) windows of the auto-correlation of the acceleration time history were converted with a 1024-point Fast Fourier Transform (resulting frequency resolution 0.2 Hz) and then averaged.

Anchor (left) and cable (right) spectra for each response axis are shown for the fast test in Figure 4.11. The anchor response to the fast test consists of frequencies primarily between 10 and 40 Hz, which is usual for high-speed traffic. Note that this record also includes significant low-frequency content in the x- and z-directions. The transverse cable response spectra in the y- and z-directions contain excited harmonics (integer multiples) of the fundamental frequency, typical taut string behavior. The spacing of the harmonics is therefore the fundamental frequency. For this unrestrained cable, the transverse y- and z-directions both show harmonic responses. The z-direction is in the vertical plane, and is better excited in this fast test. Figure 4.12 is the anchor and cable spectra for the bump and brake test. Transverse cable response is seen again in the 10 to 40 Hz range, with taut string harmonics clearly visible in both the y- and z-directions. Cable harmonic response can also be seen reflected in the anchor motion in the y-direction.

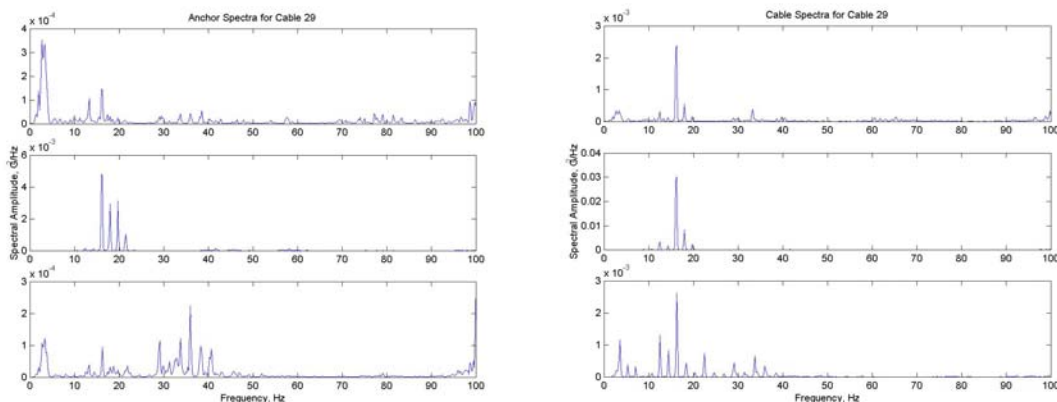


Figure 4.11 29W Fast Test Acceleration Spectra: Anchor (left) and Cable (right)

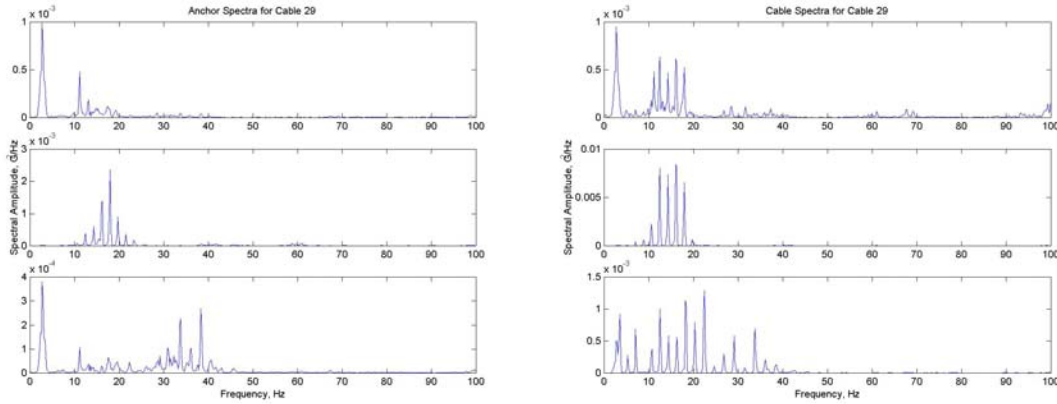


Figure 4.12 29W Bump and Brake Acceleration Spectra: Anchor (left) and Cable (right)

Automated analysis of the 20 bridge stay cable y-direction spectra was accomplished with Cepstrum signal processing (Smith, Johnson and Schrader 2000) applying a Fast Fourier Transform (FFT) size of 512 samples (no averaging) to the initial spectra computed using a 1024-point FFT. This “spectrum of a spectrum” is sometimes referred to as the “Cepstrum” (Harris 1996). In essence, this finds the frequency of the harmonics in the spectrum. Bridge stay cables, like rotating machinery where this approach is used, exhibit response spectra that include many harmonic peaks. The Cepstrum result is a dominant peak in a time-domain plot (Figure 4.13) that is the period of the fundamental frequency. The resulting time-domain resolution here is 0.01 seconds. Since the resulting period is the inverse of the fundamental frequency, this time-domain resolution gives a variance of the frequency results ranging from 0.6% for the longest cables (with fundamental frequency near 0.5 Hz) and 2.0% for the shortest cables (with fundamental frequency near 2.0 Hz).

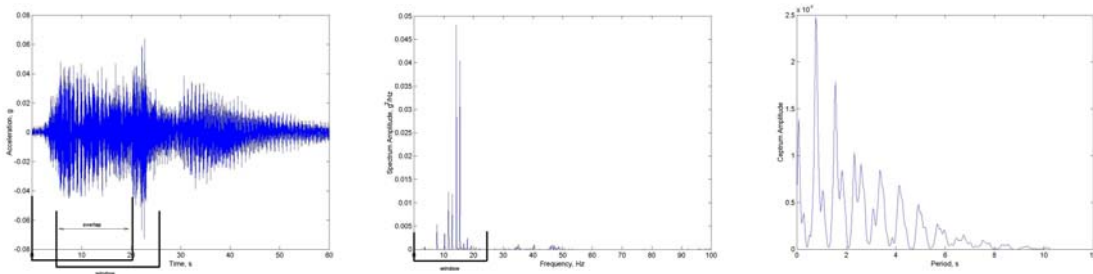


Figure 4.13 A Typical Cepstrum Analysis to Determine Fundamental Frequency: Time History (left), Spectrum (middle) and Cepstrum (right)

Table 4.2 (at the end of the field test section) presents the resulting fundamental frequencies for all cables tested determined from the transverse (y) measurements for the two recorded data sets of the first field test. These are compared to fundamental frequencies determined from the as-built specifications using a taut string model:

$$f = \frac{1}{2L} \sqrt{\frac{T}{m}}$$

where f is the fundamental frequency in cycles per second, L is the free length in feet, T is the tension in lbs, and m is the mass per unit length of the string in lbs-s²/ft².

In the transverse (y) direction, restrainers do not appreciably influence small-amplitude response, so the free length is the entire length of the cable (work points B to D on the plans). In the in-plane (z) direction, the restrainers serve to establish fixed points and to effectively shorten the cable free length. Response spectra for the Maysville cables in the y-directions showed taut-string characteristics more consistently. Therefore, y-direction spectra were used to determine the unrestrained fundamental frequencies of the Maysville cables for model correlation. The first column of Table 4.2 is the cable designation. The second column of Table 4.2 is the predicted transverse fundamental frequency using axial forces determined as the combined effect of the as-built dead load and the in-service load. The next two columns are respectively the transverse fundamental frequency results for the “fast” and “bump-and-brake” tests.

Cable fundamental frequencies determined via Cepstrum analysis of out-of-plane transverse (y-direction) response for both the fast and bump and brake tests are plotted in comparison to taut string frequencies calculated for the cables using as-built tensions in Figure 4.14. The experimental frequencies were generally greater than the taut-string predictions. The difference is larger for longer cables (21, 22, 23, 39, 40) and for shorter cables (28 through 33).

In shorter cables, bending effects omitted from the taut string model could explain the difference. Note that the anchor and cable surface temperatures during this series of tests varied from 18 to 33 degrees F as seen in Figure 4.15. Longer cables were tested at the beginning and end of the day when temperatures were generally lower. Results under these conditions will be compared to results at higher temperatures.

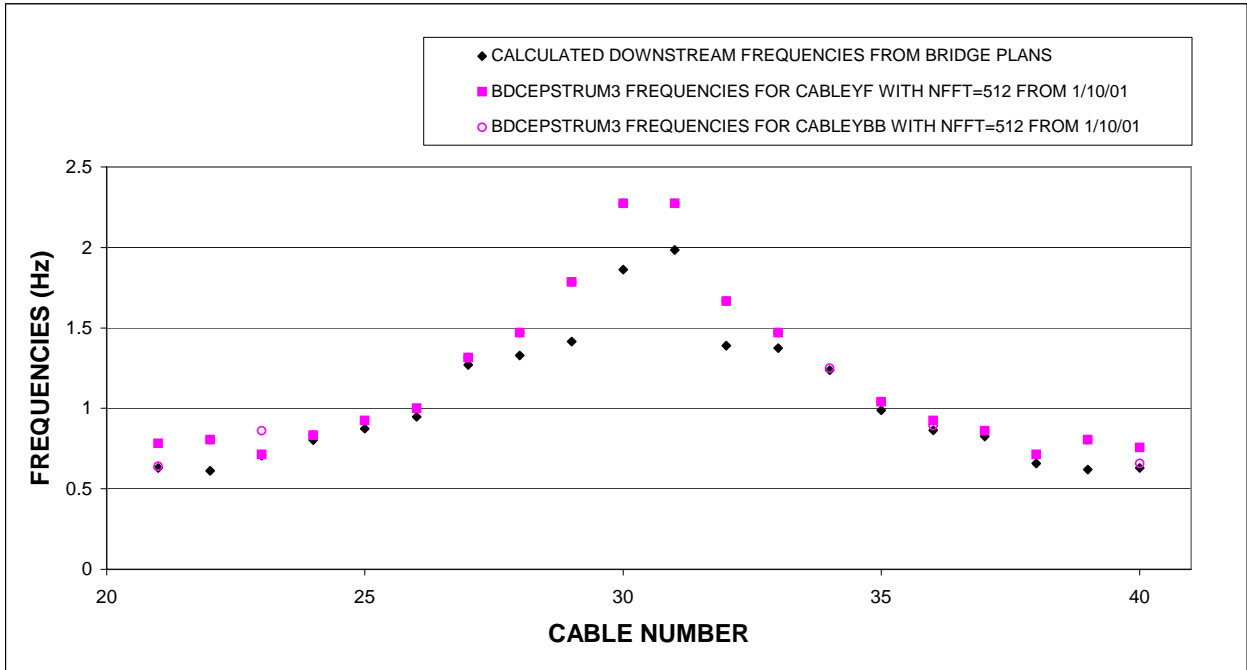


Figure 4.14 Frequencies of Cables 21-40W: String Models and First Field Test Results

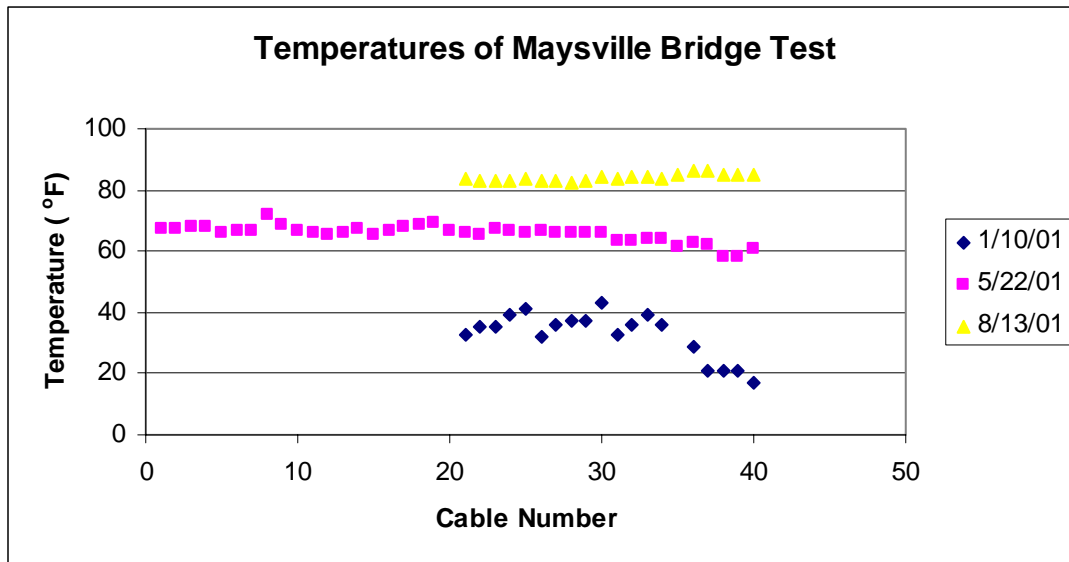


Figure 4.15 Temperatures Recorded for All Field Tests: Surface Temperatures (1/10/01) and Air Temperatures (5/22/01 and 8/13/01)

4.2.2. Second Field Test, May 22, 2001

The second field test and results are summarized in Figures 4.16 through 4.24 and in Table 4.2 (at the end of the field test section). Acceleration response measurements

were made for all 40 downstream (West) cables. The bridge was not closed to traffic for this test; excitation was provided only by the traffic crossing the bridge. At some times this was heavy, including one or two large trucks. At other times the traffic was light to very light, including only a few cars, if that. At least two measurements were recorded for each cable, noting heavier traffic and lighter traffic, if possible. For measurements of cables 31 to 40, both lanes of traffic were open and traffic traveled at normal speed (50-60 mph). For measurements of cables 1 through 30, one lane of the bridge was closed for restrainer collar installation and traffic proceeded at a slower speed. Rain fell during measurements of cables 39 and 40, but stopped as the testing proceeded from cable 39 to cable 1.

Again, two triaxial accelerometers (PCB Piezotronics, Inc. model 3703G3FD3G) were used to measure three-dimensional accelerations of each cable and anchor. Voltage signals were recorded for 60 seconds at a sampling rate of 200 Hz to a notebook PC using Iotech's Wavebook/512 12-bit, 1 MHz Data Acquisition System. The first accelerometer was placed on the anchor; the second was mounted securely to the cable as far up as could be reached without a lift. Both accelerometers were oriented with respect to the cable with the x-axis parallel to the longitudinal axis, y-axis transverse to the cable horizontally for out-of-plane motion (lateral to bridge deck), and z-axis transverse to the cable in the vertical plane of static equilibrium. Figure 4.16 includes selected pictures of the second field test.

Figure 4.17 presents typical cable accelerations for downstream cable numbers 32 and 33 near the north tower of the bridge. On the left are accelerations from a heavier-traffic measurement; on the right are a lighter-traffic measurement. The maximum amplitudes of the heavier-traffic accelerations seen here neared 0.05 g's, five times larger than maximum accelerations with lighter traffic. Overall, heavier-traffic accelerations ranged from 0.05 g's to Over 0.1 g, comparable to the accelerations seen in the January tests with the loaded trucks. Figure 4.18 presents the corresponding spectra, computed as above. Spectra for both heavy and light traffic data sets included multiple harmonics and so were useful for identification of fundamental cable frequencies.



Figure 4.16 Second field test: in the rain (top left), measuring wind speed (top right) and data acquisition system (bottom).

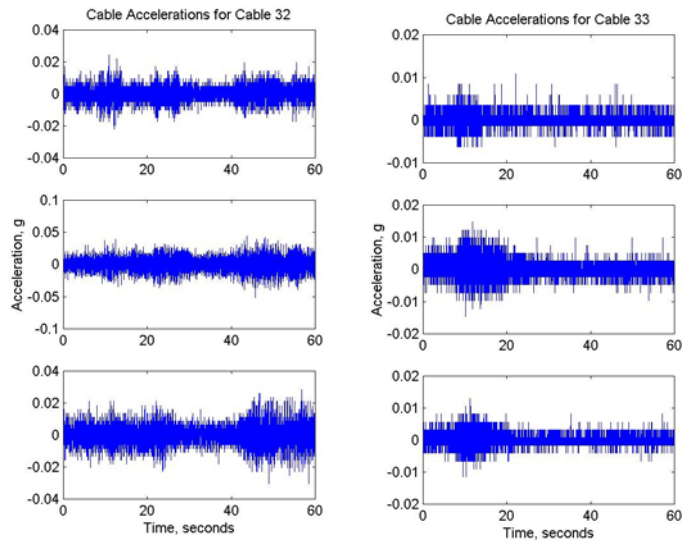


Figure 4.17 Typical Accelerations for Heavier Traffic, Cable 32 W (left) and Lighter Traffic, Cable 33 W (right) on May 22, 2001

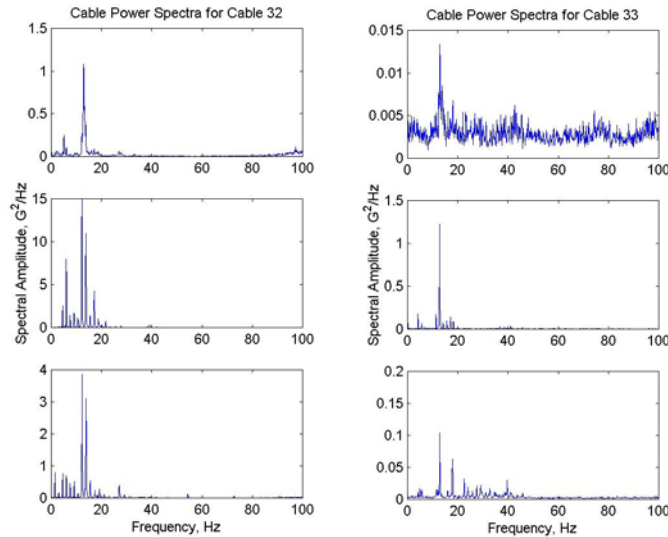


Figure 4.18 Typical Spectra for Heavier Traffic, Cable 32 W (left) and Lighter Traffic, Cable 33 W (right) on May 22, 2001

Automated analyses of 37 of the 40 bridge stay cable y-direction spectra to find fundamental cable frequencies were accomplished with Cepstrum signal processing as before. (Three cables were tested during the rain event described in the next section and omitted from these results.) Results for both heavy- and light-traffic accelerations are presented in Figure 4.19, also including results from the first field test. Results from the two tests are nearly the same, with the exception of the longer cables. For this second test, the longer cable frequencies are lower, matching the string model predictions. Shorter cable frequencies are consistent with those of the first test and higher than string-model predictions.

Temperature effects are one possible explanation for the difference between the longer cable fundamental frequencies. Many structural test programs have shown significant modal frequency differences when the structure is tested under different temperatures. Power-line cables are known to change length (and hence fundamental frequency) with temperature as well. Another possible explanation for the temperature difference is a “breaking-in” effect of the anchor castings. With use of the bridge, rough surfaces of the anchor castings are expected to wear to a certain point, thus affecting the tension in the cables and their frequency. A test of a few cables of the Maysville cable-stayed bridge is planned for January 2004 (after this project is completed) to provide answers about the magnitude of temperature effects on frequencies of the longer cables.

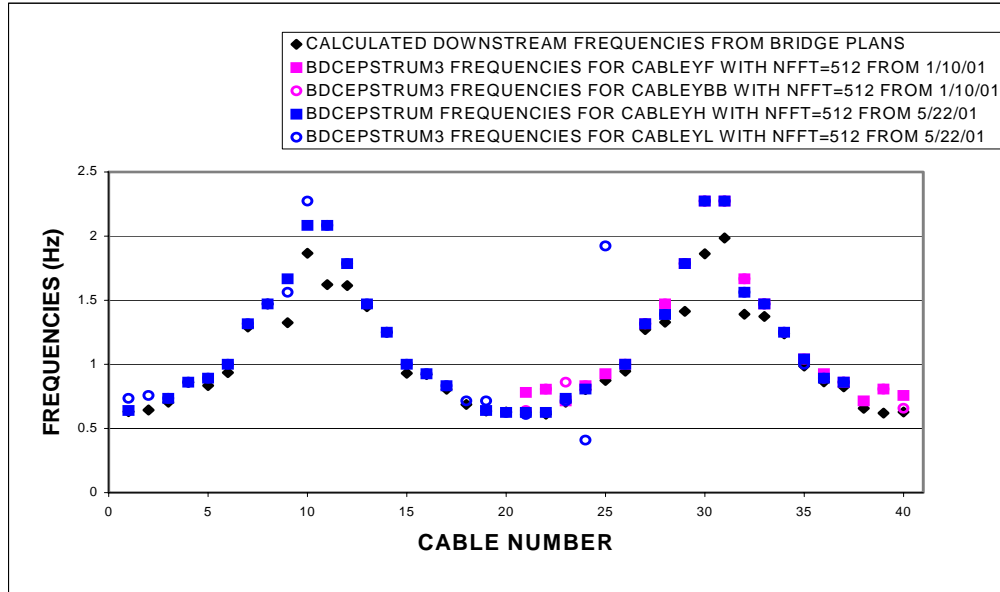


Figure 4.19 Frequencies of Cables 1-40W: String Models, First and Second Test Results

4.2.3. Rain Event during the Second Field Test, May 22, 2001

As we arrived and were setting up the equipment to start at downstream Cable 40W, a rain shower began. As seen in Figure 4.20, rivulets formed on the underside of the cable and streamed from its base. Ties (ribbons) on the restrainer collars served as wind speed and direction indicators. We watched these ribbons throughout the day and they typically were parallel indicating consistent winds at different heights above the deck. The ties were more horizontal when wind speeds were larger and more vertical when wind speeds were smaller.

The helical strand on the outside of the cables is intended to disrupt rivulet formation and flow. It did disrupt the rivulet for a short distance (approximately 1/10 the distance between the helical strands), then the rivulet returned to its uninterrupted path. Testing of cable 40W and cable 39W proceeded in the rain that then stopped for the remainder of the day.

Figures 4.21 and 4.22 are plots of the acceleration response of cables 40W and 39W with rain and traffic. In each plot, the z-direction cable acceleration time history is plotted, overlaid with the three axes of the corresponding anchor acceleration time histories. The cable response direction (z) is transverse to the cable, in the vertical plane. This is the plane of the cable restrainers.

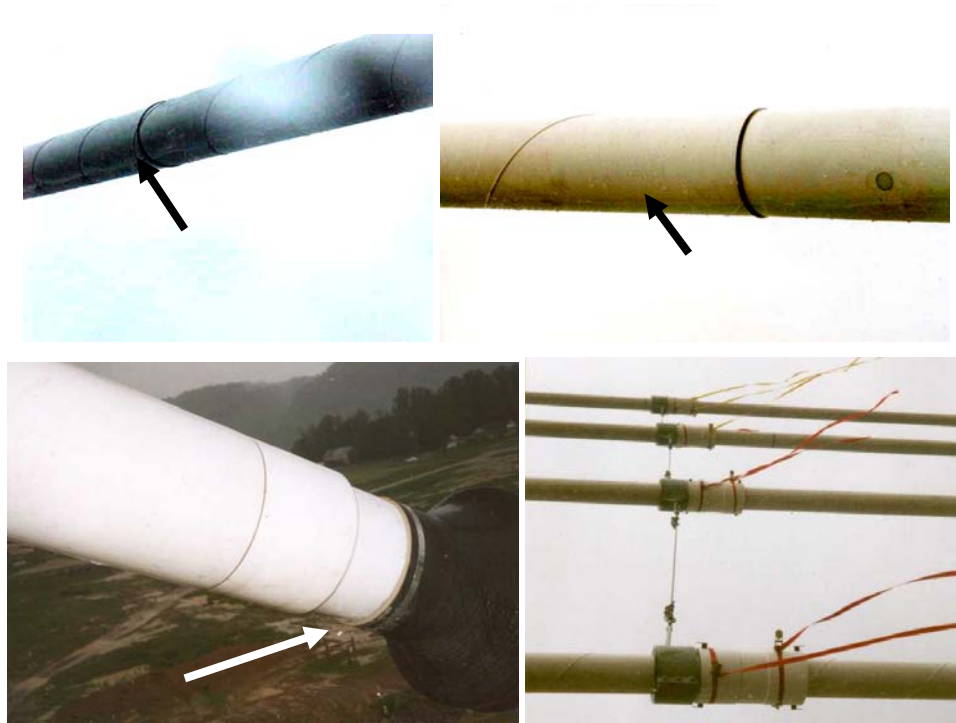


Figure 4.20 Underside rivulet on Cable 40W (top left and right, with contrast enhanced), Rivulet Stream Leaving Cable (bottom left), and Restrainer Collar Ribbons Showing Wind Speed and Direction and Underside Rivulet (bottom right)

During the heavier rain of the event, the cable response of Cable 40W (Figure 4.21) is unrelated to the anchor motion. The response is consistent throughout the record, with periodic amplitude modulations. For this heavier rain, the maximum amplitude of the response is about 0.05 g's - more than that with light traffic, but less than the maximum response with heavy traffic. Figure 4.22 presents the rain response of Cable 39 W for lighter rain, along with response after the rain had stopped. The rain response is smaller in amplitude with the lighter rain (maximum amplitude about 0.02 g's), but still consistent amplitude modulated response unrelated to the anchor motion. Once the rain stopped, the cable response is nearly identical to the anchor motion.

Response with these characteristics (limited amplitude, with modulating amplitude) is often seen with systems that can move easily between hard limits. In the z direction, the restrainer design allows the cable to move with little resistance (the elastomer pad between the cable and the surrounding pipe clamp) before coming to hard limits imposed by the pipe clamps. From this admittedly limited data, the restrainers

appear to be acting to limit the motion of the cables. Recorded accelerations did not exceed those resulting with normal heavy traffic.

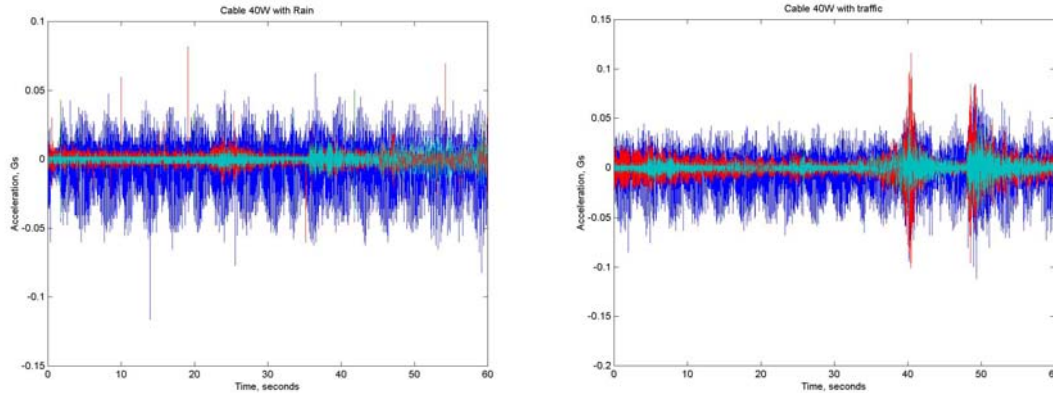


Figure 4.21 Transverse (z) acceleration of Cable 40W overlaid with tri-axial anchor accelerations in rain with light traffic (left) and heavy traffic (right)

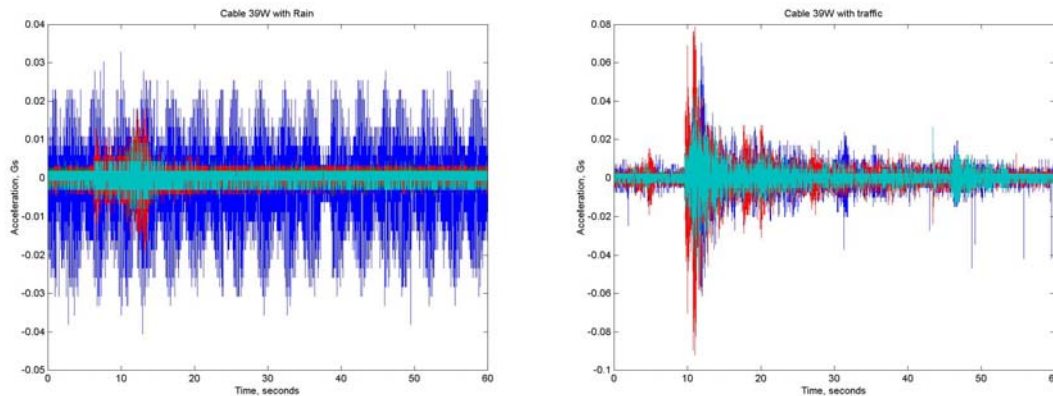


Figure 4.22 Transverse (z) acceleration of Cable 39W with tri-axial anchor accelerations in rain with light traffic (left) and after rain has stopped with heavy traffic (right)

Rain events are difficult to measure without an installation of sensors that continuously monitor rain, wind and acceleration response. Continuous monitoring systems are installed with a pc computer on site and a set of sensors. If certain threshold values are crossed, the system begins recording a large set of data for analysis (for example, Main and Jones 2001).

4.2.4 Third Field Test, August 13, 2001

The third field test and results are summarized in Figures 4.23 through 4.25 and in Table 4.2. Acceleration response measurements were made for all 40 upstream (East) cables and the 20 downstream (West) cables tested twice previously. The bridge was not closed to traffic for this test; excitation was provided only by the traffic crossing the bridge. At some times this was heavy, including large trucks. At other times the traffic was light. Two measurements were recorded for each cable, noted as A and B, along with comments on traffic. The previous test had shown that fundamental frequencies are able to be identified with response measurements resulting from both heavy and light traffic.

As with the previous two tests, two triaxial accelerometers (PCB Piezotronics, Inc. model 3703G3FD3G) were used to measure three-dimensional accelerations of each cable and anchor. Voltage signals were recorded for 60 seconds at a sampling rate of 200 Hz to a notebook PC using Iotech's Wavebook/512 12-bit, 1 MHz Data Acquisition System. The first accelerometer was placed on the anchor; the second was mounted securely to the cable as far up as could be reached without a lift. Both accelerometers were oriented with respect to the cable with x parallel to the longitudinal axis, y transverse to the cable horizontally for out-of-plane motion (this is lateral with respect to the bridge deck), and z transverse to the cable in the vertical plane of static equilibrium. Redundant accelerometers were used to provide back-up measurements in the event that problems developed with measurements in any direction. Figure 4.23 includes selected pictures of the third field test.

Automated analyses of the 40 upstream and 20 downstream bridge stay cable y-direction spectra to find fundamental cable frequencies were accomplished with Cepstrum signal processing as before. Results for both (A and B) recorded acceleration time histories for the 20 downstream cables are presented in Figure 4.24, also including results from the first and second field tests. Results from the three tests are nearly the same, with the exception of the longer cables. Here again, frequencies of the longer cables are lower than those of the first test, and closer to matching the string model predictions. Shorter cable frequencies are consistent with those of the first two tests and higher than string-model predictions.

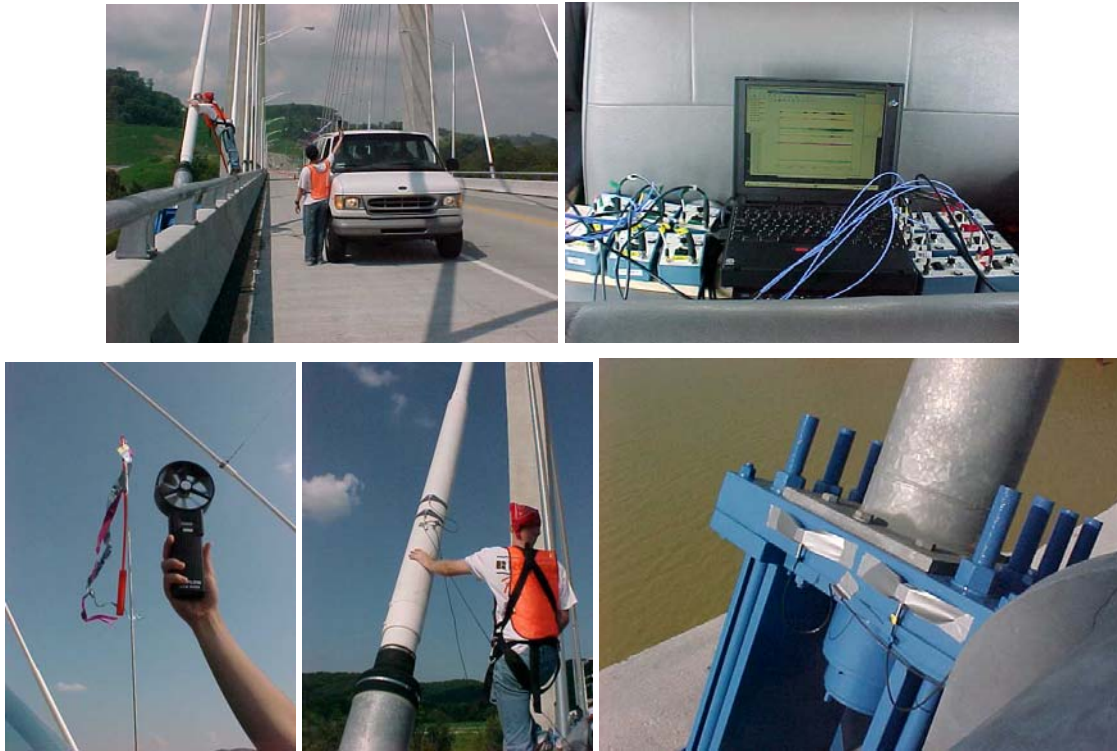


Figure 4.23 Third field test in progress (top left), data acquisition (top right), measuring wind speed and direction (bottom left), and cable / anchor sensor placement (bottom middle / right).

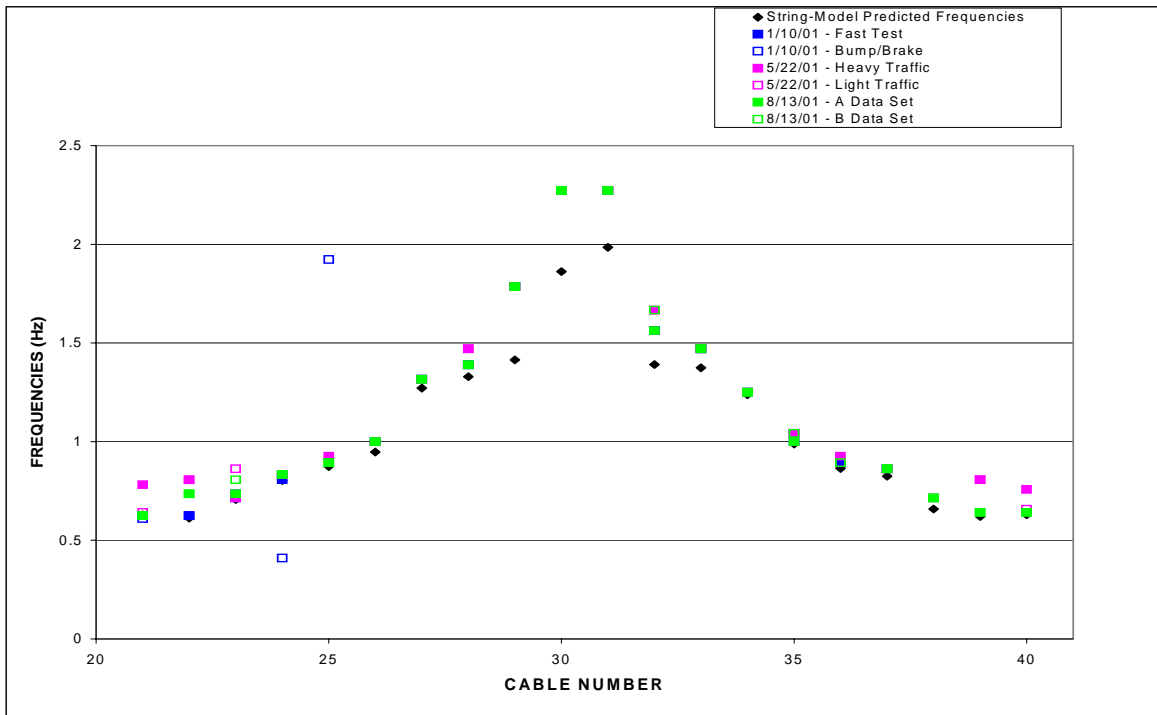


Figure 4.24 Frequencies of Cables 21-40W: String Model and All Field Test Results

Figure 4.25 presents the analysis results of the 40 upstream (East) cables, along with the computed string frequency. Since redundant sensors were used for each measurement, results for four data sets are presented: A and B for each of accelerometers #3 and #4. Four results are disregarded as not reasonable. Automated processing of large data sets occasionally results with computed Cepstrum frequencies that are not reasonable; here 4 of 160 (2.5%) results are inconsistent with other results and string frequency predictions. The remaining results are seen to have similar relationship to the string frequency predictions as seen with the downstream (West) cables. Shorter (higher-frequency) cables have higher frequencies than taut-string model predictions. Longer (lower-frequency) cables also have higher measured frequencies than taut-string model predictions. Here, however, we see the resolution of the method illustrated with differences between corresponding measurements on the same cable. From this, differences between the May and August tests of the downstream cables are within resolution of the method, but differences of the January tests for the longest cables are outside the resolution of the identification approach.

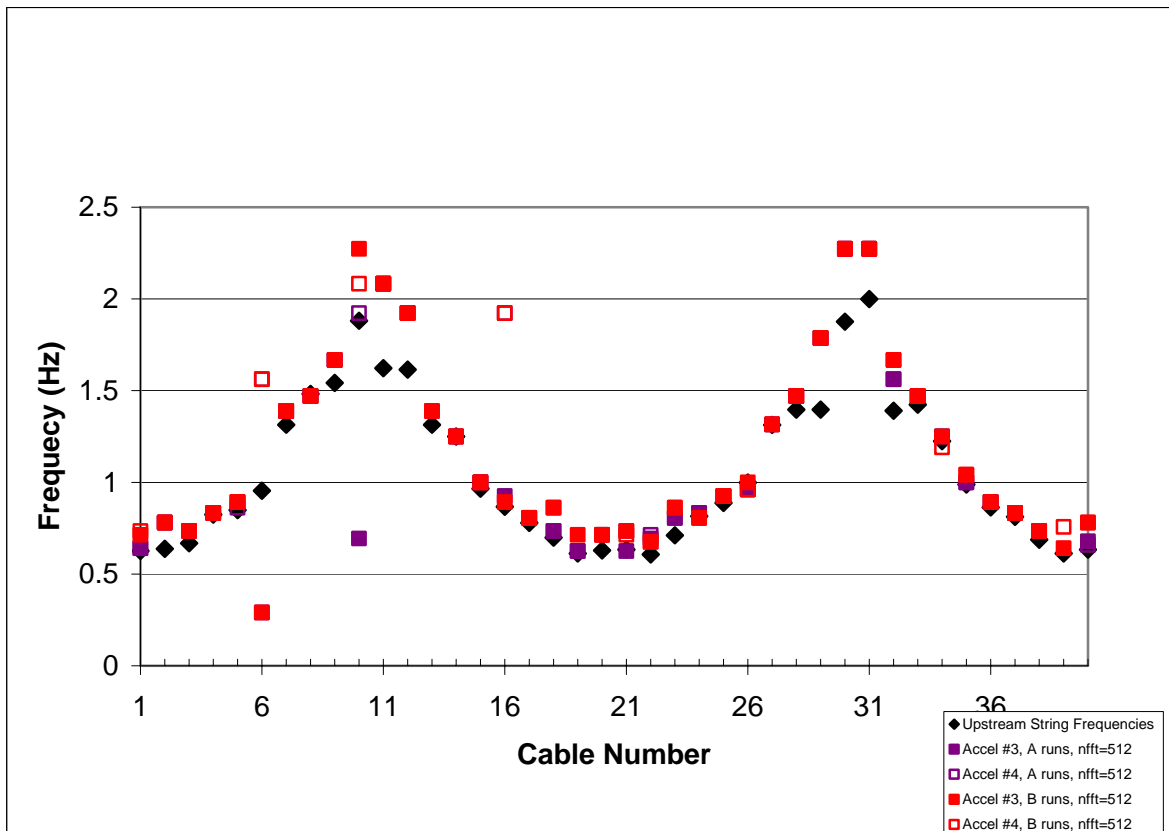


Figure 4.25 Frequencies of Cables 1-40E: String Model and All Field Test Results

Table 4.2 Numerical Results from Cepstrum Analysis of All Tested Cables

#	West String Freq.	West Fast 1/10/01	West Bump 1/10/01	West Heavy 5/22/01	West Light 5/22/01	West A 8/13/01	West B 8/13/01	East A (accel3) 8/13/01	East B (accel3) 8/13/01	East String Freq.
	Hz	Hz	Hz	Hz	Hz	Hz	Hz	Hz	Hz	Hz
1	0.631	-	-	0.641	0.735	-	-	0.641	0.714	0.626
2	0.645	-	-	-	0.758	-	-	0.781	0.781	0.637
3	0.706	-	-	0.735	0.735	-	-	0.735	0.735	0.668
4	0.860	-	-	0.862	0.862	-	-	0.833	0.833	0.825
5	0.834	-	-	0.893	0.893	-	-	0.893	0.893	0.849
6	0.936	-	-	1.000	1.000	-	-	-	-	0.954
7	1.292	-	-	1.316	1.316	-	-	1.389	1.389	1.314
8	1.471	-	-	1.471	1.471	-	-	1.471	1.471	1.482
9	1.326	-	-	1.667	1.563	-	-	1.667	1.667	1.542
10	1.866	-	-	2.083	2.273	-	-	-	2.273	1.881
11	1.622	-	-	2.083	2.083	-	-	2.083	2.083	1.622
12	1.614	-	-	1.786	1.786	-	-	1.923	1.923	1.614
13	1.450	-	-	1.471	1.471	-	-	1.389	1.389	1.314
14	1.250	-	-	1.250	1.250	-	-	1.250	1.250	1.25
15	0.930	-	-	1.000	1.000	-	-	1.000	1.000	0.966
16	0.921	-	-	0.926	0.926	-	-	0.926	0.892	0.867
17	0.805	-	-	0.833	0.833	-	-	0.807	0.807	0.779
18	0.688	-	-	-	0.714	-	-	0.735	0.862	0.698
19	0.637	-	-	0.641	0.714	-	-	0.625	0.714	0.612
20	0.629	-	-	0.625	0.625	-	-	-	0.714	0.629
21	0.629	0.781	0.641	0.625	0.610	0.625	0.625	0.625	0.735	0.633
22	0.612	0.806	0.807	0.625	0.625	0.735	0.735	0.694	0.676	0.607
23	0.706	0.714	0.862	0.735	0.714	0.735	0.807	0.807	0.862	0.711
24	0.803	0.833	0.833	0.807	0.410	0.833	0.833	0.833	0.807	0.816
25	0.874	0.926	-	-	1.923	0.893	0.893	0.926	0.926	0.888
26	0.947	1.000	-	1.000	1.000	1.000	1.000	0.962	1.000	0.999
27	1.271	1.316	1.316	1.316	1.316	1.316	1.316	1.316	1.316	1.313
28	1.329	1.471	1.471	1.389	1.389	1.389	1.389	1.471	1.471	1.397
29	1.414	1.786	1.786	1.786	1.786	1.786	1.786	1.786	1.786	1.397
30	1.862	2.273	2.273	2.273	2.273	2.273	2.273	2.273	2.273	1.876
31	1.985	2.273	2.273	2.273	2.273	2.273	2.273	2.273	2.273	1.999
32	1.391	1.667	1.667	1.563	1.563	1.563	1.667	1.563	1.667	1.391
33	1.374	1.471	1.471	1.471	1.471	1.471	1.471	1.471	1.471	1.424
34	1.238	-	1.250	1.250	1.250	1.250	1.250	1.250	1.250	1.224
35	0.988	1.042	1.042	1.042	1.000	1.000	1.042	1.000	1.042	0.988
36	0.864	0.926	0.893	0.893	0.893	-	0.893	0.893	0.893	0.864
37	0.825	0.862	0.862	0.862	0.862	0.862	0.862	0.833	0.833	0.812
38	0.658	0.714	-	-	-	0.714	0.714	0.735	0.735	0.687
39	0.620	0.807	0.807	-	-	0.641	0.641	-	0.641	0.612
40	0.629	0.758	0.658	-	-	0.641	0.641	-	0.781	0.633

4.3. Finite Element Analysis

Finite element (FE) models were developed for the Maysville Bridge cables using cable properties from the original drawings and as-built information provided after the construction was completed. This section describes the development of the FE models of the unrestrained cables and of a set of ten restrained cables, and comparison of the results to those of the field survey experiments. Cable models were developed using ANSYS finite element software. Independent model verification was performed by Jeff Gagel.

The Maysville Bridge includes 80 cables in eight sets of 10 cables. Two parallel lines of cables, designated “upstream” and “downstream” include cables numbered from 1 to 40 from the Kentucky to the Ohio side of the bridge. To describe the development of an FE model of a representative set of ten cables, downstream cables 21 to 30 will be the focus of the discussion. Data to enable development of similar models of all 80 cables is included.

Each cable model is developed using three-dimensional beam elements (ANSYS Beam Element Type 4). Prior experience modeling bridge stay cables indicated that bending effects should be included for correlated models of some cables, so beam elements were used herein. Each cable is modeled with 35 nodes, with nodes 1 and 35 respectively at the coordinates specified as Work Points B and D, and the others equally spaced between the endpoints. Thirty-four beam elements are defined between each consecutive pair of end points. Representing fixed boundary conditions, all six degrees-of-freedom (DOFs) are restrained for the two endpoints of each cable. The cable tension was incorporated in the analysis by first performing a static analysis to prestress the cables. A block Lanczos modal analysis was run to determine the fundamental frequencies of the cables.

Note that consideration of the effect of deck motion on the dynamic response of the cables is beyond the scope of this project, although separate efforts have considered nonlinear FE modeling of a cable excited by motion of the bridge deck through the anchor (Fujina, Warnitchai and Pacheco 1993, Lilien and Pinto da Costa 1994, Smith and Baker 2001, Baker and Smith 2002, Jean 2003). Some patterns of response seen in the Maysville Bridge cables, specifically the bandwidth of the response spectrum in the

horizontal (out-of-plane) direction, appear correlated to patterns of motion of the bridge deck (Campbell and Smith 2003).

Varying cable geometry and material properties necessary to develop FE models of each individual cable include diameter, Young’s modulus, mass density and initial strain. These properties are summarized, along with coordinates of the endpoints of the cables, in Table 4.3. Endpoints of the cables were defined as Work Points B and D of the drawings. As has been used on prior cable-stayed bridge projects, the effective Young’s moduli were computed using Kollbruner’s relation (Kollbruner, Hajdin and Stipanis, 1980). The mass densities were computed using the cable fabricated length, weight per unit length and cross section area. Also in the models, two additional properties were specified for all cables: Poisson’s ration and modal damping. Poisson’s ratio was specified as 0.30. Modal damping was specified to be one quarter of one percent, 0.0025. Note that modal damping does not enter into the normal modes computation performed with these models. Figure 4.26 presents the finite element model mesh with boundary conditions indicated. Table 4.4 and Figure 4.27 present the computed fundamental frequencies compared to experimental results (repeated here for ease of reference). Tables 4.5 and 4.6 present the complete geometry and properties for all cables.

Table 4.3 Cable Geometry and Material Properties for Downstream Cables 21-30

CABLE NUMBER	COORDINATE POINTS				PE PIPE	EFFECTIVE		INITIAL
	WORK POINT B		WORK POINT D		DIAMETER	YOUNG'S	DENSITY	STRAIN
	X	Y	X	Y		MODULUS		
	FT	FT	FT	FT	INCHES	KSI	SLUGS/IN ³	
21	1087.02	570.35	1568.78	783.53	8.858	27414.89	0.0002491	0.000572
22	1136.20	570.36	1568.83	777.69	8.858	27091.09	0.0002491	0.000454
23	1185.23	570.36	1568.88	771.86	8.858	27423.89	0.0002491	0.000488
24	1234.09	570.25	1568.60	765.87	7.874	27593.41	0.0002516	0.000506
25	1283.09	570.19	1568.66	760.16	7.874	27639.78	0.0002516	0.000469
26	1332.03	570.12	1568.73	754.58	7.874	27670.31	0.0002516	0.000421
27	1380.75	569.96	1568.81	749.2	6.299	27904.53	0.0002577	0.000577
28	1429.51	569.85	1568.91	743.82	6.299	27905.50	0.0002577	0.000464
29	1478.12	569.70	1569.03	738.11	6.299	27931.94	0.0002577	0.000388
30	1526.58	569.46	1569.13	728.19	6.299	27991.26	0.0002577	0.000495

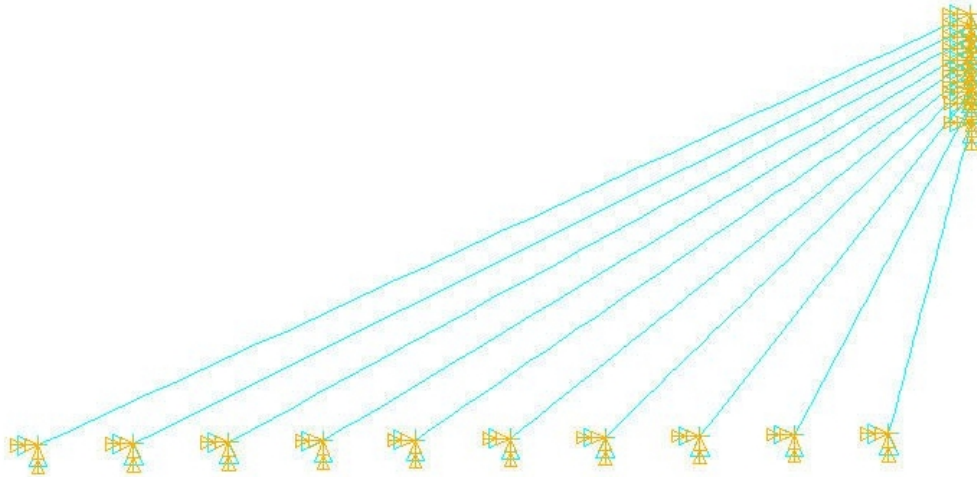


Figure 4.26 Finite Element Model of Ten Unrestrained Cables of the Maysville Bridge

Table 4.4 Finite Element Model Fundamental Frequency Results with Tests and String Model

	STRING	CABLYF	CABLYBB	CABLYH	CABLYL	cw3yb21	cw4yb21	ANSYS	ANSYS Y
Cable	FREQ	1/10/2001	1/10/2001	5/22/01	5/22/01	8/13/01	8/13/01	No Restr	Restrained
No.	Hz	Hz	Hz	Hz	Hz	Hz	Hz	Hz	Hz
21	0.629	0.781	0.641	0.625	0.610	0.625	0.625	0.647	0.647
22	0.612	0.806	0.807	0.625	0.625	0.735	0.735	0.634	0.633
23	0.706	0.714	0.862	0.735	0.714	0.735	0.807	0.735	0.727
24	0.803	0.833	0.833	0.807	0.410	0.833	0.833	0.834	0.832
25	0.874	0.926	n/a	n/a	1.923	0.893	0.893	0.915	0.912
26	0.947	1.000	n/a	1.000	1.000	1.000	1.000	1.002	0.998
27	1.271	1.316	1.316	1.316	1.3156	1.316	1.316	1.327	1.318
28	1.329	1.471	1.471	1.389	1.3889	1.389	1.389	1.407	1.405
29	1.414	1.786	1.786	1.786	1.7856	1.786	1.786	1.527	1.547
30	1.862	2.273	2.273	2.273	2.273	2.273	2.273	2.016	2.016

n/a – result not available

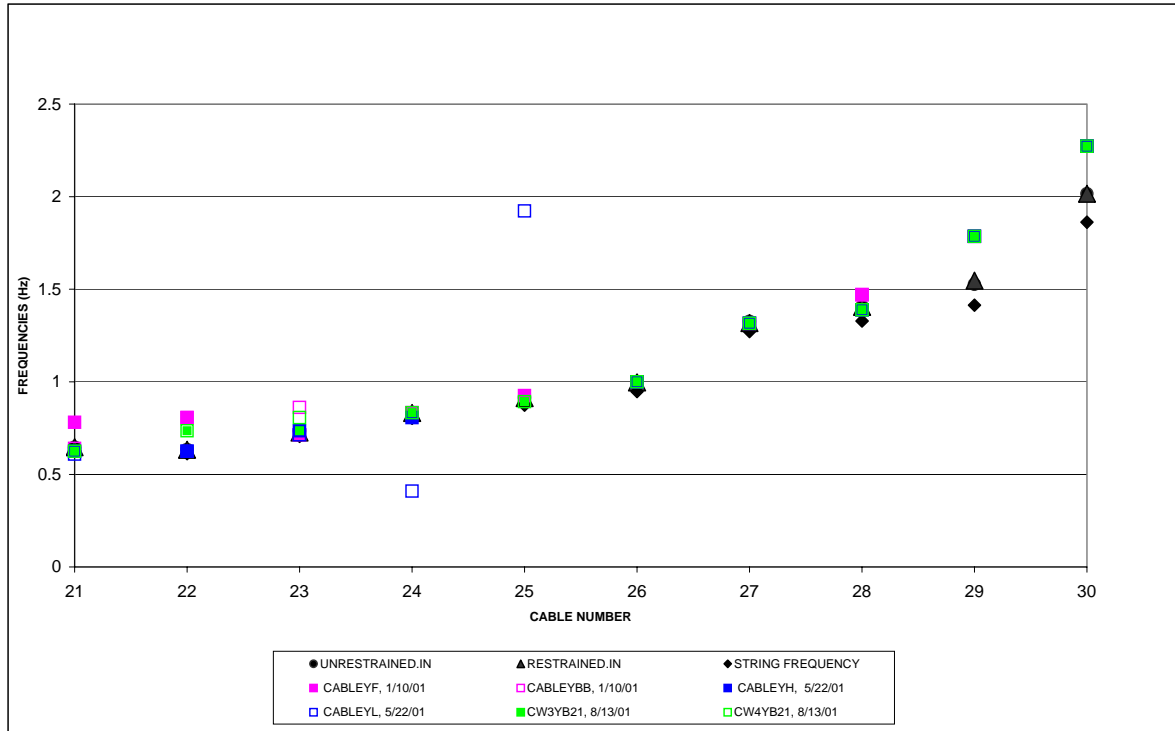


Figure 4.27 Comparison of Finite Element Model Fundamental Frequency Results for Cables 21-30 W to Experimental and String Model Frequencies

To add restrainers to a model of a set of ten cables, additional beam elements connect the nodes of the cables closest to the restrainer locations. Note that the restrainers were installed without specific locations indicated in the drawings relative to the work points that define the cable lengths. Restrainer locations in the model were established using the geometry indicated on the drawings and observations of the installed restrainers. Note also that the restrainers are a system including the following (as seen in Figure 4.5 above): an elastic interface between the cable and the collar (pipe clamp), the collar (pipe clamp), the cable tie connectors (bridge socket) and the cable ties (bridge wires) themselves. A model including all elements was considered, but the dominant stiffness in the restrained cable set response is that of the cross ties. Therefore, the restrainers were modeled as cross ties connected to specified cable nodes.

Properties of the cross ties are as follows: cross-section diameter = 0.5 inches, Young’s modulus = 20×10^6 psi, density = 0.00913 slugs/in³, Poisson’s ratio = 0.3 and modal damping ratio = 0.0025. Two lines of restrainers are installed for each set of ten cables. The restrainer locations for the model are specified by listing a cable number (in

this set the cables are numbered from 1 through 10 with 1 being the longest and 10 being the shortest) with a node number (nodes are numbered from 1 to 35 from the deck to the tower). The first restrainer line connects the following cable-nodes: 1-12, 2-10, 3-8, and 4-5. The second restrainer line connects the following cable nodes: 1-24, 2-23, 3-22, 4-20, 5-18, 6-16, 7-12 and 8-7. For the restrainers, tension-only elements are used rather than beam elements. The model mesh is presented in Figure 4.28. Fundamental frequency results of the restrained cable model are included above in Table 4.4. As noted in the field test results, the out-of-plane response of the cables is not appreciably affected by the restrainers, so the fundamental cable frequencies from the restrained cable model are nearly identical to those of the unrestrained cable model.

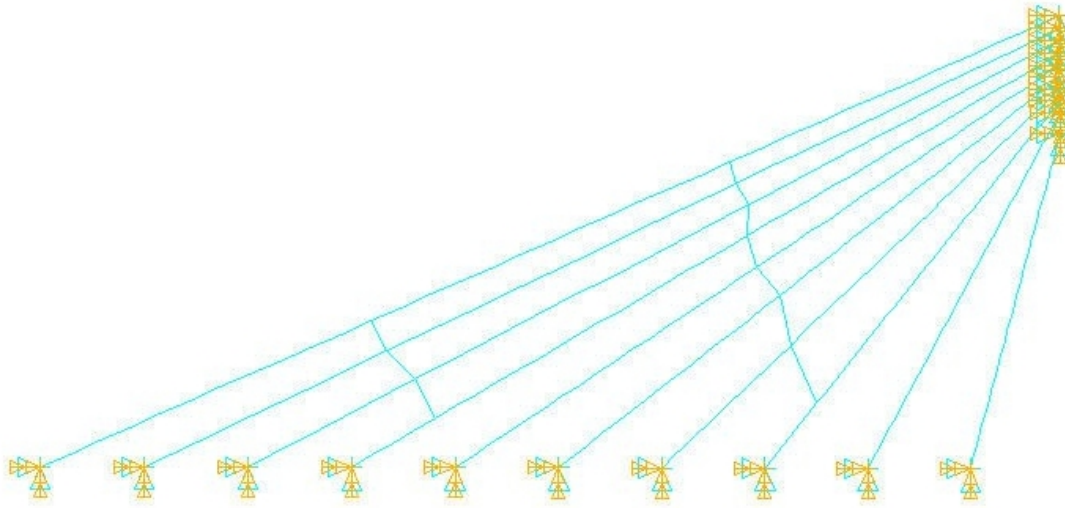


Figure 4.28 Finite Element Model of Ten Restrained Cables of the Maysville Bridge

Finally, unrestrained models of all 80 cables of the Maysville Bridge were constructed in sets of 10 as described above and using the as-built information provided in Tables 4.5 and 4.6. The fundamental frequencies resulting from these models were compared to the average field test results (May and August tests). These are presented in Figure 4.29. The FE model is seen to be well-correlated to the field test results, so no further model adjustment efforts are required.

Table 4.5 Cable Geometry and Material Properties for **Downstream** Cables 1-40

CABLE NUMBER	COORDINATE POINTS				PE PIPE	EFFECTIVE		INITIAL
	WORK POINT B		WORK POINT D		DIAMETER	YOUNG'S	DENSITY	STRAIN
	X	Y	X	Y		MODULUS		
	FT	FT	FT	FT	INCHES	KSI	SLUGS/IN ³	
1	39.28	562.70	518.80	783.6	8.858	27420.29	0.0002491	0.000577
2	88.40	563.48	518.86	777.77	8.858	27326.64	0.0002491	0.000503
3	137.23	564.23	518.91	771.96	8.858	27429.74	0.0002491	0.000490
4	185.77	564.91	518.62	765.94	7.874	27706.87	0.0002564	0.000593
5	233.16	565.58	518.67	760.25	7.874	27527.88	0.0002516	0.000436
6	282.03	566.28	518.74	754.65	7.874	27651.63	0.0002516	0.000418
7	330.74	566.89	518.82	749.27	6.299	27914.64	0.0002577	0.000605
8	379.50	567.55	518.92	743.88	6.299	27947.90	0.0002577	0.000577
9	428.12	568.17	519.03	738.18	6.299	27909.37	0.0002577	0.000346
10	476.57	568.70	519.13	728.23	6.299	27991.67	0.0002577	0.000502
11	573.42	569.46	530.87	728.19	6.299	27981.23	0.0002577	0.000376
12	621.88	569.70	530.97	738.11	6.299	27966.80	0.0002577	0.000505
13	670.49	569.85	531.09	743.82	6.299	27940.85	0.0002577	0.000552
14	719.25	569.96	531.19	749.2	6.299	27895.35	0.0002577	0.000558
15	767.97	570.12	531.27	754.58	7.874	27637.46	0.0002516	0.000406
16	816.91	570.19	531.34	760.16	7.874	27727.34	0.0002516	0.000519
17	865.91	570.26	531.40	765.87	7.874	27597.37	0.0002516	0.000507
18	914.77	570.35	531.12	771.86	8.858	27338.86	0.0002491	0.000464
19	963.80	570.36	531.17	777.69	8.858	27265.47	0.0002491	0.000490
20	1012.98	570.35	531.22	783.53	8.858	27413.42	0.0002491	0.000571
21	1087.02	570.35	1568.78	783.53	8.858	27414.89	0.0002491	0.000572
22	1136.20	570.36	1568.83	777.69	8.858	27091.09	0.0002491	0.000454
23	1185.23	570.36	1568.88	771.86	8.858	27423.89	0.0002491	0.000488
24	1234.09	570.25	1568.60	765.87	7.874	27593.41	0.0002516	0.000506
25	1283.09	570.19	1568.66	760.16	7.874	27639.78	0.0002516	0.000469
26	1332.03	570.12	1568.73	754.58	7.874	27670.31	0.0002516	0.000421
27	1380.75	569.96	1568.81	749.2	6.299	27904.53	0.0002577	0.000577
28	1429.51	569.85	1568.91	743.82	6.299	27905.50	0.0002577	0.000464
29	1478.12	569.70	1569.03	738.11	6.299	27931.94	0.0002577	0.000388
30	1526.58	569.46	1569.13	728.19	6.299	27991.26	0.0002577	0.000495
31	1623.43	568.70	1580.87	728.23	6.299	27994.10	0.0002577	0.000567
32	1671.88	568.17	1580.97	738.18	6.299	27929.42	0.0002577	0.000381
33	1720.50	567.55	1581.08	743.88	6.299	27925.01	0.0002577	0.000505
34	1769.26	566.89	1581.18	749.27	6.299	27892.53	0.0002577	0.000556
35	1817.97	566.28	1581.26	754.65	7.874	27738.55	0.0002516	0.000465
36	1866.84	565.58	1581.33	760.25	7.874	27609.24	0.0002516	0.000466
37	1914.23	564.91	1581.38	765.94	7.874	27631.31	0.0002564	0.000546
38	1962.77	564.23	1581.09	771.96	8.858	27178.02	0.0002491	0.000430
39	2011.60	563.48	1581.14	777.77	8.858	27170.55	0.0002491	0.000468
40	2060.72	562.70	1581.20	783.6	8.858	27411.97	0.0002491	0.000574

Table 4.6 Cable Geometry and Material Properties for **Upstream** Cables 1-40

CABLE NUMBER	COORDINATE POINTS				PE PIPE	EFFECTIVE		INITIAL
	WORK POINT B		WORK POINT D		DIAMETER	YOUNG'S	DENSITY	STRAIN
	X	Y	X	Y		MODULUS		
	FT	FT	FT	FT	INCHES	KSI	SLUGS/IN ³	
1	39.28	562.70	518.80	783.6	8.858	27394.68	0.0002491	0.000568
2	88.40	563.48	518.86	777.77	8.858	27279.37	0.0002491	0.000492
3	137.23	564.23	518.91	771.96	8.858	27239.21	0.0002491	0.000442
4	185.77	564.91	518.62	765.94	7.874	27631.58	0.0002564	0.000547
5	233.16	565.58	518.67	760.25	7.874	27571.11	0.0002516	0.000451
6	282.03	566.28	518.74	754.65	7.874	27684.58	0.0002516	0.000434
7	330.74	566.89	518.82	749.27	6.299	27922.12	0.0002577	0.000626
8	379.50	567.55	518.92	743.88	6.299	27949.97	0.0002577	0.000586
9	428.12	568.17	519.03	738.18	6.299	27959.22	0.0002577	0.000467
10	476.57	568.70	519.13	728.23	6.299	27992.03	0.0002577	0.000510
11	573.42	569.46	530.87	728.19	6.299	27981.23	0.0002577	0.000376
12	621.88	569.70	530.97	738.11	6.299	27966.80	0.0002577	0.000505
13	670.49	569.85	531.09	743.82	6.299	27900.02	0.0002577	0.000454
14	719.25	569.96	531.19	749.2	6.299	27895.35	0.0002577	0.000558
15	767.97	570.12	531.27	754.58	7.874	27702.79	0.0002516	0.000437
16	816.91	570.19	531.34	760.16	7.874	27624.71	0.0002516	0.000462
17	865.91	570.26	531.40	765.87	7.874	27521.51	0.0002516	0.000477
18	914.77	570.35	531.12	771.86	8.858	27384.43	0.0002491	0.000476
19	963.80	570.36	531.17	777.69	8.858	27090.78	0.0002491	0.000454
20	1012.98	570.35	531.22	783.53	8.858	27413.42	0.0002491	0.000571
21	1087.02	570.35	1568.78	783.53	8.858	27433.62	0.0002491	0.000578
22	1136.20	570.36	1568.83	777.69	8.858	27054.64	0.0002491	0.000448
23	1185.23	570.36	1568.88	771.86	8.858	27444.84	0.0002491	0.000494
24	1234.09	570.25	1568.60	765.87	7.874	27625.87	0.0002516	0.000521
25	1283.09	570.19	1568.66	760.16	7.874	27669.36	0.0002516	0.000484
26	1332.03	570.12	1568.73	754.58	7.874	27751.44	0.0002516	0.000467
27	1380.75	569.96	1568.81	749.2	6.299	27919.91	0.0002577	0.000615
28	1429.51	569.85	1568.91	743.82	6.299	27927.80	0.0002577	0.000513
29	1478.12	569.70	1569.03	738.11	6.299	27927.25	0.0002577	0.000378
30	1526.58	569.46	1569.13	728.19	6.299	27991.64	0.0002577	0.000503
31	1623.43	568.70	1580.87	728.23	6.299	27994.33	0.0002577	0.000575
32	1671.88	568.17	1580.97	738.18	6.299	27929.42	0.0002577	0.000381
33	1720.50	567.55	1581.08	743.88	6.299	27937.95	0.0002577	0.000541
34	1769.26	566.89	1581.18	749.27	6.299	27885.83	0.0002577	0.000544
35	1817.97	566.28	1581.26	754.65	7.874	27737.88	0.0002516	0.000464
36	1866.84	565.58	1581.33	760.25	7.874	27608.23	0.0002516	0.000466
37	1914.23	564.91	1581.38	765.94	7.874	27599.26	0.0002564	0.000531
38	1962.77	564.23	1581.09	771.96	8.858	27343.09	0.0002491	0.000466
39	2011.60	563.48	1581.14	777.77	8.858	27108.10	0.0002491	0.000456
40	2060.72	562.70	1581.20	783.6	8.858	27428.98	0.0002491	0.000580

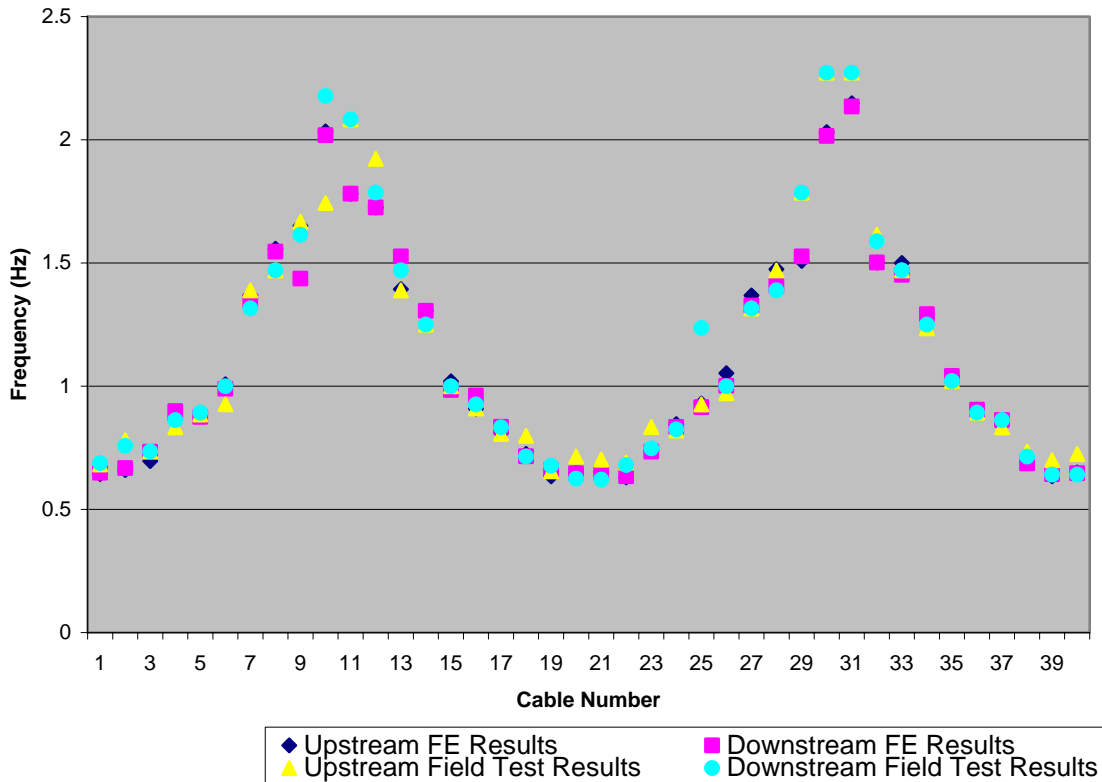


Figure 4.29 Final Comparison of Finite Element Model Results to Field Test Results

4.4. Remarks

Cable testing and modeling for the Maysville Bridge included three field tests of the cables (on 1/10/01, 5/22/01 and 8/13/01). The first of these was just before the bridge opened with excitation provided by loaded trucks. The second and third tests used ambient (typical traffic and wind) excitation. Signal processing analysis of the recorded acceleration time histories identified fundamental frequencies of the cables. Finite element models were developed for all cables using the as-built cable properties and compared to field test results showing good correlation.

Notable results include the following:

1. Short (60-second) triaxial acceleration time records were recorded for each of the 80 cables. One set of 20 cables (21-40 W) was tested during each of the three field tests for comparison. Corresponding anchor accelerations were recorded for each cable. Overall, more than 320 separate cable data sets (each set with 6 to 12 channels) were recorded.

2. Signal processing was performed to identify the fundamental cable frequency from each cable record. The cable transverse direction response (perpendicular to the vertical plane containing the parallel cables and restrainers) enabled identification of the unrestrained fundamental frequency for each cable. The Cepstrum signal processing approach, developed at the University of Kentucky for a previous cable-stayed bridge project, allowed automated processing of the data records.
3. Using short time records with Cepstrum analysis enables testing of all bridge stay cables in 1.5 days (facilitating periodic visits for cable monitoring).
4. Field tests of the cables in May 2001 and August 2001 resulted in consistent fundamental frequencies that differed from those for the longest cables of the first test just before bridge opening in January 2001. Two possible explanations for the differences include a “breaking-in” period for castings and temperature effects.
5. A rain event occurred during testing in May 2001. Response of two restrained cables was recorded during the rain showing persistent amplitude-modulated response unrelated to the anchor motion. This response stopped when the rain stopped. Rivulets were noted and photographed on the underside of the cables. The helical strikes included on the surface of the cables do not significantly disrupt the rivulet path down the cable. The motion of the cables was limited (by the restrainers), however, to acceleration amplitudes less than those seen with typical heavy traffic.
6. Technical papers related to the Maysville Bridge testing and nonlinear modeling of cables (not in the scope of this project and under separate support) have been presented at conferences. References not listed above include Smith and Campbell 2002; Jean, Baker and Smith 2003; and Campbell, Baker and Smith 2004.

Finally, note that the cable testing and modeling effort could not have been accomplished without the assistance of many colleagues and capable students who helped with the bridge testing, data analysis and model verification. Their careful attention to detail contributed to the excellent results seen herein.

5. CONCLUSIONS AND RECOMMENDATIONS

5.1. General

Maysville cable-stayed bridge, dedicated as the William H. Harsha Bridge, was completed in January 2001. It connects Maysville (Mason County), Kentucky and Aberdeen (Brown County), Ohio over the Ohio River. Since the main span length was increased and more shallow and slender stiffness girders were used in modern cable-stayed bridges, the safety of the whole bridges under service loadings and environmental dynamic loadings presents increasingly important concerns in design, construction and service. It has become essential to synthetically understand and realistically predict their response to these loadings. The present study focuses on the baseline modeling of the Maysville cable-stayed bridge. It has demonstrated that the dynamics-based structural evaluation method provides a ‘global’ way to evaluate the structural state and safety. The dynamics-based structural evaluation requires improvements in instrumentation for sensing and recording, data acquisition, algorithms for system identification, model updating and structure evaluation. The finite element model calibration through the field dynamic testing plays an important role in the dynamics-based structural evaluation. The calibrated finite element model can be used as a baseline for health assessments of the bridge structure in the future.

5.2. Finite Element Modeling and Dynamic Properties

The complete 3-D nonlinear modeling of a cable-stayed bridge has proved to be difficult. The smaller discretization would be computationally very large and inefficient. Convergence of such a large number of nonlinear elements is not always guaranteed. The displacement convergence criterion is effective and often results in the convergent solution. Due to the cable sagging, the static analysis of a cable-stayed bridge is always a geometric nonlinear. The stress stiffening of cable elements plays an important role in both the static and dynamic analysis. Nonlinear static analysis without the stress stiffening effect will lead to an aborted run due to the divergent oscillation even though the displacement convergence criterion is used. Large deflection has been demonstrated

to be the limited effect on the member forces and deck deflection of the bridge under dead loads. After introducing enough amount of initial strain in the cables, the static analysis of the Maysville cable-stayed bridge due to dead loads can be elastic and small deflection. However, the stress stiffening effect is always required to ensure the convergent solution.

The initial strain in the cables is the key factor to control the initial equilibrium configuration under the dead load. For a complete bridge, the common fact is that the initial position of the cable and bridge is unknown. The initial geometry of the bridge which was modeled is really the deflected shape of the bridge loaded by the dead load. The initial equilibrium configuration of the bridge due to dead loads can be approximately achieved by referring to the bridge plans.

It is demonstrated that a cable-stayed bridge is a highly pre-stressed structure. The self-weight effect can significantly improve the stiffness of a cable-stayed bridge. The modal or any dynamic analysis must start from the initial equilibrium configuration due to dead loads. This initial equilibrium configuration can be a small deflection static analysis because the large deflection can be ignored. The modal analysis of a cable-stayed bridge should include two steps: small deflection static analysis under the dead load and followed by pre-stressed modal analysis, so that the dead load effect on the stiffness can be included. In other words, the modal analysis of a cable-stayed bridge must be a pre-stressed modal analysis.

It is observed that one dominated mode of the Maysville cable-stayed bridge is always coupled with other modes. The dominated mode shapes of the Maysville cable-stayed bridge in the low-frequency (0~1.0 Hz) range are mainly vertical direction. This reveals the fact that the lateral stiffness of the cable stayed bridge is stronger than that of the suspension bridge (Ren and Harik 2001). From the parametric studies, it is found that the key parameters affecting the vertical modal properties are the mass, cable sectional area, cable elastic modulus and deck vertical bending stiffness. The key parameters

affecting the transverse and torsion modal properties are the mass, cable sectional area, cable elastic modulus and deck lateral bending stiffness.

5.3. Free Vibration Testing and Model Calibration

On site free vibration testing provides a fast way to obtain the real dynamic properties of a structure. The modal parameters can be effectively extracted from output-only dynamic testing by using the frequency domain based peak picking (PP) method. The peak picking identification is very fast and efficient since no model has to be fitted to the data. For real applications, the peak picking method could be used on site to verify the quality of the measurements. But the mode shapes for the transverse are not too good since the transverse excitation is not enough. The bump-and-brake test does not improve the identified results. It means that the ambient vibration measurements induced by normal traffics and natural winds are good enough to identify the modal parameters of a large cable-stayed bridge. Ambient vibration testing provides a convenient, fast and cheap way to perform the bridge dynamic testing.

A good agreement of frequencies has been found between the results of the calibrated finite element model and in *situ* free vibration testing results. The identified frequencies from the High-speed and Bump-brake measurements are quite stable. The better matching for higher modes is not expected and not realistic too, as the experimental modal properties of the bridge come from the output-only measurement. The calibrated finite element model may be used as a baseline in the future structural analysis and monitoring of the Maysville cable-stayed bridge.

5.4. Cable Testing and Modeling

Short (60-second) triaxial acceleration time records were recorded for each of the 80 cables. One set of 20 cables (21-40 W) was tested during each of the three field tests for comparison. Corresponding anchor accelerations were recorded for each cable. Overall, more than 320 separate cable data sets (each set with 6 to 12 channels) were

recorded. Signal processing was performed to identify the fundamental cable frequency from each cable record. The cable transverse direction response (perpendicular to the vertical plane containing the parallel cables and restrainers) enabled identification of the unrestrained fundamental frequency for each cable. The Cepstrum signal processing approach, developed at the University of Kentucky for a previous cable-stayed bridge project, allowed automated processing of the data records.

Using short time records with Cepstrum analysis enables testing of all bridge stay cables in 1.5 days (facilitating periodic visits for cable monitoring). Field tests of the cables in May 2001 and August 2001 resulted in consistent fundamental frequencies that differed from those for the longest cables of the first test just before bridge opening in January 2001. Two possible explanations for the differences include a “breaking-in” period for castings and temperature effects.

A rain event occurred during testing in May 2001. Response of two restrained cables was recorded during the rain showing persistent amplitude-modulated response unrelated to the anchor motion. This response stopped when the rain stopped. Rivulets were noted and photographed on the underside of the cables. The helical strikes included on the surface of the cables do not significantly disrupt the rivulet path down the cable. The motion of the cables was limited (by the restrainers), however, to acceleration amplitudes less than those seen with typical heavy traffic.

REFERENCES

- Abdel-Ghaffar, A.M. (1980). "Vertical vibration analysis of suspension bridges." *Journal of Structural Engineering*, ASCE, 106(10), 2053-2075.
- Abdel-Ghaffar, A.M. and Rubin, L.I. (1983). "Vertical seismic behavior of suspension bridges." *Earthquake Engineering and Structural Dynamics*, 11, 1-19.
- Abdel-Ghaffar, A.M. and Nazmy A.S. (1987) "Effects of three-dimensionality and nonlinearity on the dynamic and seismic behavior of cable-stayed bridges." *Proceedings of the Structures Congress (Bridges and Transmission Line Structures)*, ASCE, New York, 389-404.
- Abdel-Ghaffar, A.M. and Nazmy, A.S. (1991a). "3-D nonlinear seismic behavior of cable-stayed bridges." *Journal of Structural Engineering*, ASCE, 117(11), 3456-3476.
- Abdel-Ghaffar, A.M. and Khalifa, M.A. (1991b) "Importance of cable vibration in dynamics of cable-stayed bridges." *Journal of Engineering Mechanics*, ASCE, 117(11), 2571-2589.
- Abdel-Ghaffar, A.M. and Scanlan, R. H. (1985). "Ambient vibration studies of Golden Gate Bridge. I: suspended structure." *Journal of Engineering Mechanics*, ASCE, 111(4), 463-482.
- Andersen, P., Brincker, R. and Kirkegaard, P.H. (1996). "Theory of covariance equivalent ARMAV models of civil engineering structures." *Proceedings of IMAC14, the 14th International Modal Analysis Conference*, Dearborn, MI, 518-524.
- ANSYS5.6 (1999). *User's manual*, Swanson Analysis System, USA.
- Au, F.T.K., Cheng, Y.S., Cheung, Y.K. and Zheng, D.Y. (2001). "On the determination of natural frequencies and mode shapes of cable-stayed bridges." *Applied Mathematical Modeling*, 25, 1099-1115.
- Baker, J.R. and Smith, S.W. (2002) "Simulation of parametric response of bridge stay cables." *Proceedings of the International Modal Analysis Conference*, Los Angeles, California.
- Bathe, K.J. (1982). *Finite element procedures in engineering analysis*. Prentice-Hall, Inc., Englewood Cliffs, New Jersey.
- Bendat, J.S. and Piersol, A.G. (1993). *Engineering applications of correlation and spectral analysis*. 2nd edition, John Wiley & Sons, New York.

- Boonyapinyo, V., Miyata, T. and Yamada, H. (1999). "Advanced aerodynamic analysis of suspension bridges by state-space approach." *Journal of Structural Engineering*, ASCE, 125(12), 1357-1366.
- Boonyapinyo, V., Yamada, H. and Miyata, T. (1994). "Wind-induced nonlinear lateral-torsional buckling of cable-stayed bridges." *Journal of Structural Engineering*, ASCE, 120(2), 486-506.
- Bracewell, R.N. (2000). *The fourier transform and its applications*. Third edition, McGraw Hill.
- Brownjogn, J.M.W. and Xia, P.Q.(2000). "Dynamic assessment of curved cable-stayed bridge by model updating." *Journal of Structural Engineering*, ASCE, 126(2), 252-260.
- Brownjohn, J.M.W., Dumanoglu, A.A. and Severn, R.T. (1992). "Ambient vibration survey of the Faith Sultan Mehmet (Second Bosphorus) suspension bridge." *Earthquake Engineering and Structural Dynamics*, 21, 907-924.
- Caetano, E., Cunha, A. and Taylor, C.A. (2000a) "Investigation of dynamic cable-deck interaction in a physical model of a cable-stayed bridge, part I: modal analysis." *Earthquake Engineering and Structural Dynamics*, 29(4), 481-498.
- Caetano, E., Cunha, A. and Taylor, C.A. (2000b) "Investigation of dynamic cable-deck interaction in a physical model of a cable-stayed bridge, part II: seismic response." *Earthquake Engineering and Structural Dynamics*, 29(4), 499-521.
- Campbell, J.E. and Smith, S.W. (2003) "Comparison of field survey test results of four cable stayed bridges: deck/cable response and controlled/ambient traffic excitation." *Proceedings of the Fifth International Symposium on Cable Dynamics*, Santa Margarita Ligure, Italy, 517-524.
- Campbell, J.E., Baker, J.R. and Smith, S.W. (2004) "Simulations and tests of bridge stay-cable dynamics based on experimental deck motion measurements." *Proceedings of the International Modal Analysis Conference*, Detroit, Michigan.
- Casas, J.R. and Aparicio, A.C. (1994). "Structural damage identification from dynamic-test data." *Journal of Structural Engineering*, ASCE, 120(8), 2437-2450.
- Chang, C.C., Chang, T.Y.P. and Zhang, Q.W. (2001). "Ambient vibration of long-span cable-stayed bridge." *Journal of Bridge Engineering*, ASCE, 6(1), 46-53.
- Chen, H.L., Spyrakos, C.C. and Venkatesh, G. (1995). "Evaluating structural deterioration by dynamic response." *Journal of Structural Engineering*, ASCE, 121(8), 1197-1204.

Cunha, A., Caetano, E. and Delgado, R. (2001). "Dynamic tests on large cable-stayed bridge." *Journal of Bridge Engineering*, ASCE, 6(1), 54-62.

DADiSP (1996). *User Manual, DADiSP Worksheet, Data Analysis and Display Software*. DSP Development Corporation, Cambridge, Massachusetts.

De Roeck, G. and Peeter, B. (1999). *MACCEC2.0 – Modal Analysis on Civil Engineering Constructions*, Department of Civil Engineering, Catholic University of Leuven, Belgium.

De Roeck, G., Peeters, B. and Ren, W.X. (2000). "Benchmark study on system identification through ambient vibration measurements." *Proceedings of IMAC-XVIII*, the 18th International Modal Analysis Conference, San Antonio, Texas, 1106-1112.

Doebbling, S.W., Farrar, C.R., Prime, M.B. and Shevitz, D.W. (1996). "Damage identification and health monitoring of structural and mechanical systems from changes in their vibration characteristics: A literature review." *Research report LA-13070-MS, ESA-EA*, Los Alamos National Laboratory, New Mexico, USA.

Ewins, D.J. (1986). *Modal testing: theory and practice*. Research Studies Press Ltd., England.

Fleming, J.F. and Egeseli, E.A. (1980). "Dynamic behavior of a cable-stayed bridge." *Earthquake Engineering and Structural Dynamics*, 8, 1-16.

Friswell, M.I. and Mottershead, J.E. (1995). *Finite element model updating in structural dynamics*, Kluwer Academic Publishers, Netherlands.

Fujina, Y., Warnitchai, P. and Pacheco, B.M. (1993) "An experimental and analytical study of autoparametric resonance in a 3dof model of a cable-stayed beam," *Nonlinear Dynamics*, 4, 111-138.

Gupta, A.K. (1992). *Response Spectrum Method in Seismic Analysis and Design of Structures*, CRC Press, Ann Arbor, Michigan.

Harik, I.E., Allen, D.L., Street, R.L., Guo, M., Graves, R.C., Harrison, J. and Gawry, M.J. (1997). "Free and ambient vibration of brent-spence bridge." *Journal of Structural Engineering*, ASCE, 123(9), 1262-1268.

Harik, I.E., Allen, D.L., Street, R.L., Guo, M., Graves, R.C., Harrison, J. and Gawry, M.J. (1997). "Seismic evaluation of brent-spence bridge." *Journal of Structural Engineering*, ASCE, 123(9), 1269-1275.

Harik, I.E., Vasudevan, K., Madasamy, C., Chen, D., Zhou, L., Sutterer, K., Steet, R. and Allen, D.L. (1999). "Seismic evaluation of the US41 Southbound bridge over the Ohio

River at Henderson, KY.” *Research Report KTC-99-17*, Kentucky Transportation Center, University of Kentucky.

Harris, C.M., ed. (1996) *Shock and Vibration Handbook, Fourth Edition*, McGraw-Hill, New York, 14.34-14.37.

Hearn, G. and Testa, R.B. (1991). “Modal analysis for damage detection in structures.” *Journal of Structural Engineering*, ASCE, 117(10), 3042-3063.

Hikami, Y. and Shiraishi, N. (1988) “Rain-wind induced vibrations of cables in cable stayed bridges.” *J. Wind Engineering and Industrial Aerodynamics*, 29, 409-418.

James III, G.H., Carne, T.G. and Lauffer, J.P. (1995). “The natural excitation technique (NExT) for modal parameter extraction from operating structures.” *International Journal of Analytical and Experimental Modal Analysis*, 10(4), 260-277.

Jean, D.P., Baker, J.R., Smith, S.W. and Li J. (2003) “Phased development of nonlinear finite element simulations of deck-excited response of sagged bridge stay cables.” *Proceedings of the Fifth International Symposium on Cable Dynamics*, Santa Margarita Ligure, Italy, 173-180.

Jean, D.P., Baker, J.R. and Smith, S.W. (2003) “Nonlinear finite element simulations of sagged bridge stay cables.” *Proceedings of the International Modal Analysis Conference*, Kissimmee, Florida.

Jean, D.P. (2003) “Nonlinear finite element simulations of large oscillations of flexible structures with applications to bridge stay cables.” *Masters Thesis, University of Kentucky*.

Johnson, M.L. (1999) “Vibration reduction for rain-wind induced vibrations of the stay cables of the Fred Hartman bridge.” *Masters Thesis, University of Kentucky*.

Juneja, Y., Haftka, R.T. and Cudney, H.H. (1997). “Damage detection and damage detectability - analysis and experiments.” *Journal of Aerospace Engineering*, ASCE, 10(4), 135-142.

Kollbruner, C., Hajdin, N. and Stipanis, B. (1980) “Contribution to the analysis of cable-stayed bridges.” *Institut Fuer Bauwissenschaftliche Forsch Publikation* (Switzerland), 48, 1-45.

Lall, J. (1992). “Analytical modelling of the J.A. Roebling suspension bridge.” A thesis submitted to the Department of Civil and Environmental Engineering, University of Cincinnati in partial fulfillment of the requirements for the degree of Master of Science.

Lilen, J.L. and Pinto da Costa, A. (1994) “Amplitudes caused by parametric excitations on cable stayed structures.” *Journal of Sound and Vibration*, 174(1), 64-90.

Liu, P.L. (1995). "Identification and damage detection of trusses using modal data." *Journal of Structural Engineering*, ASCE, 121(4), 599-608.

Ljung, L. (1987). *System identification: theory for the user*. Prentice-Hall Inc., Englewood Cliffs, New Jersey.

Maia, N.M.M. and Silva, J.M.M. Edited. (1997). *Theoretical and experimental modal analysis*. Research Studies Press Ltd., England.

Main, J.A. and Jones, N.P. (1999) "Full-scale measurements of stay cable vibration." *Proceedings of the 10th International Conference on Wind Engineering*, Copenhagen, Denmark.

Main, J.A. and Jones, N.P. (2001) "Characterization of rain-wind induced stay-cable vibrations from full-scale measurements." *Proceedings of the Fourth International Symposium on Cable Dynamics*, Montreal, Canada, 235-242.

Matsumoto, M., Shiraishi, N. and Shirato, H. (1992) "Rain-wind induced vibration of cables of cable stayed bridges." *J. Wind Engineering and Industrial Aerodynamics*, 2011-2022.

Mazurek, D.F. and Dewolf, J.T. (1990). "Experimental study of bridge monitoring technique." *Journal of Structural Engineering*, ASCE, 116(9), 2532-2549.

Nazmy, A.S. and Abdel-Ghaffar, A.M. (1990). "Three-dimensional nonlinear static analysis of cable-stayed bridges." *Computers and Structures*, 34(2), 257-271.

Okauchi, I., Miyata, T., Tatsumi, M. and Sasaki, N. (1997). "Field vibration test of a long span cable-stayed bridge using large exciters." *Journal of Structural Engineering /Earthquake Engineering*, Tokyo, 14(1), 83-93.

Peeters, B. and De Roeck, G. (2000). "Reference based stochastic subspace identification in civil engineering." *Inverse Problems in Engineering*, 8(1), 47-74.

Peeters, B., et al. (2003) "Continuous monitoring of the Oresund Bridge: system and data analysis." *Proceedings of International Modal Analysis Conference*, Kissimmee, FL.

Pinto da Costa, A., et. al. (1996) "Oscillations of bridge stay cables induced by periodic motions of deck and/or towers," *Journal of Engineering Mechanics*, 122(7), 613-622.

Podolny, W. and Fleming, J.F. (1972). "History development of cable-stayed bridges." *J. Strut. Div.*, ASCE, 98(9), 2079-2095.

Ren, W.X. (1999). "Ultimate behavior of long span cable-stayed bridges." *Journal of Bridge Engineering*, ASCE, 4(1), 30-37.

- Ren, W.X., Harik, I.E. and Blandford, G.E. (2001). *Structural evaluation of the John A. Roebling suspension bridge over the Ohio river*. Kentucky Transportation Center Research Report KTC- - . University of Kentucky, Lexington, Kentucky.
- Ren, W.X., Harik, I.E., Lenett, M. and Basehearh, T. (2001). "Modal properties of the Roebling suspension bridge – FEM modeling and ambient testing." Proceedings of IMAC-XX: A Conference on Structural Dynamics, Kissimmee, Florida, February 5-8, 1139-1145.
- Ren, W.X. and Obata, M. (1999). "Elastic-plastic seismic behavior of long span cable-stayed bridges." *Journal of Bridge Engineering*, ASCE, 4(3), 194-203.
- Ren, W.X., Shen, J.Y. and De Roeck, G. (2000c). "Structural Stiffness Matrix Identification with Maximum Likelihood Estimation Method." Proceedings of IMAC-XVIII, the 18th International Modal Analysis Conference, San Antonio, Texas, 418-423.
- Ren, W.X. and Chen, G. (2003) "Experimental modal analysis of bridge stay cables." *Proceedings of International Modal Analysis Conference*, Kissimmee, Florida.
- Salawu, O.S. (1997). "Detection of structural damage through changes in frequency: a review." *Engineering Structures*, 19(9), 718-723.
- Schrader, M.D. (1999) "Stay Cable Properties for vibration analysis model comparisons: Veterans Memorial and Maysville bridges." *Masters Thesis, University of Kentucky*.
- Smith, S.W. and Johnson, M.L. (1998) "Field test to determine frequencies of bridge stay cables." *Proceedings of the 17th International Modal Analysis Conference*, Kissimmee, Florida.
- Smith, S.W., Johnson, M.L. and Schrader, M.D. (2000) "Correlation of bridge stay cable models using short time record data." *Proceedings of the AIAA Dynamics Specialists Conference*, Atlanta, Georgia, USA.
- Smith, S.W. and Baker, J.R. (2001) "Toward simulating parametric response of bridge stay cables resulting from motion of the deck and tower." *Proceedings of the Fourth International Symposium on Cable Dynamics*, Montreal, Canada, 361-368.
- Smith, S.W. and Campbell, J.E. (2002) "Testing and model verification of the Maysville Kentucky bridge stay cables." *Proceedings of the International Modal Analysis Conference*, Los Angeles, California.
- Spyrakos, C.C., Kemp, E.L. and Venkatareddy, R. (1999). "Validated analysis of Wheeling suspension bridge." *Journal of Bridge Engineering*, ASCE, 4(1), 1-7.

- Stubbs, N., Sikorsky, C., Park, S., Choi, S. and Bolton, R. (1999). "A methodology to nondestructively evaluate the structural properties of bridges." *Proceedings of IMAC17, the 17th International Modal Analysis Conference*, 1260-1268, Kissimmee, Florida, USA.
- Van der Auweraer, H. and Hermans, L. (1999). "Structural modal identification from real operating conditions." *Sound and Vibration*, 33(1), 34-41.
- Van Overschee, P. and De Moor, B. (1996). *Subspace identification for linear systems: theory, implementation and applications*, Kluwer Academic Publishers, Dordrecht, Netherlands.
- West, H.H., Suhoski, J.E. and Geschwindner Jr., L.F. (1984). "Natural frequencies and modes of suspension bridges." *Journal of Structural Engineering*, ASCE, 110(10), 2471-2486.
- Wilson, J.C. and Gravelle, W. (1991). "Modeling of a cable-stayed bridge for dynamic analysis." *Earthquake Engineering and Structural Dynamics*, 20, 707-721.
- Wilson, J.C. and Liu, T. (1991). "Ambient vibration measurements on a cable-stayed bridge." *Earthquake Engineering and Structural Dynamics*, 20, 723-747.
- Xu, Y.L., Ko, J.M. and Zhang, W.S. (1997). "Vibration studies of Tsing Ma Suspension Bridge." *Journal of Bridge Engineering*, ASCE, 2, 149-156.
- Yang, F.H. and Fonder, G.A. (1998). "Dynamic response of cable-stayed bridges under moving loads." *Journal of Engineering Mechanics*, ASCE, 124(7), 741-747.
- Yang, Y.B. and McGuire, W. (1986). "A stiffness matrix for geometric non-linear analysis." *Journal of Structural Engineering*, ASCE, 112(4), 853-877.
- Yang, Y.B. and McGuire, W. (1986). "Joint rotations and geometric non-linear analysis." *Journal of Structural Engineering*, ASCE, 112(4), 879-905.
- Yoshimura, T., Savage, M.G. and Tanaka, H. (1995) "Wind-induced vibrations of bridge stay cables." *Proceedings of the International Symposium on Cable Dynamics*, A.I.M., Liege, Belgium, 437-444.
- Zhang, Q.W., Chang, T.Y.P. and Chang, C.C. (2001). "Finite-element model updating for the Kap Shui Mun cable-stayed bridge." *Journal of Bridge Engineering*, ASCE, 6(4), 285-293.
- Zhu, L.D., Xiang, H.F. and Xu, Y.L. (2000). "Triple-girder model for modal analysis of cable-stayed bridges with warping effect." *Engineering Structures*, 22, 1313-1323.